AD-A110 274 PRINCETON UNIV NJ DEPT OF MECHANICAL AND AEROSPACE --ETC F/G 1/2
DIGITAL COMMAND AUGMENTATION FOR LATERAL-DIRECTIONAL AIRCRAFT D--ETC(U)
MAY 81 D ATZHORN N00014-78-C-0257
UNCLASSIFIED MAE-1511 ONR-CR-300-003-2 NL

1 of 3

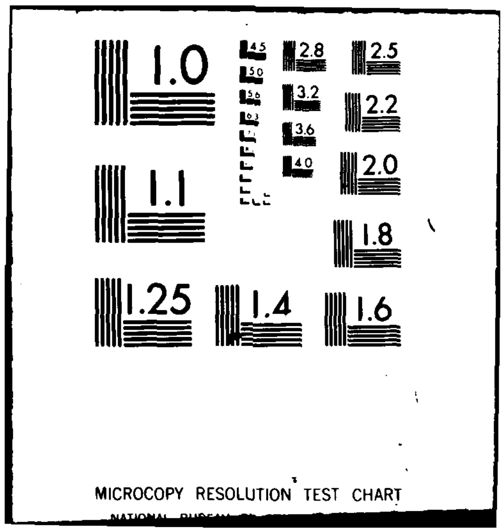
1.0
1.1
1.25
1.4
1.6
1.8
2.0
2.2
2.5
2.8
3.2
3.6
4.0
MICROCOPY RESOLUTION TEST CHART

REPORT ONR-CR-300-003-2

(12)

OFFICE OF NAVAL RESEARCH

DIGITAL COMMAND AUGMENTATION FOR LATERAL-DIRECTIONAL AIRCRAFT DYNAMICS

DAVID ATZHORN

FLIGHT RESEARCH LABORATORY
DEPARTMENT OF MECHANICAL AND AEROSPACE ENGINEERING
PRINCETON UNIVERSITY

PRINCETON, NEW JERSEY 08544

CONTRACT N00014-78-C-0257
ONR TASK 300-003

MAY 1981

ANNUAL TECHNICAL REPORT FOR PERIOD
1 FEBRUARY 1979 - 31 JANUARY 1980

PREPARED FOR THE
OFFICE OF NAVAL RESEARCH - 800 N. Quincy - Arlington, VA 22217

SECURITY CLASSIFICATION OF THIS PAGE (When Data Entered)

REPORT DOCUMENTATION PAGE		READ INSTRUCTIONS BEFORE COMPLETING FORM
1. REPORT NUMBER ONR-CR-300-003-2	2. GOVT ACCESSION NO. AD-A110 274	3. RECIPIENT'S CATALOG NUMBER
4. TITLE (and Subtitle) Digital Command Augmentation for Lateral-Directional Aircraft Dynamics		5. TYPE OF REPORT & PERIOD COVERED Annual - Technical 1 FEB 1979 - 31 JAN 1980
		6. PERFORMING ORG. REPORT NUMBER MAE Report No. 1511
7. AUTHOR(s) David Atzhorn		8. CONTRACT OR GRANT NUMBER(s) N00014-78-C-0257
9. PERFORMING ORGANIZATION NAME AND ADDRESS Flight Research Laboratory, Department of Mechanical and Aerospace Engineering, Princeton University, Forrestal Campus, Princeton, N.J.08544		10. PROGRAM ELEMENT, PROJECT, TASK AREA & WORK UNIT NUMBERS ONR Task 300-003
11. CONTROLLING OFFICE NAME AND ADDRESS Office of Naval Research Code 260 800 N. Quincy St., Arlington, VA 22217		12. REPORT DATE May 1981
		13. NUMBER OF PAGES 193
14. MONITORING AGENCY NAME & ADDRESS(if different from Controlling Office)		15. SECURITY CLASS. (of this report) Unclassified
		15a. DECLASSIFICATION/DOWNGRADING SCHEDULE

16. DISTRIBUTION STATEMENT (of this Report)

Approved for public release; Distribution unlimited

17. DISTRIBUTION STATEMENT (of the abstract entered in Block 20, if different from Report)

18. SUPPLEMENTARY NOTES

Principal Investigator: Robert F. Stengel, Associate Professor of Mechanical and Aerospace Engineering and Director, Flight Research Laboratory

19. KEY WORDS (Continue on reverse side if necessary and identify by block number)

Aircraft flight control; digital control; aircraft flying qualities; modern control theory; atmospheric flight mechanics; flight testing techniques; microprocessor systems; variable-response research aircraft.

20. ABSTRACT (Continue on reverse side if necessary and identify by block number)

Linear-quadratic sampled-data regulator theory is used to design several Type 0 and Type 1 control laws for lateral-directional aircraft dynamics. Control structures are defined for singular command inputs and for control rate outputs; the former allows for precise following of a command whose integral appears in the state vector, while the latter uses both a difference approximation and the Tustin transform to characterize control rate in the discrete-time domain. Type 0 controllers with control rate restraint and "equivalent" Type 1 controllers are implemented in a microprocessor-based digital flight

DD FORM 1 JAN 73 1473 EDITION OF 1 NOV 65 IS OBSOLETE

411732

SECURITY CLASSIFICATION OF THIS PAGE (When Data Entered)

20. continued

control system, and flight tests are conducted using Princeton University's Variable-Response Research Aircraft. The control system, entitled CAS-4, offers four combinations of control: direct (unaugmented) control, Type 0 control with both roll rate/sideslip angle and roll rate/lateral acceleration command combinations, and Type 1 control with roll/sideslip angle command.

Ground-based hybrid simulation and flight test results show that major closed-loop response features are unaffected by the choice of sampling rate when sampled-data regulator theory is used. Consequently, much lower sampling rates than would normally be expected can be used when control laws are derived in this manner (a sampling rate of 10 sps is primarily used in this investigation, though lower sampling rates are investigated as well). The control laws provide improved command response and exhibit improved steady-state decoupling over the open-loop dynamics at all sampling rates investigated. Hybrid simulations show the Type 1 system to be extremely sensitive to noise inputs. Flight tests verify this sensitivity to disturbances and measurement noise, indicating the need for state estimation and/or control law restructuring. The Type 0 controller provides satisfactory performance without state estimation.

The results derived through this investigation and presented herein provide additional evidence that digital flight control through modern control theory will be a practical way of implementing flight control systems in future high performance aircraft.

ACKNOWLEDGMENTS

I wish to express my deepest appreciation to Professor Robert F. Stengel for his guidance and patience throughout the duration of this investigation. In addition, I would like to thank George E. Miller, whose invaluable experience and assistance made possible the successful completion of this project. Further appreciation is extended to Barry W. Nixon and Barton Reavis, whose professional experience made possible successful flight evaluations presented herein. I would like to extend a special thank you to Karen Praul and Marion Sandvik for their time and patience in typing this report. I wish to acknowledge the Office of Naval Research, which provided funding for this investigation under Contract No. N00014-78-C-0257.

This report carries the report number MAE-1511 in the Department of Mechanical and Aerospace Engineering.

TABLE OF CONTENTS

LIST OF FIGURES

LIST OF TABLES

LIST OF SYMBOLS

Variables	Description
a_y	Lateral acceleration
C	Type 1 optimal gains
E	Expected value
e	2.71828...
F	System dynamics matrix (continuous-time system)
$\underline{f}$	Nonlinear functions for equations of motion
G	Control effects matrix (continuous-time system)
g	Gravitational acceleration
H	• Observation matrix
	• Measurement matrix
I	Identity matrix
J	Scalar cost functional
K	• Type 0 optimal gains
	• Kalman filter gains
L	• Disturbance effects matrix (continuous-time system)
	• Roll moment
M	State and control weighting matrix
N	• State, control, and control weighting matrix
	• Yaw moment
P	• Riccati equation solution
	• State covariance matrix
p	Roll rate
Q	• State weighting matrix
	• Disturbance covariance matrix
q	Pitch rate
R	• Control weighting matrix
	• Control rate weighting matrix
	• Measurement error covariance matrix
r	Yaw rate
S	Estimation error weighting matrix
S_{11}	Steady-state state vector mapping matrix
S_{12}	Steady-state state vector mapping matrix

Variables	Description
S_{21}	Steady-state control vector mapping matrix
S_{22}	Steady-state control vector mapping matrix
s	Laplace transform variable
T	Time interval
t	Time
u	x-axis velocity
$\underline{u}$	Control vector
V	Total velocity
v	y-axis velocity
$\underline{v}$	Random noise vector
W	Disturbance covariance matrix
w	z-axis velocity
$\underline{w}$	Disturbance vector
$\underline{x}$	State vector
Y	Aerodynamic force along the y-axis
$\underline{y}$	Command vector
z	Tustin transform variable
$\underline{z}$	Measurement vector

Variables (Greek)	
β	Sideslip angle
Γ	Control effects matrix (discrete-time system)
γ	Vertical flight path angle
δA	Aileron deflection
δE	Elevator deflection
δF	Flap deflection
δR	Rudder deflection
δSF	Side-force panel deflection
δT	Throttle deflection
ζ	Damping ratio
θ	Pitch attitude angle
Λ	Disturbance effects matrix (discrete-time system)
λ	Eigenvalue
Φ	State-transition matrix (discrete-time system)
ϕ	Roll attitude angle

Variables (Greek)	Description
ψ	Yaw attitude angle
ω	Natural frequency

Subscripts

C	Continuous time index
CL	Closed-loop
D	Discrete-time index
DR	Dutch roll
d	Desired value
F	Fast mode dynamics
k	Sampling instant index
o	Nominal value
p	Sensitivity to roll rate
R	Rolling convergence
r	Sensitivity to yaw rate
S	• Spiral mode • Slow mode dynamics
β	Sensitivity to sideslip angle
δA	Sensitivity to aileron deflection
δR	Sensitivity to rudder deflection
∞	Steady-state value

Punctuation

$(\dot{\ })$	Derivative of quantity with respect to time
$(\underline{\ })$	Vector quantity
$\partial(\ )/\partial(\ )$	Partial derivative of one variable with respect to another
$\Delta(\ )$	Perturbation variable
$(\ )^*$	Steady-state value
$(\ )^T$	Transpose of a vector or matrix
$(\ )^{-1}$	Inverse of a matrix
$(\tilde{\ })$	Error quantity
$(\hat{\ })$	• Discrete-time weighting matrix • Estimate
$(\ )'$	Augmented or reduced-order system

Punctuation	Description
(-)	Estimate made prior to measurement
(+)	Estimate updated with measurement

Acronyms	
A/D	Analog to digital
AFCS	Automatic flight control system
APL	A Programming Language
ASCII	American Standard Code For Information Interchange
CAS	Command augmentation system
CCV	Control configured vehicle
CDU	Control display unit
CPU	Central processing unit
D/A	Digital to analog
DFCS	Digital flight control system
FCCU	Flight control computer unit
FCLP	Field carrier landing practice
FCS	Flight control system
FRL	Flight Research Laboratory
HQR	Handling qualities ratings
IAS	Indicated airspeed
I/O	Input/output
KIAS	Knots, indicated airspeed
Micro-DFCS	Microprocessor-based digital flight control system
MSL	Mean sea level
NATC	Naval Air Test Center
PROM	Programmable read-only memory
RAM	Random access memory
RF	Radio frequency
SBC	Single board computer
sps	Samples per second
VRA	Variable-response research aircraft
VTOL	Vertical takeoff and landing

1. INTRODUCTION

Future high performance aircraft will require some form of command or stability augmentation to meet handling qualities requirements while achieving performance objectives. Reasons for such systems include the relaxed static stability and increased pilot workloads inherent in future high-performance aircraft. Flight control technologies which promote the development of complex and reliable control systems are therefore essential to continued successful progress in aircraft development.

Modern control theory and digital microprocessors can be expected to play complementary roles in these developments; they provide both the method for designing complex control structures and the means for implementing them in flight. Modern control theory makes use of state space, time domain, and optimal control concepts, as well as frequency domain methods (1). Relying heavily on matrix theory and linear algebra, modern control uses high-speed digital computers to generate gains for complex control structures. It is the tremendous computational capability of digital computers which allows these complex control laws to be put into practice. Recent developments in large-scale integrated circuit technology have provided us with microprocessor-based computers that contain much of the computational ability of larger computers, but with significant reductions in size and cost. Together, these technologies form an attractive approach to digital flight control, but both must be proven in flight as a logical step to acceptance.

This report presents an experimental program designed to study the application of modern control theory to aircraft control and the use of microprocessors in performing the control computations. Lateral-directional control laws resulting in two-input/two-output command modes based on Type 0 and Type 1 structures are formulated. The control laws are coded for use by the microprocessor-based digital flight control system (Micro-DFCS) installed in a research aircraft, and actual flight tests are conducted.

1.1 THE NATURE OF DIGITAL FLIGHT CONTROL

It is becoming increasingly apparent that digital implementation of control logic is necessary to realize the full potential of flight control. Analog logic can perform the basic functions; however, as the requirements imposed on the flight control system increase, the control and monitoring functions are more effectively accomplished with digital processors. Advantages afforded by digitally mechanized flight control systems include the following:

- Easy implementation of advanced control laws
- Flexibility in adding or changing functions
- Ability to schedule gains according to flight condition
- Repeatability of performance
- System integration and hardware economy
- Increased reliability
- Potential for future growth

The first two advantages can be attributed directly to the digital computer's computational ability and flexibility. The normal instruction set of a digital computer allows routine performance of many mathematical operations that would cause severe hardware problems in an equivalent analog system. Mathematically complex control algorithms that would tax an analog system can be performed routinely by a digital computer. Similarly, the software implementation of control algorithms provides much more design flexibility than does analog hardware implementation. Once the digital system hardware is implemented--that is, once the necessary interfaces between pilot command, aircraft sensors, surface actuators, and the computer itself are implemented--all that is required to alter a control law or to add a new mode of operation is a program change. While a program change is not necessarily easier than a hardware change, the logistics involved are much less painful. In the long run, this will benefit not only the airframe manufacturer and equipment suppliers during the development program, but the user as well, as field modifications will be easier to accomplish [2].

The third advantage is a result of the digital computer's conditional logic. Because the control laws are derived with respect to a given flight condition, fixed gains may not be acceptable everywhere in the flight envelope. The digital computer can accept inputs from the sensors, evaluate the flight condition, and adapt to the changing environment by choosing new gains from a table in memory or by choosing an entirely different mode of operation.

The digital computer provides more repeatable performance than do analog systems [3]. One reason is that the digital computer is less sensitive to power supply variations than are analog systems, i.e., computations are not altered by voltage or current fluctuations. Digital computations are not subject to accumulation of null offsets or gain and time constant tolerances as are analog signal paths; roundoff and truncation provide similar error in the digital system, though at a hopefully lower level of significance. The digital computer also significantly reduces the number of separate components through system integration.

Perhaps the greatest potential improvement in flight control technology offered by digital systems is increased reliability through redundancy and built-in test logic. The conditional logic of a digital system allows much more comprehensive built-in test capability without additional hardware expenditures. A typical analog built-in test system with 85 to 95 percent test coverage requires circuitry that amounts to 20 or 25 percent of the total system hardware, while in an equivalent system mechanized digitally, test functions account for 1 to 4 percent of the total system hardware [4]. The digital computer allows more effective redundancy management through signal voting, and it can reorganize itself to accommodate system failures. The ability of the computer to integrate functions reduces the number of interfaces, which in turn provides better in-flight testing, easier fault isolation, and simplified maintenance.

While improvements in analog systems continue to be made, improvements in digital systems are occurring at a much greater rate. This is

especially true in the case of large-scale integrated circuit technology, where advancements in design and manufacturing technology allow increasingly complex functions to be accomplished with significant hardware reductions. Reliable, inexpensive single-board computers capable of performing the math, sequencing, and input/output operations required of a digital flight control system (DFCS) will provide sizable reductions in the cost, size, weight, and power dissipation of flight control systems. These improvements, along with improvements in the computational speed and word length of microprocessors, have provided us with microcomputers with much of the computational ability of a large computer. Based on these technologies and on the advantages presented herein, digital flight control systems will allow more effective implementation of advanced control concepts than will analog systems.

1.2 PREVIOUS RESEARCH IN DIGITAL FLIGHT CONTROL

There have been several actual flight investigations of digital flight control systems in recent years (There have been important theoretical digital control developments as well; these will be referenced in the chapter on control law development.). The most recent of these investigations have differed from the earlier applications in the methodologies employed. The areas of major differences include the types of computers used to implement the control systems, the complexity of the control functions attempted, and the methods of obtaining sampled-data control laws, whether by digitizing continuous-time control laws or by designing in the discrete-time domain. Despite the differences in approach, however, the results from these investigations seem to validate the advantages to be gained through digital flight control. [3], [4]

The first applications of digital technology to flight control involve digital implementation of the basic autopilot functions. Reference [5] documents one of the first flight tests of a digital autopilot, which featured triple redundancy, sensor voting, and failure detection based on a voter monitor system. References [6] and [7] document similar applications of digital flight control. The major conclusions drawn from these

studies was that improved monitoring and fault isolation capabilities of digital systems offered great promises for improvement in maintenance management.

These early flight investigations also provided a favorable outlook for digital control systems; they did not, however, test the advanced flight control functions that will be required of future high performance aircraft. Since then, several major research efforts have been undertaken to design and implement advanced control laws for command and stability augmentation of high performance aircraft.

Reference [8] documents the development of the digital automatic flight control system for the SAAB JA-37 aircraft. The specific design objectives were presented as the following:

- Prove that a digital automatic flight control system (AFCS) can provide performance which is equivalent to an analog AFCS; and
- Identify any potential problems that could affect the final development and production of the digital AFCS for the JA-37.

The digital control laws were obtained by digitizing the existing command augmentation system (CAS) control laws and were tested against analog control by side-by-side execution of identical tests under identical flight conditions. While the tests showed that the two systems provided identical command response, they uncovered several problem areas in the digital mechanization. It was discovered that the servos responded to the quantization noise present in the output signals, and that disengagement of the flight control system occurred, partially due to the error build-up between samples. These problems required only minor adjustments: a filter on the servo command signals to eliminate quantization noise and a minor program change to minimize the error build-up. This program provided valuable insight into the nature of digital flight control systems.

References [9], [10], and [11] present a comprehensive investigation of digital flight control using the A-7D aircraft, in which the aircraft's stability and command augmentation functions, plus multimode functions tailored to specific mission tasks, are implemented digitally. The

objectives given include:

- To determine if the standard A-7D stability and command augmentation systems had been duplicated by the DFCS; and
- To provide a technology base for the future development of digital and multimode flight control functions.

The results showed that the DFCS duplicated the analog system with one exception: the phase lag introduced by sampling increased the DFCS susceptibility to limit cycles and should be accounted for in the design process. The ability to make program changes rather than hardware changes is reported to be a definite asset to the flight test phase of the program.

Whereas the emphasis in these programs was directed towards the design of digital flight control systems for aircraft, several other studies have been conducted whose major emphasis was placed on the development of advanced flight control laws for implementation in digital systems. References [12], [13], and [14] describe NASA's advanced control law program for the F-8 digital fly-by-wire aircraft. Broad objectives of the program included:

- To provide technology required for implementing advanced, reliable digital fly-by-wire flight control systems; and
- To investigate and promote advanced control laws for flight experimentation.

A more specific goal of the investigation was to explore the use of modern control design methodology to achieve the desired performance results, with emphasis on control configured vehicle (CCV) benefits. The control law design procedures presented are based on linear-quadratic regulator theory, and provide for design in either the continuous-time or discrete-time domains. Results of these investigations include the following:

- Both a pitch CAS and lateral-directional CAS can achieve conventional handling qualities in statically unstable airframes. Using advanced control concepts, acceptable handling qualities can be achieved in airframes designed for efficiency rather than unaugmented handling characteristics.
- Conventional autopilot modes are completely compatible with inner loops designed with optimal control methods.

- Application of the quadratic procedure is an iterative process of choosing responses and weighting matrices. Their choice is expedited by the designer's past experience and his understanding of the control problem. The procedure does not replace classical techniques but is a powerful design aid.

In addition, several conclusions are drawn with respect to digital control:

- Computational requirements of adaptive control and the computational ability of present day digital flight computers are compatible.
- Concepts of adaptation to system failures appear to offer a means whereby increased safety of flight or reduced levels of hardware redundancy can be achieved.

Reference [15] presents guidance and control aspects of NASA's Vertical Takeoff and Landing (VTOL) Approach and Landing Technology Program; its objectives include developing the technology base for guidance and control requirements for future VTOL aircraft. Significant features of the VTOL digital control design processes include the design of discrete-time proportional-integral controllers to meet continuous-time specifications and evaluation of the control system response. The evaluation of the optimal control laws designed resulted in the following observations and conclusions:

- The linear-optimal control laws correspond to "classical" control laws in their use of proportional-integral compensation, gain scheduling, and linear feedback/airspeed loops.
- Linear-optimal control laws can operate at lower sampling rates as a result of being designed directly in the discrete-time domain and are designed with less reliance on the designer's intuition than equivalent classical control laws.
- A principal advantage of optimal design techniques is that the necessary control structure is visible early in the design process; all reasonable state-control paths are identified, allowing the designer to evaluate the relative importance of each path and to eliminate those which contribute little to system performance.

These advanced concepts of digital flight control system design and control law development have been combined with the advanced concept of the CCV in the German CCV-F104G program [16, 17]. The objectives of this program are:

- Development of an advanced CCV-flight control system (FCS); and
- Investigation of FCS performance and demonstration of handling qualitites in the complete flight envelope with up to twenty percent negative static margin.

The control laws to be implemented in the CCV-FCS were designed directly in the discrete-time domain using linear-optimal control theory for multi-variable systems, resulting in a sampling rate of 16 samples per second (sps). While the modifications intended to destabilize the F104G to test the CCV concept have yet to be demonstrated, the superior flight mechanical performance of the CCV-FCS has been compared with that of the basic F104G on the basis of simulator results. These simulations revealed the following:

- Significant improvement in dutch roll and short period characteristics in the CCV-FCS;
- Good turn coordination with the CCV-FCS;
- Smoother roll response with the CCV-FCS,
- The augmented CCV had a much higher maximum roll rate than the basic airplane during high-'g' maneuvers;
- The augmented CCV had a slower initial response due to the slow sampling rate; and
- The MIL-F-8785B [18] was not a satisfactory guideline for the design, as it was not written for aircraft with complex fly-by-wire control systems.

Test flights to date have tested the CCV-FCS only in the open-loop mode, so direct validation of the closed-loop simulations cannot be made. Preliminary assessments of the design process have, however, been made from initial flights. These include the following:

- The digital system provides more flexibility than analog systems, but care must be taken since the word length of the A/D and D/A converters do not match the computer word length. The use of floating point arithmetic is recommended.

- The resulting control system required less hardware and fewer interfaces than an equivalent analog design.

The German CCV-F104G program has shown modern control theory and digital control to be valuable tools in the design of flight control systems for next-generation aircraft. The application of microprocessors to aircraft flight control, however, has yet to be sufficiently demonstrated; to date, only one aircraft has flown with a microprocessor-based digital flight control system as a primary method of control.

In 1978, Princeton University's Flight Research Laboratory (FRL), under contract to the Office of Naval Research, undertook research on the development of a Micro-DFCS [19]. Specifically, the objectives of the program were as follows:

- To successfully demonstrate Princeton University's Variable-Response Research Aircraft Fly-by-Wire system augmented with the Micro-DFCS.
- To provide results for the investigation of optimal control laws in flight.
- To provide experimental evidence for sampling-rate requirements.

The flight control program implemented, entitled CAS-1, featured single pilot input (longitudinal stick), a single control output (elevator displacement), and three command modes: a direct mode, pitch rate command, and normal acceleration command. The program was highly successful, with the major results summarized below:

- Commercially available microcomputer equipment provides substantial capability for conducting advanced research in digital flight control.
- Step responses obtained from the digital model, analog simulation, and flight test results show that major response features are not affected by sampling rate. This verifies that the lag associated with sampling is accounted for in the design process.
- The pilot is not aware of the sampled nature of the control system at a sampling rate of 10 sps. No performance degradation is noted in the pitch rate mode down to a rate of 7 sps. In the direct mode, a sampling rate of 3 sps was found to be

acceptable in the landing flare, but a minimum of 10 sps is desired for the short final segment of the approach.

In summary, a Micro-DFCS, using modern control theory, was found to be a highly satisfactory method of implementing digital flight control.

These examples (there may be others not cited here) have traced the development of digital flight control. Improvements in technology have allowed microprocessors to implement the control functions once limited to general purpose digital computers. Similarly, control functions implemented in a DFCS have grown in complexity from basic autopilot functions to stabilization of Control-Configured Vehicles. Modern control theory has been shown to be an effective basis for designing advanced control laws, but several questions remain to be answered. These questions include the control law structures to be implemented, the effects of the sampling rate on closed-loop control, the control law disturbance response and sensitivity to parameter variations, coupling effects, effects of time delays introduced by sampling, and others. While technology continues to dictate the direction DFCS hardware structures will take, the answers to these questions remain a fundamental goal of digital flight control research.

1.3 RESEARCH OBJECTIVES AND SUMMARY OF MAJOR RESULTS

Specific objectives of this investigation are defined as the following:

- To develop design and analysis methodologies for advanced lateral-directional CAS control laws, and, ultimately, to demonstrate their operation in flight;
- To develop "equivalent" Type 0 and Type 1 command structures, and to demonstrate the characteristics of each under less than optimal conditions; and
- To determine and provide experimental evidence on the effects of sampling rate and cost function weighting factors on the closed-loop aircraft dynamics.

The ultimate goal of this investigation is to demonstrate, in flight, a digital command augmentation system designed using modern control theory and implemented using microprocessor technology. This goal can only be achieved, however, if design and analysis tools which allow advanced control concepts to be put into practive are used. Type 0 controllers with control rate restraint and equivalent Type 1 controllers for lateral-directional dynamics are developed and implemented in the Micro-DFCS. Of special interest in this investigation is the reaction of these controllers to less than ideal conditions. Though the Type 0 and Type 1 control laws provide nearly identical command responses, the two structures do not provide the same response to disturbances, and command responses are different when the aircraft model used in the design and the actual aircraft are mismatched. These differences are investigated.

The effects of varying the sampling rate are examined with a two-fold purpose in mind. One is to verify that the sampled-data regulator theory takes into account the time interval and provides identical command response at all sampling rates. The second purpose is to determine the effects of lower sampling rates on the closed-loop system, especially with regard to pilot opinions of handling qualities and response characteristics. Finally, the use of various weighting factors is examined to determine their utility in the design process and in altering the closed-loop aircraft response characteristics.

Flight verification of the control laws derived in this investigation was conducted at Princeton University's FRL with the Variable-Response Research Aircraft (VRA). For the testing of the lateral-directional control laws, longitudinal response was fixed at satisfactory levels to allow the evaluation pilot to concentrate on lateral-directional criteria. Qualitative and quantitative data were collected with the Micro-DFCS operating using both Type 0 control laws with rate restraint and Type 1 control laws. All control laws implemented in the Micro-DFCS treated lateral center stick motions as roll rate commands, while the foot pedals commanded either sideslip angle or lateral acceleration. An alternate form of the Type 0 control law in which the foot pedal commands yaw rate was

developed late in the program and was not implemented in the Micro-DFCS, although it was simulated using the digital computer.

The control law evaluation tests included tracking tasks at altitude and step responses to pilot commands. Telemetry records and pilot opinions of the aircraft responses were examined, and the control laws were evaluated using the military flying qualities specification [18] as a guide.

Many results of this investigation are presented throughout the body of this text; a few of the major results are summarized here. The step response traces from the digital model, hybrid simulation, and flight tests show that the major command response features are not affected by the sampling rate when sampled-data regulator theory is used. The Type 0 command structure with control rate restraint using a difference approximation to characterize the control derivative provides improved command response, lateral-directional decoupling, and disturbance response over the open-loop VRA dynamics at all sampling rates; the initial response of the controller, however, cannot be altered in the design process. An alternate form of this control structure, one which uses the Tustin transform to characterize the control derivative in the discrete-time domain, is developed; this makes the initial command response dependent upon the linear optimal gains. The Type 1 structure proves superior to the Type 0 controller when the linear model used in the design and the actual aircraft dynamics were mismatched; the Type 1 system, however, is found to be unduly sensitive to disturbance inputs and measurement noise, indicating the need for state estimation or control law restructuring. The Micro-DFCS used in this investigation is capable of implementing advanced concepts of command and stability augmentation at the sampling rate afforded through the use of sampled-data regulator theory.

1.4 ORGANIZATION OF REPORT

This report is divided into five chapters and four appendices. Chapter 2 presents the development of the control laws using linear-optimal regulator theory. The linear model of the VRA's lateral-directional

dynamics is presented, along with the responses of the various control laws as predicted analytically. Chapter 3 shows how the control laws are actually implemented in the Micro-DFCS. The flight control computer unit is described, as well as the operational control program. Hybrid simulation of the Micro-DFCS is conducted on an analog computer, and the results are compared with those predicted in Chapter 2.

Chapter 4 presents the actual flight testing of the Micro-DFCS. Specific flight test objectives are presented, the flight test systems and procedures are described, and flight test results are given. Chapter 5 presents the conclusions drawn from the investigation and gives recommendations towards areas of future research.

Appendices A and B present the derivations of the Type 0 regulator with rate restraint using the Tustin transform and the Type 1 regulator for commands whose integral appears in the state vector, respectively. Appendix C describes all of the APL computer programs used in this investigation, while Appendix D describes all the routines of the Micro-DFCS control program, entitled CAS-4. Appendix E describes the research system used in this investigation, including the VRA and ground station.

2. DIGITAL CONTROL LAW DEVELOPMENT

This chapter presents the design objectives, optimal control theory, and analytical results for the lateral-directional CAS implemented in the Micro-DFCS. Type 0 control laws with control rate restraint and equivalent Type 1 control laws are developed using a fourth-order model of lateral-directional dynamics for the VRA. The development of a sideslip-angle estimator is also presented.

2.1 DESIGN OBJECTIVES

The primary design objectives of the lateral-directional CAS are to provide improved command response and to provide steady-state decoupling of lateral and directional dynamics. Evaluation of the resulting control laws is accomplished using conventional step response criteria, computer generated responses, and the Military Specifications on Flying Qualities [18].

Improved command response is specified for the resulting control laws using conventional step response figures of merit, rise time and percent overshoot. Control laws with various response characteristics will be designed with the minimum acceptable performance criteria being those set forth in the Military Specifications. While there are no step response criteria for rudder inputs, roll response criteria are set forth. Specifically, Level 1 requirements for a Class I aircraft in cruise are such that a bank angle of 60 degrees must be attainable in 1.7 seconds, with the roll rate at the first response minimum being not less than 25 percent of the roll rate at the first response peak. Additional roll rate oscillation limitations, as indicated by the parameter p_{OSC}/p_{AV}, are shown in Fig. 2-1. The unaugmented VRA's characteristics are marked and are seen to meet Level 1 requirements.

State decoupling is evaluated using both step responses and the Military Specifications. Computer generated responses provide a measure of the degree of coupling, while adverse yaw limits are set forth in

Reference 18. Specifically, the ratio of sideslip angle to the parameter k (as defined therein) shall be less than 10 degrees, with the roll command held fixed until the bank angle has reached 90 degrees. Additionally, sideslip excursion requirements for small inputs are given in Fig. 2-2, where the maximum sideslip angle is that attained within 2 seconds of the command. Again, the unaugmented VRA is shown to meet Level 1 requirements.

In its unaugmented state, the VRA provides a highly stable base from which to conduct research. As such, stability augmentation is not a necessity, and great changes in the dynamic characteristics cannot be major design goals. Comparison and evaluation of the various control laws still can be accomplished, however, using the criteria presented above. This demonstrates the utility of control laws developed herein in providing stability augmentation and in altering the VRA's dynamic response characteristics.

2.2 LINEAR MODEL OF LATERAL-DIRECTIONAL DYNAMICS

Although the dynamics of aircraft motion are basically nonlinear, linear models have shown great utility in stability-and-control analysis, and they provide the basis for this investigation.

Neglecting disturbance inputs, the nonlinear equations governing vehicle dynamics can be expressed as the vector differential equation

$$\dot{\underline{x}}(t) = \underline{f}[\underline{x}(t),\underline{u}(t)] \tag{2.2-1}$$

The state vector, generally of length n, contains three components each of translational rate, angular rate, and attitude,

$$\underline{x}^T = [u \ v \ w \ p \ q \ r \ \phi \ \theta \ \psi] \tag{2.2-2}$$

where (u,v,w) are body-axis velocities, (p,q,r) are body-axis rotational rates, and (ϕ,θ,ψ) are the Euler angles of the aircraft's attitude in an inertial frame. The control vector, of length m, includes elevator, throttle, flap, rudder, aileron, and side force control surface deflections,

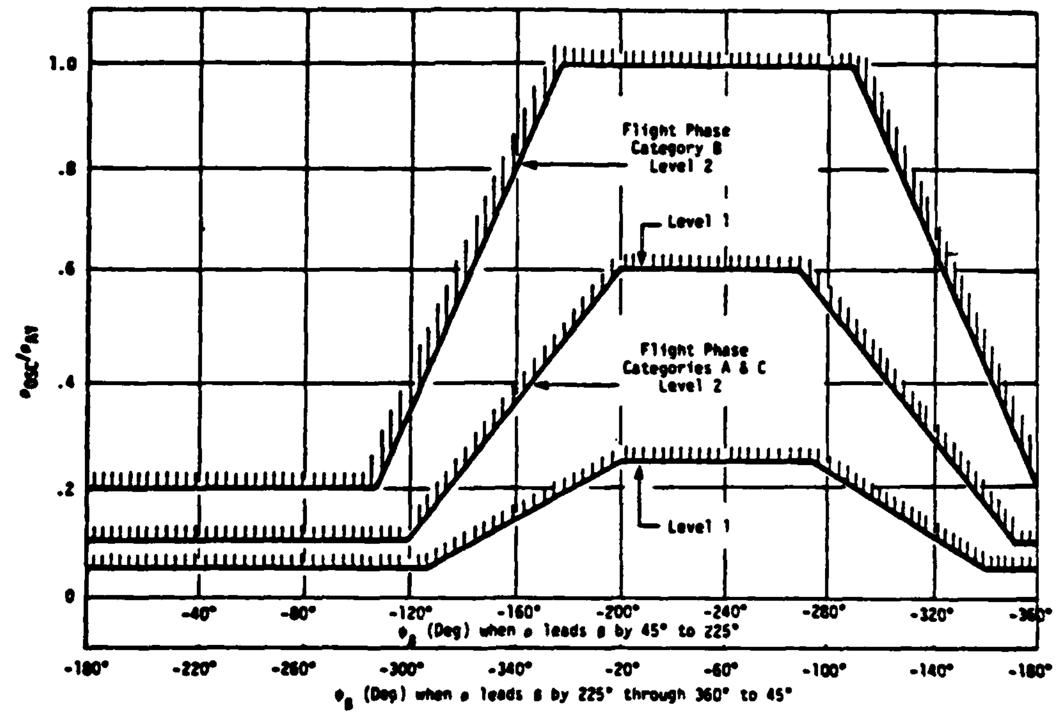

Figure 2-1. Roll Rate Oscillation Limitations.

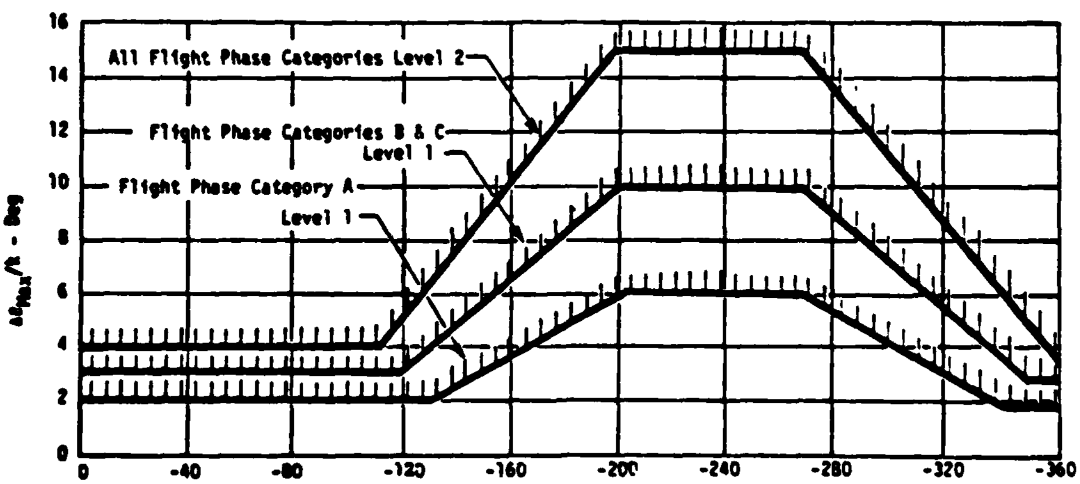

Figure 2-2. Sideslip Angle Excursion Limitations.

$$\underline{u}^T = [\delta E \; \delta T \; \delta F \; \delta R \; \delta A \; \delta SF] \tag{2.2-3}$$

The reduced-order state vector which contains rolling and yawing dynamics of aircraft motion, referred to as "lateral" and "directional" respectively, is

$$\underline{x}^T = [v \; p \; r \; \phi] \tag{2.2-4}$$

Because side velocity is difficult to measure, it is replaced in the state vector by sideslip angle. Conventionally, the state vector is reordered to allow partitioning of the directional and lateral variables, as

$$\underline{x}^T = [r \; \beta \; p \; \phi] \tag{2.2-5}$$

It specifically includes yaw rate, sideslip angle, roll rate, and roll angle. The lateral-directional control vector includes rudder and aileron control deflections,

$$\underline{u}^T = [\delta R \; \delta A] \tag{2.2-6}$$

The total state and control can be divided into nominal and perturbation components,

$$\underline{x}(t) = \underline{x}_o(t) + \Delta\underline{x}(t) \tag{2.2-7}$$

$$\underline{u}(t) = \underline{u}_o(t) + \Delta\underline{u}(t) \tag{2.2-8}$$

A first-order Taylor series expansion of Eq. 2.2-1, using Eq. 2.2-7 and 2.2-8, leads to a nonlinear differential equation in the nominal component,

$$\dot{\underline{x}}_o(t) = \underline{f}[\underline{x}_o(t), \underline{u}_o(t)] \tag{2.2-9}$$

and a linear vector differential equation in the perturbation component,

$$\Delta\dot{\underline{x}}(t) = F(t)\Delta\underline{x}(t) + G(t)\Delta\underline{u}(t) \tag{2.2-10}$$

The system dynamics matrix, F(t), is given by

$$F(t) = \frac{\partial}{\partial \underline{x}} \underline{f}[\underline{x}_o(t), \underline{u}_o(t)] \tag{2.2-11}$$

and the control effects matrix, G(t), by

$$G(t) = \frac{\partial}{\partial \underline{u}} \underline{f}[\underline{x}_o(t), \underline{u}_o(t)] \tag{2.2-12}$$

Stability derivatives, inertial effects, and kinematic relationships are contained in F,

$$F = \begin{bmatrix} N_r & N_\beta & N_p & 0 \\ (Y_r/V-1) & Y_\beta/V & Y_p/V & g/V \cos\gamma \\ L_r & L_\beta & L_p & 0 \\ 0 & 0 & 1 & 0 \end{bmatrix} \tag{2.2-13}$$

where angles and angular rates are measured in stability axes and in units of radians and radians per second. The subscripted capital letters represent the sensitivities of the specific forces and moments to the state variables, g is the gravitational acceleration, γ is the flight path angle, and V is the nominal aircraft velocity. The control effect matrix, G, contains control derivatives,

$$G = \begin{bmatrix} N_{\delta R} & N_{\delta A} \\ Y_{\delta R}/V & Y_{\delta A}/V \\ L_{\delta R} & L_{\delta A} \\ 0 & 0 \end{bmatrix} \tag{2.2-14}$$

where the subscripted capital letters represent the sensitivities of the forces and moments to control surface deflections. With the directional variables defined as r, β, and δR, and the lateral variables as

p, ϕ, and δ_A, both F and G can be partitioned as

$$\left[\begin{array}{c|c} \text{Directional Effects} & \text{Lateral-to-Directional Coupling} \\ \hline \text{Directional-to-Lateral Coupling} & \text{Lateral Effects} \end{array}\right]$$

where the lateral-directional coupling is indicated by the magnitude of the off-diagonal blocks.

While the calculation of the nominal states and controls remains a nonlinear problem, linear control laws still can be designed based on certain observations and assumptions. It can be see that F(t) and G(t) are explicit functions of flight conditions rather than time; hence, control laws can be designed with respect to specific flight conditions rather than a specific flight profile. By scheduling gains throughout the flight profile as functions of the flight condition, control laws based on a linear, time-invariant model of aircraft dynamics,

$$\Delta\dot{\underline{x}}(t) = F\Delta\underline{x}(t) + G\Delta\underline{u}(t) \qquad (2.2\text{-}15)$$

can be utilized [15].

2.3 LINEAR-QUADRATIC REGULATORS

Using linear, time-invariant models of aircraft dynamics and linear-quadratic regulator theory, discrete-time control laws are derived. Advanced control structures, Type 0 controllers with control rate restraint and equivalent Type 1 controllers, with non-zero set points, are designed as extensions of the basic linear-quadratic regulator problem [20].

2.3.1 The Basic Regulator

The basic linear-quadratic regulator problem can be stated as follows: determine the control, $\underline{u}(t)$, which minimizes the quadratic cost function,

$$J_c = \int_0^{\infty} \left[\Delta\underline{x}^T(t)\, Q\, \Delta\underline{x}(t) + \Delta\underline{u}^T(t)\, R\, \Delta\underline{u}(t) \right] dt \tag{2.3-1}$$

subject to the dynamic constraint imposed by the linear differential equations of motion (Eq. 2.2-15);

$$\Delta\dot{\underline{x}}(t) = F\Delta\underline{x}(t) + G\Delta\underline{u}(t)$$

Matrices Q and R weight the perturbations in state and control, respectively. The solution to this optimization problem is a linear control law of the form

$$\Delta\underline{u}(t) = -K\Delta\underline{x}(t) \tag{2.3-2}$$

where K is the optimal gain matrix.

The goal here, however, is not to derive continuous-time optimal control laws: it is to derive a discrete-time control law which drives the system along a trajectory that is as close as possible to that obtained using the above continuous-time control law. These discrete-time control laws are derived directly in the discrete-time domain using sampled-data regulator theory. The resulting controller will drive the continuous-time system using piecewise-constant inputs that change only at the sampling instant (zero-order hold).

The sampled data regulator problem is identical to the linear-quadratic regulator problem: that is, to determine the control which minimizes the discrete-time cost function subject to the dynamic constraint imposed by the equations of motion. Because the control changes only at discrete instances, however, the discrete-time cost function is a summation rather than an integral,

$$J_D = \sum_{k=0}^{\infty} \left\{ [\underline{\Delta x}^T \; \underline{\Delta u}^T]_K \begin{bmatrix} \hat{Q} & \hat{M} \\ \hat{M}^T & \hat{R} \end{bmatrix} \begin{bmatrix} \underline{\Delta x} \\ \underline{\Delta u} \end{bmatrix} \right\} \tag{2.3-3}$$

The dynamic constraint imposed by the equations of motion becomes the discrete-time equivalent of equation (2.2-15),

$$\underline{\Delta x}_{K+1} = \Phi \underline{\Delta x}_K + \Gamma \underline{\Delta u}_K \tag{2.3-4}$$

where Φ, the state transition matrix, and Γ, the discrete control effect matrix, are given by,

$$\Phi = e^{F\Delta t} = I + F\Delta t + \frac{(F\Delta t)^2}{2} + \frac{(F\Delta t)^3}{6} + \ldots \tag{2.3-5}$$

$$\Gamma = \Phi[F^{-1} (I - \Phi^{-1})]G \tag{2.3-6}$$

and Δt is the sampling interval.

The goal of sampled-data regulator theory is to choose discrete-time weighting matrices, $\hat{Q}$, $\hat{M}$, and $\hat{R}$ such that the control which minimizes the discrete-time cost function minimizes the continuous-time cost function as well, thereby penalizing errors in the states and controls continuously in time and driving the system along a trajectory nearly identical to that obtained by the continuous-time controller. The method of choosing these matrices is presented in Reference [21]. Decomposing the continuous-time cost function into the sum of N integrals and equating it with the discrete-time cost function, the following relationships are derived:

$$\hat{Q} = \int_0^{\Delta t} \Phi^T(t) \, Q\Phi(t) \, dt \tag{2.3-7}$$

$$\hat{M} = \int_0^{\Delta t} \Phi^T(t) \, Q\Phi(t) \, dt \tag{2.3-8}$$

$$\hat{R} = \int_0^{\Delta t} [R + \Gamma^T(t) \, Q \, \Gamma(t)] \, dt \tag{2.3-9}$$

where Q is positive semi-definite and R is positive definite.

Provided that the system is completely controllable and completely observable [22], and using these relationships for the discrete-time weighting matrices, the resulting discrete-time optimal control law is given as

$$\Delta \underline{u}_K = -K \Delta \underline{x}_K \tag{2.3-10}$$

where, K, the optimal gain matrix, is given by

$$K = (\hat{R} + \Gamma^T P \Gamma)^{-1} (\Gamma^T P \Phi + \hat{M}^T) \tag{2.3-11}$$

and P is the positive-definite solution of the discrete-time matrix Riccati equation,

$$P = \Phi^T P \Phi - (\Gamma^T P \Phi + \hat{M}^T)^T (\hat{R} + \Gamma^T P \Gamma)^{-1} (\Gamma^T P \Phi + \hat{M}^T) + \hat{Q} \tag{2.3-12}$$

The advantages of designing control laws in this manner is clear: weighting matrices can be specified for the continuous-time cost function based on an intuitive understanding of the continuous-time system and of the trade-offs between weightings of state and control for a continuous-time problem, rather than trying to specify discrete-time weightings directly.

Of particular interest in the design of sampled-data regulators is the determination of the sampling rate required to drive a continuous-time system. Past solutions to this problem used a rule of thumb, based on Shannon's Sampling Theorem, that the sampling frequency be 10 times faster than the highest frequency present in the waveform being sampled. In practice, however, much lower frequencies may be used [23].

The linear differential state equation (Eq. 2.2-10) has the solution

$$\Delta \underline{x}(t) = e^{F(t-t_o)} \Delta \underline{x}(t_o) + \int_{t_o}^{t} e^{F(t-\tau)} G \Delta \underline{u}(\tau)\, d\tau \tag{2.3-13}$$

The only unknown is $\Delta \underline{x}(t_o)$, and $\Delta \underline{u}(t)$ is arbitrary. Assuming that F and G are known exactly, and assuming there are no disturbance inputs to the system, one sample of $\Delta \underline{x}(t_o)$ is all that is needed to completely specify

the solution, $\Delta\underline{x}(t)$. It is because the above assumptions are not realistic situations, that is, disturbances are present and F and G are imprecisely known, that additional sampling is required to specify $\Delta\underline{x}(t)$.

Since the purpose of the linear-quadratic regulator is to maintain aircraft states within specified bounds, the sampling rate should be chosen such that such bounds are not exceeded by the error propagation while the system is running open loop (between sampling instants). Propagation of the state errors is governed by the equation,

$$\dot{P}(t) = FP(t) + P(t)F^T + W \tag{2.3-14}$$

where P is the state covariance matrix and W is the disturbance covariance matrix. Assuming that the uncertainty at the start of a sampling period is eliminated, Eq. 2.3-14 is integrated with the initial condition,

$$P(0) = 0 \tag{2.3-15}$$

After some elapsed time, one or more of the error variances will exceed the pre-determined error bounds, and this elapsed time is defined to be the maximum allowable sampling interval.

Also of particular interest is the evaluation of the closed-loop characteristics of the sampled-data regulator. Combining the linear-optimal control law (Eq. 2.3-10) and the discrete-time equation (Eq. 2.3-4) leads to

$$\Delta\underline{x}_{K+1} = (\Phi - \Gamma K)\Delta\underline{x}_K \tag{2.3-16}$$

where $(\Phi - \Gamma K)$ represents the closed-loop state transition matrix. The eigenvalues of a stable closed-loop discrete-time system lie within the unit circle: they are not easily related to the aircraft's modal characteristics by any conventional analysis techniques. This discrete-time system can, however, be mapped into the continuous-time domain, where its major characteristics can be easily identified [24]. Since a

continuous-time plant is converted to its discrete-time equivalent using a matrix exponential, a discrete-time system can be mapped into its equivalent continuous-time system using the natural logarithm of a matrix:

$$F_{CL} = \frac{1}{T} \ln \Phi_{CL} = \frac{1}{T}\{(\Phi_{CL} - I) - \frac{1}{2}(\Phi_{CL} - I)^2 + \frac{1}{3}(\Phi_{CL} - I)^3 - \dots\} \tag{2.3-17}$$

In this manner, the control laws derived using sampled-data regulator theory can be evaluated using conventional eigenvalue analysis.

This section has presented a method for designing digital control laws for a continuous-time system. The discrete-time control laws corresponding to continuous-time cost functions are derived, and Eq.2.3-17 transforms the digital result to the analog domain for conventional evaluation. This basic regulator problem can be amended easily to accommodate pilot command inputs by defining a suitable shift of coordinates.

2.3.2 Steady State Response to Command Inputs

Assuming that the pilot may command any linear combination of state and control, the discrete-time system dynamics are governed by

$$\Delta\underline{x}_{K+1} = \Phi\Delta\underline{x}_K + \Gamma\Delta\underline{u}_K \tag{2.3-18}$$

$$\Delta\underline{y}_K = H_x\Delta\underline{x}_K + H_u\Delta\underline{u}_K \tag{2.3-19}$$

where $\Delta\underline{y}$ is the output vector, and H_x and H_u are the state and control observation matrices, respectively. In response to a command input, then, the steady-state values of state and control must necessarily satisfy,

$$\Delta\underline{x}^* = \Phi\Delta\underline{x}^* + \Gamma\Delta\underline{u}^* \tag{2.3-20}$$

$$\Delta\underline{y}_d = H_x\Delta\underline{x}^* + H_u\Delta\underline{u}^* \tag{2.3-21}$$

or, equivalently,

$$\begin{bmatrix} 0 \\ \Delta \underline{y}_d \end{bmatrix} = \begin{bmatrix} (\Phi - I) & \Gamma \\ H_y & H_u \end{bmatrix} \begin{bmatrix} \Delta \underline{x}^* \\ \Delta \underline{u}^* \end{bmatrix} \tag{2.3-22}$$

where $\Delta \underline{y}_d$ is the pilot's command vector, and the star indicates steady-state values of state and control.

In cases where the inverse

$$\begin{bmatrix} (\Phi - I) & \Gamma \\ H_x & H_u \end{bmatrix}^{-1} = \begin{bmatrix} S_{11} & S_{12} \\ S_{21} & S_{22} \end{bmatrix} \tag{2.3-23}$$

exists, the desired steady-state values of state and control are uniquely specified by,

$$\Delta \underline{x}^* = S_{12}\ \Delta \underline{y}_d \tag{2.3-24}$$

$$\Delta \underline{u}^* = S_{22}\ \Delta \underline{y}_d \tag{2.3-25}$$

In cases where the state vector includes a pure integration of a pilot command variable, however, this matrix is singular and its inverse does not exist. This is true of lateral-directional dynamics, where roll angle is the pure integration of roll rate; hence,a different relationship exists between pilot command inputs and steady-state values of state and control.

In order to find this relationship, two factors must be considered: first, the roll angle state variable must be eliminated from the state vector to allow the above inverse to exist, and, second, its effects on the remaining state variables must be maintained in the equations of motion to provide an accurate description of system dynamics. These can be achieved by treating roll angle as a disturbance.

A new state vector for lateral-directional dynamics is written as

$$\Delta\underline{x}' = [\Delta r\ \Delta\beta\ \Delta p]^T \tag{2.3-26}$$

and the linear differential equations of motion which treat roll angle as a disturbance can be written as

$$\Delta\dot{\underline{x}}'(t) = F'\Delta\underline{x}'(t) + G'\Delta\underline{u}(t) + L\Delta\phi(t) \tag{2.3-27}$$

Matrices F' and G' are found by eliminating the roll angle dynamics from F and G respectively, and matrix L represents the effects of roll angle on the remaining state variables, i.e., the last column of F. By writing the system dynamics equation in this manner, roll angle has been eliminated as a state variable, yet the equations of motion are exact, in that they still include roll angle dynamics.

The discrete-time equations of motion are now written as

$$\Delta\underline{x}'_{K+1} = \Phi'\Delta\underline{x}'_K + \Gamma'\Delta\underline{u}_K + \Lambda\Delta\phi_K \tag{2.3-28}$$

where Φ and Γ are derived as before and Λ is given by

$$\Lambda = \Phi[F^{-1}(I - \Phi)^{-1}]L \tag{2.3-29}$$

The output equation is written as

$$\Delta\underline{y}_K = H'_x\ \Delta\underline{x}'_K + H_u\ \Delta\underline{u}_K \tag{2.3-30}$$

where H'_x reflects the change in the state vector. In response to pilot commands, the steady-state values of state and control must satisfy,

$$\Delta\underline{x}'^* = \Phi'\Delta\underline{x}'^* + \Gamma'\Delta\underline{u}^* + \Lambda\Gamma\phi^* \tag{2.3-31}$$

$$\Delta\underline{y}_d = H'_x\Delta\underline{x}'^* + H_u\Delta\underline{u}^* \tag{2.3-32}$$

or, equivalently,

$$\begin{bmatrix} (\Phi' - I) & \Gamma \\ H_x' & H_u \end{bmatrix} \begin{bmatrix} \Delta\underline{x}'^* \\ \Delta\underline{u}^* \end{bmatrix} = \begin{bmatrix} -\Lambda\Delta\phi^* \\ \Delta\underline{y}_d \end{bmatrix} \tag{2.3-33}$$

Now the inverse

$$\begin{bmatrix} (\Phi' - I) & \Gamma' \\ H_x & H_u \end{bmatrix}^{-1} = \begin{bmatrix} S_{11}' & S_{12}' \\ S_{21}' & S_{22}' \end{bmatrix} \tag{2.3-34}$$

does exist, and the steady-state relationships for state and control are written as

$$\Delta\underline{x}'^* = -S_{11}'\Lambda\Delta\phi^* + S_{12}'\Delta\underline{y}_d \tag{2.3-35}$$

$$\Delta\underline{u}^* = -S_{21}'\Lambda\Delta\phi^* + S_{22}'\Delta\underline{y}_d \tag{2.3-36}$$

and

$$\Delta\phi^* = \int_0^t \Delta p^*(\tau)\ d\tau \tag{2.3-37}$$

which can be approximated in the discrete-time case as

$$\Delta\phi_K^* = \sum_{K=1}^{n} p_K^*\ \Delta t \tag{2.3-38}$$

Now that the desired relationships between state and control steady-state values and pilot command inputs have been established, the desired shift of coordinates which allows for non-zero set point regulation can be achieved. Defining two new variables,

$$\Delta\underline{\tilde{x}}_K = \Delta\underline{x}_K - \Delta\underline{x}_K^* \tag{2.3-39}$$

$$\Delta\underline{\tilde{u}}_K = \Delta\underline{u}_K - \Delta\underline{u}_K^* \tag{2.3-40}$$

the linear-optimal regulator control law can be rewritten as

$$\Delta\underline{\tilde{u}}_K = -K\Delta\underline{\tilde{x}}_K \tag{2.3-41}$$

or, equivalently, as

$$\Delta\underline{u}_K = \Delta\underline{u}^*_K - K(\Delta\underline{x} - \Delta\underline{x}^*)_K \tag{2.3-42}$$

This controller regulates the system about the desired non-zero setpoint.

2.3.3 Linear-Quadratic Regulator with Rate Restraint

The basic linear-quadratic regulator provides proportional Type 0 control, in that the resulting control law contains no pure integration (or summation) of control [25] and in that the feedback term is directly proportional to the state. Proportional-integral controllers can be formed by penalizing control difference (or rate) in the cost function and by augmenting the equations of motion to include control rate dynamics.

A continuous-time cost function which penalizes control rates is defined by

$$J_C = \int_0^\infty \left\{ [\Delta\underline{\tilde{x}}^T \; \Delta\underline{\tilde{u}}^T] \, Q \begin{bmatrix} \Delta\underline{\tilde{x}} \\ \Delta\underline{\tilde{u}} \end{bmatrix} + \Delta\underline{\tilde{v}}^T R \Delta\underline{\tilde{v}} \right\} dt \tag{2.3-43}$$

where Q now weights both state and control, R weights the control rates, and $\Delta\underline{v}$ represents the control rate vector--the derivative of the control vector $\Delta\underline{u}$. While this cost function is not directly involved in the design of sampled-data systems, the weighting matrices Q and R are used to define the weighting matrices to be used in the equivalent sampled-data cost function,

$$J_C = \sum_{K=0}^{\infty} \left\{ [\Delta\underline{\tilde{x}}^T \Delta\underline{\tilde{u}}^T]_K \hat{Q} \begin{bmatrix} \Delta\underline{\tilde{x}} \\ \Delta\underline{\tilde{u}} \end{bmatrix}_K + [\Delta\underline{\tilde{x}}^T \Delta\underline{\tilde{u}}^T]_K \hat{N} \Delta\underline{\tilde{v}}_K + \Delta\underline{\tilde{v}}_K^T \hat{R} \Delta\underline{\tilde{v}}_K \right\} \tag{2.3-44}$$

The equations of motion used as the dynamic constraint for the cost function to be minimized must be augmented to allow for control rate dynamics and can be written as

$$\begin{bmatrix} \Delta\underline{\tilde{x}} \\ \Delta\underline{\tilde{u}} \end{bmatrix}_{K+1} = \begin{bmatrix} \Phi & \Gamma \\ 0 & I \end{bmatrix} \begin{bmatrix} \Delta\underline{\tilde{x}} \\ \Delta\underline{\tilde{u}} \end{bmatrix}_K + \begin{bmatrix} 0 \\ \Delta t I \end{bmatrix} \Delta\underline{\tilde{v}}_K \tag{2.3-45}$$

or, equivalently, as

$$\begin{bmatrix} \Delta\underline{\tilde{x}} \\ \Delta\underline{\tilde{u}} \end{bmatrix}_{K+1} = \Phi' \begin{bmatrix} \Delta\underline{\tilde{x}} \\ \Delta\underline{\tilde{u}} \end{bmatrix}_{K} + \Gamma' \, \Delta\underline{\tilde{v}}_K \tag{2.3-46}$$

where $\Delta\underline{\tilde{v}}_K$ represents the discrete-time equivalent of control rate. By stating the cost function to be minimized and the dynamic constraint equation in these forms, the problem reduces to the basic sampled-data regulator problem, and all of the relationships developed in the previous sections apply.

The discrete-time weighting matrices are derived from the continuous-time weighting matrices according to Equations 2.3-7 and 2.3-9, where the primed terms now apply:

$$\hat{Q} = \int_0^{\Delta t} \Phi'(t)^T \, Q \, \Phi'(t) \, dt \tag{2.3-47}$$

$$\hat{N} = \int_0^{\Delta t} \Phi'(t)^T \, Q \, \Gamma'(t) \, dt \tag{2.3-48}$$

$$\hat{R} = \int_0^{\Delta t} [R + \Gamma'(t)^T \, Q \, \Gamma'(t)] \, dt \tag{2.3-49}$$

Using these relationships, the control which minimizes the discrete-time cost function (and the continuous-time cost function) subject to the augmented dynamic constraint is given by

$$\Delta\underline{\tilde{v}}_K = -K_1 \Delta\underline{\tilde{x}}_K - K_2 \Delta\underline{\tilde{u}}_K \tag{2.3-50}$$

where the optimal discrete-time gains are defined by

$$[K_1 \;\; K_2] = (\hat{R} + I'^T p \Gamma')^{-1} \, (\Gamma' p \Phi' + \hat{N}^T) \tag{2.3-51}$$

and P is the steady-state solution to the discrete-time matrix Riccati equation:

$$P = \Phi' T p \Phi' - (\Gamma'^T p \Phi' + \hat{N}^T) \, (\hat{R} + \Gamma'^T p \Gamma')^{-1} \, (\Gamma'^T p \Phi' + \hat{N}^T) + \hat{Q} \tag{2.3-52}$$

This proportional-integral control law specifies the control rate as a linear function of both state and control; the closed-loop system dynamics, given by,

$$\begin{bmatrix} \Delta\underline{\tilde{x}} \\ \Delta\underline{\tilde{u}} \end{bmatrix}_{K+1} = (\Phi' - \Gamma' K) \begin{bmatrix} \Delta\underline{\tilde{x}} \\ \Delta\underline{\tilde{u}} \end{bmatrix}_{K} \qquad (2.3\text{-}53)$$

contain both state and control dynamics.

It is necessary to alter the form of this control law because control position, rather than control difference, is the required output. The approach that normally is taken is to use a first-difference approximation as the discrete-time equivalent of control rate,

$$\Delta\underline{\tilde{v}}_K = (\Delta\underline{\tilde{u}}_{K+1} - \Delta\underline{\tilde{u}}_K)/\Delta t \qquad (2.3\text{-}54)$$

and to write the proportional-integral control law, using this approximation, as

$$\Delta\underline{\tilde{u}}_K = (I - \Delta t K_2)\Delta\underline{\tilde{u}}_{K-1} - \Delta t K_1 \, \Delta\underline{\tilde{x}}_{K-1} \qquad (2.3\text{-}55)$$

or, equivalently, as

$$\Delta\underline{u}_K = \Delta\underline{u}^*_K + (I - \Delta t K_2)(\Delta\underline{u} - \Delta\underline{u}^*)_{K-1} - \Delta t K_1(\Delta\underline{x} - \Delta\underline{x}^*)_{K-1} \qquad (2.3\text{-}56)$$

where the steady-state values of state and control are derived using the appropriate method presented in the preceding section.

One interesting property of the control laws written in this form is that the initial system response is determined entirely by $\Delta\underline{u}^*$; the linear optimal gains and weightings have no effect on the initial response. In cases where the steady-state control position is near the equilibrium or nominal position, this drawback has no serious consequences. In other cases, where the steady-state control position is far from the nominal position, the system response may be very objectionable to the pilot: the initial control deflections will be very large,

causing large transients in the dynamic response characteristics of the system as well as severely loading the structure and control surface actuators. In these cases, a different form of the control law is desired: the method used in obtaining control position control from the control law (Eq. 2.3-50) must allow shaping of the initial response in the design process.

An alternate form of the control law which gives the desired control position output can be obtained by using transform techniques rather than the difference approximation for control rate. The commanded control rate in Eq. 2.3-50 is rewritten as

$$\Delta\underline{\tilde{v}}_K = \Delta\dot{\underline{\tilde{u}}}_K = \Delta\dot{\underline{u}}_K \tag{2.3-57}$$

since the steady-state value of control rate is zero. Taking the Laplace Transform of Eq. 2.3-50, the above substitution yields

$$(sI + K_2)\Delta\underline{u}_K(s) = -K_1\Delta\underline{\tilde{x}}_K(s) + K_2\Delta\underline{u}^*_K(s) \tag{2.3-58}$$

"Discretizing" the above equation using the Tustin Transform (see Appendix A for the complete derivation), the desired form of the control law can be expressed as,

$$\Delta\underline{u}_K = \left(\frac{2}{\Delta t} I + K_2\right)^{-1}\left[\left(\frac{2}{\Delta t} I - K_2\right)\Delta\underline{u}_{K-1} - K_1(\Delta\underline{\tilde{x}}_K - \Delta\underline{\tilde{x}}_{K-1}) + K_2(\Delta\underline{u}^*_K + \Delta\underline{u}^*_{K-1})\right] \tag{2.3-59}$$

With the control law written in this form, the initial response depends upon the desired steady-state control, $\Delta\underline{u}^*$, but it also depends upon the optimal gains K. Consequently, parameters used in the design process have an immediate effect on the resulting controller output, whereas the other form of the control law gives the same initial response regardless of the design parameters chosen.

Both forms of the linear-quadratic regulator with control rate restraint represent Type 0 proportional-integral controllers; the integrating action arises from the accumulation of past commands. They are not Type 1 controllers because the gains on the accumulated control, which

can generally be expected to be less than I, and the multiplication of several terms by Δt produces a low-pass filtering effect rather than a pure integration [26]. As such, the controllers do not null steady-state errors under all circumstances. If the actual aircraft and the design model are mismatched, the control laws will settle at the wrong values of $\Delta \underline{u}^*$ and $\Delta \underline{x}^*$. In addition, since disturbances are not modeled in the derivation of $\Delta \underline{x}^*$ and $\Delta \underline{u}^*$, there will be a finite "hangoff" error when such disturbances are present in the state measurements. Consequently, these forms of the Type 0 proportional-integral controller use integration to restrict control rates (by low-pass filtering) rather than to null steady-state error.

2.3.4 Type 1 Proportional Integral Control

An interesting property of the Type 0 proportional-integral controller derived using the difference approximation for control rate (Eq. 2.3-56) is that it can be transformed to a Type 1 controller with *nearly identical command response.* Knowledge of the system dynamics provides the method of introducing this Type 1 property.

The derivation of the Type 1 controller begins with the following transformation [23]:

$$[C_1 \quad C_2] \begin{bmatrix} (\Phi - I) & \Gamma \\ H_x & H_u \end{bmatrix} = [\Delta t K_1 \quad \Delta t K_2] \tag{2.3-60}$$

This transformation allows the desired gains for the Type 1 system, C_1 and C_2, to be calculated from the Type 0 gains, K_1 and K_2, provided the compound matrix above is non-singular. Assuming the matrix is invertible, the Type 1 gains are given by

$$C_1 = \Delta t K_1 S_{11} + \Delta t K_2 S_{21} \tag{2.3-61}$$

$$C_2 = \Delta t K_1 S_{12} + \Delta t K_2 S_{22} \tag{2.3-62}$$

with S_{11}, S_{12}, S_{21}, and S_{22} defined as in Eq. 2.3-23.

Rewriting the control law which gives Type 0 control with rate restraint (Eq. 2.3-56) using the substitutions for the optimal gains (Eq. 2.3-60) produces

$$\Delta\underline{\tilde{u}}_K - \Delta\underline{\tilde{u}}_{K-1} = -C_1[(\Phi - I)\Delta\underline{\tilde{x}}_K + \Gamma\underline{\tilde{u}}_K] - C_2(H_x\Delta\underline{\tilde{x}}_{K-1} - H_u\Delta\underline{\tilde{u}}_{K-1}) \tag{2.3-63}$$

or, equivalently,

$$\Delta\underline{\tilde{u}}_K - \Delta\underline{\tilde{u}}_{K-1} = -C_1(\Delta\underline{\tilde{x}}_K - \Delta\underline{\tilde{x}}_{K-1}) - C_2(H_x\Delta\underline{\tilde{x}}_{K-1} - H_u\Delta\underline{\tilde{u}}_{K-1}) \tag{2.3-64}$$

By making several assumptions, the desired form of the Type 1 control law can be obtained.

Assuming that each pilot command can be treated as a step input and that the pilot is limited to command only the state variables directly, the following relationships hold:

$$\Delta\underline{x}^*_K = \Delta\underline{x}^*_{K-1} = \Delta\underline{y}_d \tag{2.3-65}$$

$$\Delta\underline{u}^*_K = \Delta\underline{u}^*_{K-1} \tag{2.3-66}$$

Using these relationships, the Type 1 control law expressed in Eq. 2.3-64 can be written as

$$\Delta\underline{u}_K = \Delta\underline{u}_{K-1} - C_1(\Delta\underline{x}_K - \Delta\underline{x}_{K-1}) - C_2(H_x\Delta\underline{x}_{K-1} - \Delta\underline{y}_{d_K}) \tag{2.3-67}$$

Note that the index on $\Delta\underline{y}_d$ has been changed from K-1 to K to be consistent with the non-zero set point problem ($\Delta\underline{u}_o$ is defined by $\Delta\underline{y}_o$, not $\Delta\underline{y}_{-1}$).

The Type 1 properties of the control law are evident when written in this form. Pure integration is achieved by the accumulation of control [26], and the absente of the steady-state values in the control law ensures zero steady-state error. Model mismatch will not affect the steady-state values of state and control, nor will disturbance inputs, as the calculation of steady-state values according to these parameters does not enter the control process.

When the compound matrix in Eq. 2.3-60 is non-singular, the desired form of the equivalent Type 1 controller is derived as shown above; it was noted earlier, however, that in the case of the fourth-order model of lateral-directional dynamics, this matrix is singular. In this case, a slightly different approach which closely parallels the approach taken in Section 2.3.2 must be followed. This derivation proceeds as follows:

A reduced-order state vector is defined as in Eq. 2.3-26, and roll angle is treated as a disturbance. With the discrete-time equations of motion written as in Eq. 2.3-28, the following transformation is defined:

$$[C_1' \quad C_2] \begin{bmatrix} (\Phi - I)' & \Gamma' \\ H_x' & H_u' \end{bmatrix} = [\Delta t K_1' \quad \Delta t K_2] \qquad (2.3\text{-}68)$$

The compound matrix is now a 5x5 non-singular matrix, and K_1' and C_1' represent the gains associated with the reduced-order state vector. Now, the inverse exists, and

$$C_1' = S_{11}' \, \Delta t K_1' + S_{21}' \, \Delta t K_2 \qquad (2.3\text{-}69)$$

$$C_2' = S_{12}' \, \Delta t K' + S_{22}' \, \Delta t K_2 \qquad (2.3\text{-}70)$$

where S_{11}', S_{12}', S_{21}', and S_{22}' are defined as in Eq. 2.3-34. Following the approach used in the first case, the Type 1 control law using the reduced-order state vector can be written (a complete derivation of this control law is presented in Appendix B),

$$\Delta\tilde{\underline{u}}_K - \Delta\tilde{\underline{u}}_{K-1} = -C_1(\Delta\underline{x}_K' - \Delta\underline{x}_{K-1}') - C_2(H_x\Delta\tilde{\underline{x}}_{K-1}' - H_u\Delta\tilde{\underline{u}}_{K-1}) \qquad (2.3\text{-}71)$$

Using the assumption that $\Delta\underline{y}_d$ is constant over the control interval and that the pilot commands the state variables directly, plus the relationships for $\Delta\underline{x}^*$ and $\Delta\underline{u}^*$ given by Equations 2.3-35 through 2.3-38, the following relationships are obtained:

$$\Delta\underline{x}_K^* - \Delta\underline{x}_{K-1}^* = S_{11}' \, \Lambda \, (\Delta\phi_K^* - \Delta\phi_{K-1}^*) \qquad (2.3\text{-}72)$$

$$\Delta \underline{u}_K^* - \Delta \underline{u}_{K-1}^* = S_{21}' \Lambda (\Delta \phi_K^* - \Delta \phi_{K-1}^*) \tag{2.3-73}$$

and

$$(\Delta \phi_K^* - \Delta \phi_{K-1}^*) = \Delta p^* \Delta t \tag{2.3-74}$$

Substituting these relationships into Eq. 2.3-71 produces the desired form of the Type 1 control law,

$$\Delta \underline{u}_K = \Delta \underline{u}_{K-1} - S_{21}' \Lambda (\Delta p^* \Delta t) - C_1' [(\Delta \underline{x}_K' - \Delta \underline{x}_{K-1}') + S_{11}' \Lambda (\Delta p^* \Delta t)] - C_2 (H_x \Delta \underline{x}_{K-1}' - \Delta \underline{y}_{d_K}) \tag{2.3-75}$$

In this Type 1 control law, the accumulation of past control is apparent. It may appear that due to the presence of the steady-state term in the control law, model mismatch or the presence of disturbance inputs may cause a hangoff error. It should be noted, however, that this alternative derivation of the Type 1 control law is necessary only when roll rate is commanded. Consequently, the desired value of roll rate is determined exactly by the pilot's command, and no hangoff error will exist.

2.3.5 Summary of Control Laws

The preceding sections have presented several different control laws for sampled data systems: the basic sampled-data regulator, with zero and non-zero set point regulation; Type 0 proportional-integral control with control rate restraint, using two different approaches; and an equivalent Type 1 control law. These forms, both with and without a non-singular compound matrix, are summarized here.

The basic sampled-data regulator takes the form

$$\Delta \underline{u}_K = -K \Delta \underline{x}_K \tag{2.3-10}$$

where K is the linear-optimal gain matrix. Non-zero set point regulation is achieved by shifting the coordinates, as

$$\Delta \underline{u}_K = \Delta \underline{u}_K^* - K(\Delta \underline{x}_K - \Delta x_K^*) \tag{2.3-42}$$

where $\Delta \underline{u}^*$ and $\Delta \underline{x}^*$ are given in Equations 2.3-24 and 2.3-25 for a non-singular compound matrix, or as in Eqs. 2.3-35 through 2.3-38 for a singular matrix.

Control rate restraint was included in the control laws by augmenting the difference equations of motion to include control rate dynamics. The resulting control law was expressed as

$$\Delta \underline{\tilde{v}}_K = -K_1 \Delta \underline{\tilde{x}}_K - K_2 \Delta \underline{\tilde{u}}_K \tag{2.3-50}$$

Because control position rather than control rate is the necessary output, two methods were presented to produce the necessary output.
The first used a difference approximation for control rate, and resulted in a control law of the form

$$\Delta \underline{\tilde{u}}_K' = (I - \Delta t K_2) \Delta \underline{\tilde{u}}_{K-1} - (\Delta t k_2) \Delta \underline{\tilde{x}}_{K-1} \tag{2.3-55}$$

The second approach used both Laplace and Tustin transform techniques to produce control position output, resulting in a control law of the form

$$\Delta \underline{u}_K = (\frac{2}{\Delta t} I + K_2)^{-1} [(\frac{2}{\Delta t} I - K_2) \Delta \underline{u}_{K=1} - K_1 (\Delta \underline{\tilde{x}}_K - \Delta \underline{\tilde{x}}_{K=1}) + K_2 (\Delta \underline{u}_K^* + \Delta \underline{u}_{K-1}^*)] \tag{2.3-59}$$

Type 1 control laws were derived from the first form of the Type 0 control law with control rate restraint using the transformation presented in Section 2.3.4. With a non-singular compound matrix, this control law can be written as

$$\Delta \underline{u}_K = \Delta \underline{u}_{K-1} - C_1 (\Delta \underline{x}_K - \Delta \underline{x}_{K-1}) - C_2 (H_x \Delta x_{K-1} - \Delta \underline{y}_{d_K}) \tag{2.3-67}$$

When this matrix is singular, the control law can be written as

$$\Delta \underline{u}_K = \Delta \underline{u}_{K-1} - S_{21}' A (\Delta p^* \Delta t) - C_1 [(\Delta \underline{x}_K' - \Delta \underline{x}_{K-1}') + S_{11}' A (\Delta p^* \Delta t)] - C_2 (H_x \Delta \underline{x}_{K-1} - \Delta \underline{y}_{d_K}) \tag{2.3-75}$$

where the primed terms are associated with the reduced-order state vector.

The remainder of this investigation will deal only with Type 0 control laws with control rate restraint and with equivalent Type 1 controllers. Reference 19 presents an in-depth investigation of basic sampled-data regulators with non-zero set point regulation.

2.3.6 Application of Design Objectives in Control Design

The design process used to obtain the desired control objectives is an iterative procedure. Once the flight control system parameters, such as nominal flight conditions and pilot command variables, are set, the process consists of adjusting weighting matrices Q and R as necessary to produce the desired response. This procedure essentially follows that shown in Fig. 2-3.

Given the linear model of aircraft dynamics (referenced to a particular flight condition), the first step in the design process is to define the pilot's command variables by choosing matrices H_x and H_u (Eq. 2.3-19). The sampling rate is chosen next because it is used to calculate Φ, Γ, and Λ in Eqs. 2.3-5, 2.3-6, and 2.3-29.

Once these parameters have been established, it is necessary to compute the relationship between pilot inputs and steady-state values of state and control. For a lateral-directional CAS, however, it was noted that these relationships could only be found by using a reduced-order state vector. Consequently, the next step in the design process involves eliminating roll angle from the state vector and defining reduced-order matrices F', G', and L such that the linear equations of motion, Eq. 2.3-27, remain exact. This accomplished, Φ', Γ', and Λ are computed using Eqs. 2.3-5, 2.3-6, and 2.3-29, and the desired relationship between steady-state values of state, control, and pilot commands (S'_{11}, S'_{12}, S'_{21} and S'_{22}) are found (Eq. 2.3-34). It also is necessary to compute Φ and Γ associated with the fourth-order state vector, since these are used to solve the Riccati equation, to calculate the linear

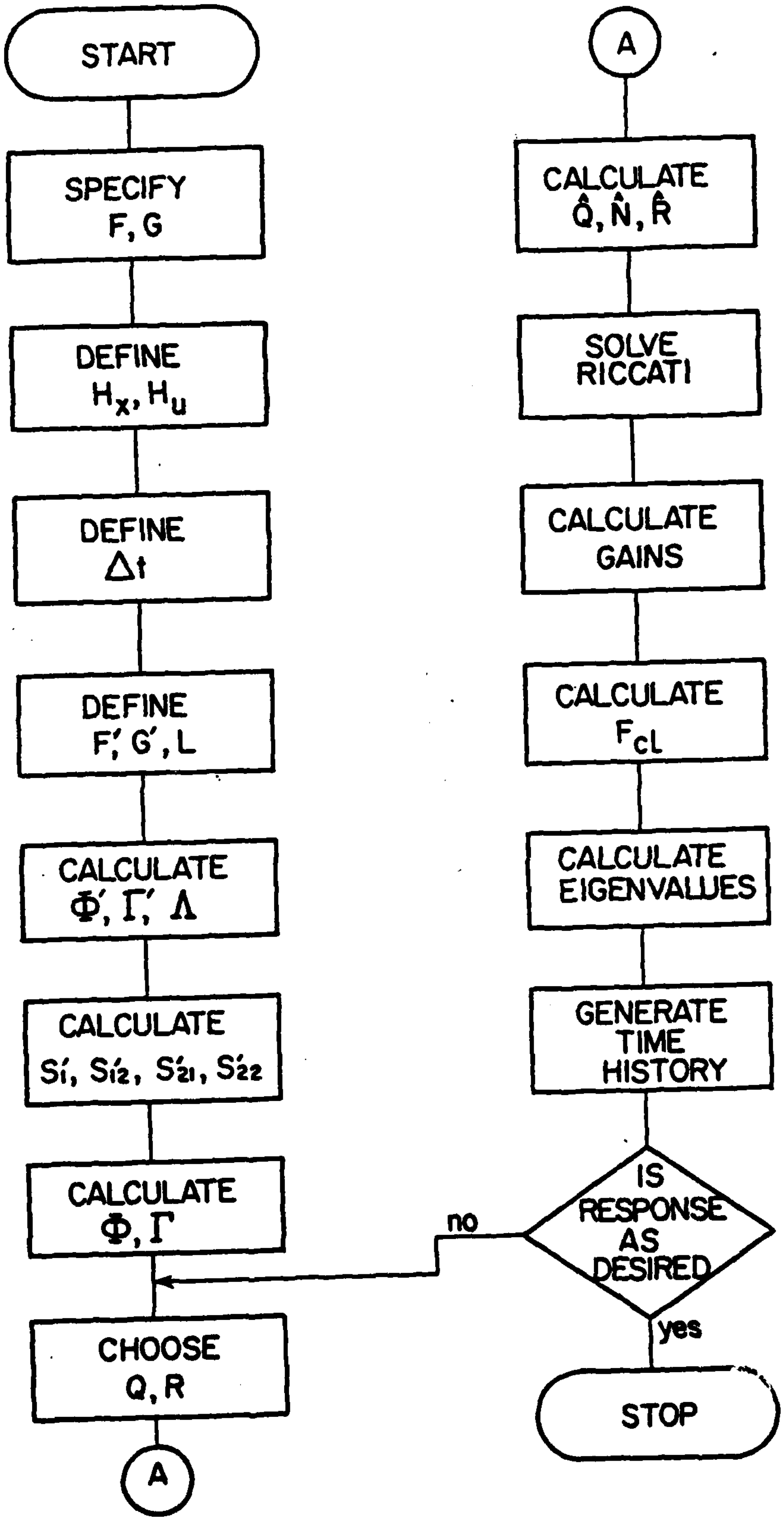

Figure 2-3. Procedure for Finding Optimal Gains.

optimal gain matrices, and to generate time histories for evaluating control laws. These are computed using Eqs. 2.3-5 and 2.3-6.

The iterative part of the design process begins by specifying elements of weighting matrices Q and R. These matrices weight the importance of suppressing perturbations in state, control, and control rate away from the commanded value, and can be thought of as the inverses of the maximum-allowable mean-square values of system values [27]. State, control, state-rate, and command weighting are expressed in the (m+n)x(m+n) symmetric matrix,

$$Q = \begin{bmatrix} 1/\Delta x_1^2 & & & & & 0 \\ & \ddots & & & & \\ & & 1/\Delta x_n^2 & & & \\ & & & 1/\Delta u_1^2 & & \\ & & & & \ddots & \\ 0 & & & & & 1/\Delta u_n^2 \end{bmatrix}_{MAX} + \begin{bmatrix} F^T \\ G^T \end{bmatrix} \begin{bmatrix} 1/\Delta \dot{x}_1^2 & & 0 \\ & \ddots & \\ 0 & & 1/\Delta \dot{x}_n^2 \end{bmatrix}_{MAX} [F \quad G]$$

$$+ \begin{bmatrix} H_x^T \\ H_u^T \end{bmatrix} \begin{bmatrix} 1/\Delta y_1^2 & & 0 \\ & \ddots & \\ 0 & & 1/\Delta y_\ell^3 \end{bmatrix}_{MAX} [H_x \quad H_u] \qquad (2.3\text{-}76)$$

while control rate weightings are contained in

$$R = \begin{bmatrix} 1/\Delta \dot{u}_1^2 & & 0 \\ & \ddots & \\ 0 & & 1/\Delta \dot{u}_m^2 \end{bmatrix}_{MAX} \qquad (2.3\text{-}77)$$

Following the initial choice of weighting matrices Q and R, discrete-time weighting matrices $\hat{Q}$, $\hat{N}$, and $\hat{R}$ are found by integrating equations 2.3-47 through 2.3-49. The Riccati equation (Eq. 2.3-52) is then solved, yielding P, which is used in Eq. 2.3-51 to determine the linear-optimal gain matrix, K.

The closed-loop system characteristics must be evaluated, both by eigenvalue analysis and by observing the time history. The closed-loop eigenvalues can be found by computing the closed-loop F matrix using Eq. 2.3-17, where,

$$\Phi_{CL} = \Phi - \Gamma K \tag{2.3-78}$$

then solving for the roots of the characteristic equation specified by the determinant,

$$|sI - F_{CL}| = 0 \tag{2.3-79}$$

Continuing the process, time histories are generated using Eq. 2.3-4 and 2.3-55. If the time history generated or the eigenvalues of the closed-loop system does not exhibit the desired characteristics, it will be necessary to go back and change Q and R as necessary until all performance criteria are met.

In summary, this section has presented the iterative process used in designing command augmentation systems using modern control theory. This procedure, together with the equations derived using modern control theory presented in the previous sections, provides the basis for the command augmentation control laws to be presented later in this report.

2.4 ALGORITHMS FOR SIDESLIP ANGLE ESTIMATION

The lateral-directional control laws presented in the preceding sections contain sideslip angle (β) as a state variable. While it is not difficult to measure sideslip angle reliably on research aircraft such as the VRA, it is difficult to obtain the measurement on operational aircraft. As a result, very few flight control systems employ sideslip angle as a feedback variable. In this section, algorithms for estimating sideslip angle which do not require β measurements are presented. These estimators are dynamically similar to a Kalman filter [28], and they are based upon actual measurements of roll rate, yaw rate, roll angle, and lateral acceleration.

2.4.1 The Optimal Linear Filter

The primary objective of a filter is to estimate the time-varying mean value of the state vector, $\Delta\underline{x}$, based upon the measurement vector, $\Delta\underline{z}$, the dynamic model (Φ, Γ, and Λ), and a prior knowledge of the measurement error covariance matrix, R_K, the disturbance input covariance matrix, Q_K, and the deterministic input vector, $\Delta\underline{u}$. This estimate of the state is optimal if it minimizes the estimation error in a well-defined statistical sense. This section presents the development of an optimal linear filter (Kalman filter) which meets these objectives. Because we are dealing with sampled data systems, the discrete-time Kalman filter is presented.

Taking into account disturbance inputs, the linear difference equations of motion can be written as,

$$\Delta\underline{x}_K = \Phi_{K-1}\Delta\underline{x}_{K-1} + \Gamma_{K-1}\Delta\underline{u}_{K-1} + \Lambda_{K-1}\Delta\underline{w}_{K-1} \tag{2.4-1}$$

where $\Delta\underline{w}_K$ is a zero mean, white sequence of covariance, Q_K. The measurement vector equation is written as

$$\Delta\underline{z}_K = H_K\Delta\underline{x}_K + \Delta\underline{v}_K \tag{2.4-2}$$

where $\Delta\underline{z}_K$ is the vector of measurements at time t_K, H_K is the measurement matrix, and $\Delta\underline{v}_K$ represents the vector or random noise quantities (zero mean, covariance R_K) corrupting the measurements. Based on an estimate of the system state prior to the measurement being taken, $\Delta\hat{\underline{x}}_K(-)$ (the hat denotes the estimate; the (-) denotes prior to the measurement), we seek an updated estimate of the state $\Delta\hat{\underline{x}}_K(+)$ that is improved by the measurement vector $\Delta\underline{z}_K$ (the (+) denotes the estimate after the measurement). Based on these quantities, we assume the form of the filter to be

$$\Delta\hat{\underline{x}}_K(+) = K'_K\Delta\hat{\underline{x}}_K(-) + K_K\Delta\underline{z}_K \tag{2.4-3}$$

where K'_K and K_K are time-varying weighting matrices.

The form of the Kalman filter is obtained from the assumed form by ensuring that the estimate is unbiased; that is, by ensuring that the expected value of the estimation error will be zero. By substituting the measurement equation (Eq. 2.4-2) and the relationships defining the estimation error ((˜) denotes an error quantity),

$$\Delta\hat{\underline{x}}_K(+) = \Delta\underline{x}_K + \Delta\tilde{\underline{x}}_K(+) \qquad (2.4\text{-}4)$$

$$\Delta\hat{\underline{x}}_K(-) = \Delta\underline{x}_K + \Delta\tilde{\underline{x}}_K(-) \qquad (2.4\text{-}5)$$

into the assumed form of the filter, the estimation error is obtained:

$$\Delta\tilde{\underline{x}}(+) = [K'_K + K_K H_K - I]\Delta\underline{x}_K + K'_K \tilde{\underline{x}}_K(-) + K_K \underline{v}_K \qquad (2.4\text{-}6)$$

Because the expected value of the error must be zero, the bracketed quantity must be zero as well. Using this relationship in the general form of the filter yields the Kalman filter,

$$\Delta\hat{\underline{x}}_K(+) = \Delta\hat{\underline{x}}_K(-) + K_K[\Delta\underline{z}_K - H_K\Delta\hat{\underline{x}}_K(-)] \qquad (2.4\text{-}7)$$

As was noted earlier, this filter is optimal only when the estimate of the state minimizes the estimation error in a well-defined statistical sense; this is ensured by a judicious choice of the Kalman gain matrix, K_K. Assuming that the estimation error vector is an n-dimensional gaussian vector, all its statistical properties are defined by the mean and covariance. Since the Kalman filter estimates the time-varying mean value, all the statistical properties of the estimation error are characterized by its covariance matrix P, given by

$$P_K = E[\Delta\tilde{\underline{x}}_K\ \Delta\tilde{\underline{x}}_K^T] \qquad (2.4\text{-}8)$$

where E indicates the expected value of the quantity in brackets. Therefore, the choice of the optimal gain matrix K_K must necessarily minimize the variance of the estimation errors in some manner.

The criterion for choosing K_K is to minimize the weighted scalar sum of the diagonal elements of the error covariance matrix after the measurements have been taken. The scalar cost function to be minimized can be written

$$J_K = E[\Delta\underline{\tilde{x}}_K(+)\ S\Delta\underline{\tilde{x}}_K(+)^T] \tag{2.4-9}$$

where S is any positive semidefinite weighting matrix [29]. Choosing S=I yields

$$J_K = \text{trace}[P_K(+)]$$

which is equivalent to minimizing the length of the estimation error vector. To find the K_K that minimizes J_K, we solve

$$\frac{\partial J_K}{\partial K_K} = 0 \tag{2.4-10}$$

which yields the expression for the optimal gain matrix

$$K_K = P_K(-)\ H_K^T[H_K P_K(-) H_K^T + R_K]^{-1} \tag{2.4-11}$$

Now that we have developed the optimal linear filter, we must use these equations in a sequence to provide the best estimate of the state vector $\Delta\underline{x}$ based on the measurement vector $\Delta\underline{z}$. This process is described as follows. First, estimates of the state and covariance (before any measurements are taken of the state) at time t_K are computed using the best estimates of each at time t_{K-1}, using a knowledge of the dynamic model and the deterministic input, $\Delta\underline{u}_K$. These estimates are extrapolated according to the following equations:

$$\Delta\underline{\hat{x}}_K(-) = \Phi_{K-1}\Delta\underline{\hat{x}}_{K-1}(+) + \Gamma_{K-1}\Delta\underline{u}_{K-1} \tag{2.4-12}$$

$$P_K(-) = \Phi_{K-1}\ P_{K-1}(+)\ \Phi_{K-1}^T + \Lambda_{K-1}\ Q_{K-1}\ \Lambda_{K-1}^T \tag{2.4-13}$$

Using the value for $P_K(-)$, the optimal Kalman filter gains can be computed using Eq. 2.4-11, and the state estimate can be updated according

to the Kalman filter, Eq. 2.4-7. Finally, the covariance is updated by

$$P_K(+) = (I - K_K H_K) P_K(-) \tag{2.4-14}$$

and the next estimate of both state and covariance can be extrapolated.

These equations are used in this sequence to provide continuing estimates of the state which are optimal in a well defined sense, based on statistics of the noise present in the state and in the measurement. When the sampled data system is used to control a continuous process, however, the statistics of the noise are continuous rather than discrete. Therefore, the statistics used to determine the state estimate, R_K and Q_K, must be found from continuous-time statistics. These relationships are derived in [29], and are summarized here. The statistics of the random forcing function, $\Lambda_K \Delta w_K$, are derived using

$$\Lambda_K Q_K \Lambda_K = \int_{t_K}^{t_{K+1}} \Phi(t_{K+1},\tau)\ L(\tau)\ Q(\tau)\ L^T(\tau)\ \Phi^T(t_{K+1},\tau)\ d\tau \tag{2.4-15}$$

where Q(t) represents the spectral density matrix of the continuous-time disturbance forcing function. The measurement covariance R_K is derived from the continuous-time spectral density matrix R by

$$R_K = R/\Delta t \tag{2.4-16}$$

where Δt represents the sampling interval.

This section has presented the development of the Kalman filter used to estimate the state of a system at discrete points in time when that system is disturbed continuously in time. These equations are summarized in Table 2-1 [28].

Table 2-1 Summary of Discrete Kalman Filter Equations

System Model	$\Delta \underline{x}_K = \Phi_{K-1}\Delta \underline{x}_{K-1} + \Gamma_{K-1}\Delta \underline{u}_{K-1} + \Lambda_{K-1}\Delta \underline{w}_{K-1}$
Measurement Model	$\Delta \underline{z}_K = H_K \Delta \underline{x}_K + \Delta \underline{v}_K$
State Estimate Extrapolation	$\Delta \hat{\underline{x}}_K(-) = \Phi_{K-1}\Delta \hat{\underline{x}}(+)_{K-1} + \Gamma_{K-1}\Delta \underline{u}_{K-1}$
Error Covariance Extrapolation	$P_K(-) = \Phi_{K-1}P(+)_{K-1}\Phi^T_{K-1} + \Lambda_{K-1}Q_{K-1}\Lambda^T_{K-1}$
State Estimate Update	$\Delta \hat{\underline{x}}_K(+) = \Delta \hat{\underline{x}}_K(-) + K_K[\Delta \underline{z}_K - H_K \Delta \hat{\underline{x}}_K(-)]$
Error Covariance Update	$P_K(+) = [I - K_K H_K]P_K(-)$
Kalman Gain Matrix	$K_K = P_K(-)H_K^T[H_K P_K(-) + R_K]^{-1}$
Disturbance Covariance	$\Lambda_K Q_K \Lambda^T_K = \int_{t_K}^{t_{K-1}} \Phi(t_{K+1},\tau)L(\tau)Q(\tau)L(\tau)\Phi^T(t_{K+1},\tau)d\tau$
Measurement Covariance	$R_K = R(t)/\Delta t$

2.4.2 Reduced-Order Models for Lateral-Directional Dynamics

The Kalman filter algorithms presented in the previous section allow us to estimate sideslip angle based on measurements of other state variables, and in that sense we could eliminate the measurement of β and still use it as a feedback variable. However, the Kalman filter approach has one serious drawback for the purposes of this investigation: that is, it requires the estimation of all the state variables in each iteration. Because we are merely trying to eliminate the measurement of sideslip angle, rather than to find the "best estimate" of all the state variables, this process is somewhat too complex. It requires additional (possibly unnecessary) computations, which increases Micro-DFCS computation time. One possible alternative is to use the Kalman filter to estimate sideslip angle using a reduced-order model to keep the number of necessary computations to a minimum.

One method of reducing the order of the system is merely to truncate the fourth-order system into two second-order systems. [29] As was noted earlier, the F and G matrices can be partitioned as

$$\left[\begin{array}{c|c} \text{Directional Effects} & \text{Lateral-to-Directional Coupling} \\ \hline \text{Directional-to-Lateral Coupling} & \text{Lateral Effects} \end{array}\right]$$

If we assume that the coupling terms are negligible, then this system reduces to two second-order approximations: the Dutch roll approximation, for the directional effects; and the roll mode approximation, for the lateral effects. Using this method, sideslip angle dynamics are entirely specified by

$$F = \begin{bmatrix} N_r & N_\beta \\ -1 & Y_\beta/V \end{bmatrix} \; ; \; G = \begin{bmatrix} N_{\delta R} \\ Y_{\delta R}/V \end{bmatrix} \; ; \; \Delta \underline{x} = \begin{bmatrix} \Delta r \\ \Delta \beta \end{bmatrix} \tag{2.4-17}$$

The other method of reducing the order of the model of lateral-directional dynamics is known as residualization, or singular perturbation analysis. [29] In this analysis, the characteristic modes of lateral-directional dynamics are characterized as either fast modes or slow modes. Using this, the linear equations of motion governing aircraft dynamics are written

$$\begin{bmatrix} \Delta \dot{\underline{x}}_S \\ \Delta \dot{\underline{x}}_F \end{bmatrix} = \begin{bmatrix} F_S & F_F^S \\ F_S^F & F_F \end{bmatrix} \begin{bmatrix} \Delta \underline{x}_S \\ \Delta \underline{x}_F \end{bmatrix} + \begin{bmatrix} G_S & G_F^S \\ G_S^F & G_F \end{bmatrix} \begin{bmatrix} \Delta \underline{\delta}_S \\ \Delta \underline{\delta}_F \end{bmatrix} \tag{2.4-18}$$

or as

$$\Delta \dot{\underline{x}}_S = F_S \, \Delta \underline{x}_S + F_F^S \, \Delta \underline{x}_F + G_S \, \Delta \underline{\delta}_S + G_F^S \, \Delta \underline{\delta}_F \tag{2.4-19}$$

$$\Delta \dot{\underline{x}}_F = F_S^F \, \Delta \underline{x}_S + F_F \, \Delta \underline{x}_F + G_S^F \, \Delta \underline{\delta}_S + G_F \, \Delta \underline{\delta}_F \tag{2.4-20}$$

Using residualization, the slow mode behaves as if the fast mode is in its equilibrium condition, while the fast mode sees the slow mode as a slowly changing bias. Consequently, the fast mode affects the dynamics of the slow mode, but the reverse effect is negligible. These effects are calculated by setting,

$$\Delta\dot{\underline{x}}_F = 0 \tag{2.4-21}$$

solving for $\Delta\underline{x}_F$, and substituting this into the equation governing slow mode dynamics:

$$\Delta\underline{x}_F = -F_F^{-1}(F_S^F\,\Delta\underline{x}_S + G_S^F\,\Delta\underline{\delta}_S + G_F\,\Delta\underline{\delta}_F) \tag{2.4-22}$$

$$\Delta\dot{\underline{x}}_S = F_S\,\Delta\underline{x}_S + F_F^S[-F_F^{-1}(F_S^F\,\Delta x_S + G_S^F\,\Delta\underline{\delta}_S + G_F\,\Delta\underline{\delta}_F)] + G_S\,\Delta\underline{\delta}_S + G_F^S\,\Delta\underline{\delta}_F \tag{2.4-23}$$

Solving for the residualized slow mode dynamics results in a new system dynamics matrix,

$$F_S' = F_S - F_F^S\,F_F^{-1}F_S^F \tag{2.4-24}$$

and a new control effects matrix characterized by

$$G_S' = G_S - F_F^S\,F_F^{-1}\,G_S^F \quad ; \quad G_F^{S\prime} = G_F^S - F_F^S\,F_F^{-1}\,G_F \tag{2.4-25}$$

while the equations governing the fast mode dynamics remain unchanged. Using this approach, three possible cases exist.

The first possibility is a fast roll mode, neutral spiral, and slow Dutch roll mode. Here, roll angle is neglected, and the equations of motion are partitioned as

$$\begin{bmatrix} \Delta\dot{r} \\ \Delta\dot{\beta} \\ \Delta\dot{p} \end{bmatrix} = \begin{bmatrix} N_r & N_\beta & N_p \\ -1 & Y_\beta/V & 0 \\ L_r & L_\beta & L_p \end{bmatrix} \begin{bmatrix} \Delta r \\ \Delta\beta \\ \Delta p \end{bmatrix} + \begin{bmatrix} N_{\delta R} & N_{\delta A} \\ Y_{\delta R}/V & 0 \\ L_{\delta R} & L_{\delta A} \end{bmatrix} \begin{bmatrix} \Delta\delta R \\ \Delta\delta A \end{bmatrix} \tag{2.4-26}$$

Using the equations governing residualized systems, for this case, the following represent the reduced-order residualized dynamics governing β:

$$F = \begin{bmatrix} (N_r - N_p L_p^{-1} L_r) & (N_\beta - N_p L_p^{-1} L_\beta) \\ -1 & Y_\beta/V \end{bmatrix} \tag{2.4-27}$$

$$G = \begin{bmatrix} (N_{\delta R} - N_p L_p^{-1} L_{\delta R}) & (N_{\delta A} - N_p L_p^{-1} L_{\delta A}) \\ Y_{\delta R}/V & 0 \end{bmatrix} \tag{2.4-28}$$

$$\Delta \underline{x}^T = [\Delta r \quad \Delta\beta] \tag{2.4-29}$$

The second possibility involves a fast roll mode, slow spiral mode, and a slow Dutch roll mode. The equations of motion are partitioned as

$$\begin{bmatrix} \Delta\dot{r} \\ \Delta\dot{\beta} \\ \Delta\dot{\phi} \\ \hline \Delta\dot{p} \end{bmatrix} = \left[\begin{array}{ccc|c} N_r & N_\beta & 0 & N_p \\ -1 & Y_\beta/V & g/V & 0 \\ 0 & 0 & 0 & 1 \\ \hline L_r & L_\beta & 0 & L_p \end{array}\right] \begin{bmatrix} \Delta r \\ \Delta\beta \\ \Delta\phi \\ \hline \Delta p \end{bmatrix} + \left[\begin{array}{cc} N_{\delta R} & N_{\delta A} \\ Y_{\delta R}/V & 0 \\ 0 & 0 \\ \hline L_{\delta R} & L_{\delta A} \end{array}\right] \begin{bmatrix} \Delta\delta R \\ \Delta\delta A \end{bmatrix} \tag{2.4-30}$$

In this case, sideslip angle belongs to a residualized third-order state vector containing yaw rate, sideslip angle, and roll angle whose dynamics are governed by

$$F = \begin{bmatrix} (N_r - \frac{L_r N_p}{L_p}) & (N_\beta - \frac{L_\beta N_p}{L_p}) & 0 \\ -1 & Y_\beta/V & g/V \\ -L_r/L_p & -L_\beta/L_p & 0 \end{bmatrix} \tag{2.4-31}$$

$$G = \begin{bmatrix} \left(N_{\delta R} - \dfrac{N_p L_{\delta R}}{L_p}\right) & \left(N_{\delta A} - \dfrac{N_p L_{\delta A}}{L_p}\right) \\ Y_{\delta R}/V & 0 \\ -L_{\delta R}/L_p & -L_{\delta A}/L_p \end{bmatrix} \qquad (2.4\text{-}32)$$

The third possibility, which involves a fast Dutch roll, slow roll, and slow spiral results in a second-order model containing yaw rate and sideslip angle. The system dynamics matrix, F, is the same as that obtained by truncating the model, since fast dynamics are not affected by slow mode dynamics. In this case, however, the roll-spiral dynamics are altered. They no longer are given by the roll mode approximation; they must be found according to the above procedure.

By comparing the eigenvalues of one of these reduced-order models with those of the fourth-order model, the validity of these approximations can be established. By combining one of these reduced-order versions of sideslip angle dynamics with the Kalman filter, a valid estimate of sideslip angle can be obtained, while at the same time minimizing the number of necessary computations.

2.4.3 Reduced-Order Sideslip Angle Estimators

The reduced-order models presented in the previous section, when combined with the Kalman filter equations, provide several possibilities for reduced-order sideslip angle estimators. Using any of the reduced-order models presented in the previous section, second- or third-order Kalman filters can be obtained. In addition, by taking into account the linear relationship between sideslip angle and lateral acceleration, a first-order estimator based on Kalman filter dynamics is developed.

The expression which relates lateral acceleration to sideslip angle is written as

$$\Delta a_y = Y_\beta \, \Delta\beta + Y_{\delta R} \, \Delta_{\delta R} \tag{2.4-33}$$

By assuming that the state vector contains only β, this direct relationship between the two variables can be used in the Kalman filter. With this approximation, the following represent the variables governing system dynamics:

$$\Delta \underline{x} = [\Delta\beta] \quad ; \quad \Delta \underline{u} = [\Delta\delta R] \quad ; \quad F = [Y_\beta/v] \quad ; \quad G = [Y_{\delta R}/v] \tag{2.4-34}$$

Using these expressions for system dynamics, a Kalman filter based on a first-order model of sideslip angle dynamics can be used.

In addition to reduced order, the Kalman filters to be compared in the next section will have constant gains. This eliminates updates of the error covariance matrix and of the gains themselves. By combining the Kalman gain equation, the error covariance update equation, and the error covariance extrapolation equation (Equations 2.4-11, 2.4-14, and 2.4-13, respectively), a single equation for the error covariance is obtained:

$$P = \Phi P \Phi - \Phi P H^T [H P H^T + R_K]^{-1} H P \Phi^T + \Lambda Q_k \Lambda \tag{2.4-35}$$

Solving this equation with constant Q and R yields the steady-state error covariance, P_∞, which in turn yields the steady-state Kalman filter gains:

$$K = P_\infty H^T [H P_\infty H^T + R\ ]^{-1} \tag{2.4-36}$$

The use of steady-state gains in the Kalman filter assumes several things. It assumes that the linear model governing system dynamics is time-invariant, and also that the statistics governing the disturbance inputs are time-invariant as well. More important, it assumes that measurements are available for a sufficiently long period of time such that the steady-state condition of the filter is reached before critical points (as defined by system accuracy) in time are reached. In this

investigation, it is assumed that the sideslip angle dynamics are sufficiently slow to allow such an assumption to be made.

These sections have presented the Kalman filter algorithms to be used in a sideslip angle estimator. Reduced-order models were presented to simplify the approach; specifically, third-, second-, and first-order models were presented to reduce the computational burden required of the Micro DFCS. The actual Kalman filters were not developed here; these will be derived and evaluated in the following section.

2.5 COMMAND AUGMENTATION CONTROL LAWS

This section presents the actual command augmentation control laws developed for implementation in the Micro-DFCS. Using the algorithms presented in the previous sections, control laws are designed, and analytical results are presented. Reduced-order sideslip angle estimators are compared and evaluated, and Type 0 and Type 1 control laws are compared when the design model and actual aircraft are mismatched. First, however, the unaugmented dynamics of the VRA are presented to provide the basis for design and comparison of advanced command augmentation control laws.

As was noted earlier, the linear model of lateral-directional dynamics used in the design of command augmentation control laws must be referenced to a particular flight condition; for this investigation, straight-and-level flight at 105 KIAS presents the nominal flight condition. At this flight condition, lateral-directional dynamics of the VRA (see Appendix E for a description of the VRA) are given by

$$F = \begin{bmatrix} -.75 & 5.9 & -.26 & 0 \\ -1. & 0.40 & 0 & 0.181 \\ 1.16 & -11.5 & -6.5 & 0 \\ 0 & 0 & 1. & 0 \end{bmatrix} \qquad (2.5\text{-}1)$$

$$G = \begin{bmatrix} -6.1 & -.252 \\ -.07 & 0 \\ 0.58 & 21. \\ 0 & 0 \end{bmatrix} \qquad (2.5\text{-}2)$$

where F and G are referenced to stability axes (at this flight condition, the difference between stability axes and body axes is assumed to be negligible).

At this flight condition and based on the above F and G matrices, Figure 2-4 depicts the VRA's unaugmented flight characteristics, as generated by Princeton University's IBM 370/158 time-sharing computer. Figure 2-4a presents the VRA's yaw rate, sideslip angle, and roll rate responses to a rudder command of 5 degrees, while Figure 2-4b shows the same responses for a 5-degree step in aileron. Positive rudder deflection (that which produces positive, i.e., left, sideslip) is seen to produce a rapid change in yaw rate and sideslip angle, with the nose of the aircraft swinging to the left. As a result, the dihedral effect of the VRA produces a substantial negative rolling motion. The dominant feature of the VRA's response to positive aileron deflection (that which produces positive, i.e., right, roll) is seen to be a rapid acquisition of roll rate. This response is well damped due to the VRA's high roll damping coefficient, L_p. The adverse yaw is seen in the yaw rate response, as a slightly negative yaw rate is produced before the VRA begins tracking in the desired direction of turn. These plots show the major response characteristics of the unaugmented VRA, and to some extent, the degree of coupling of lateral and directional dynamics.

The modal characteristics of the VRA's lateral directional dynamics are given by its eigenvalues and eigenvectors. The eigenvalues of the linear model of lateral-directional dynamics are shown in Table 2-2 below, while the corresponding eigenvectors are given in Table 2-3 (the eigenvector magnitudes have been normalized with respect to sideslip angle for purposes of comparison). The roll mode is seen to be almost exclusively a rolling phenomenon, and its large time constant is responsible

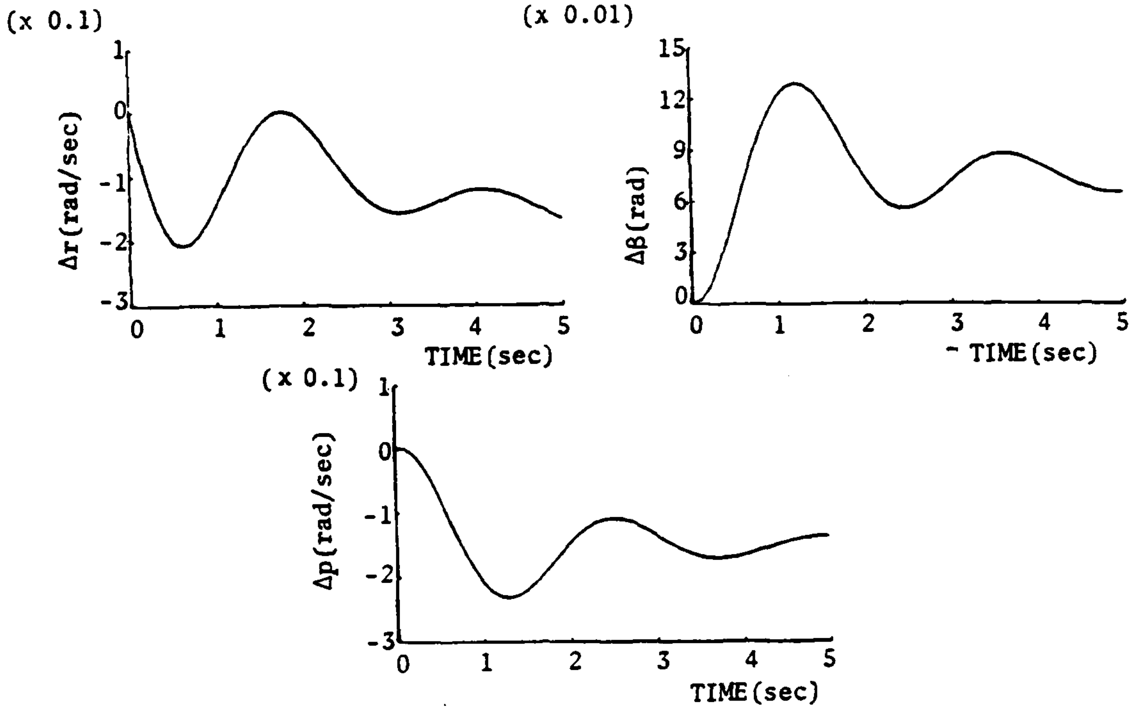

a. Response for ΔδR = 5°

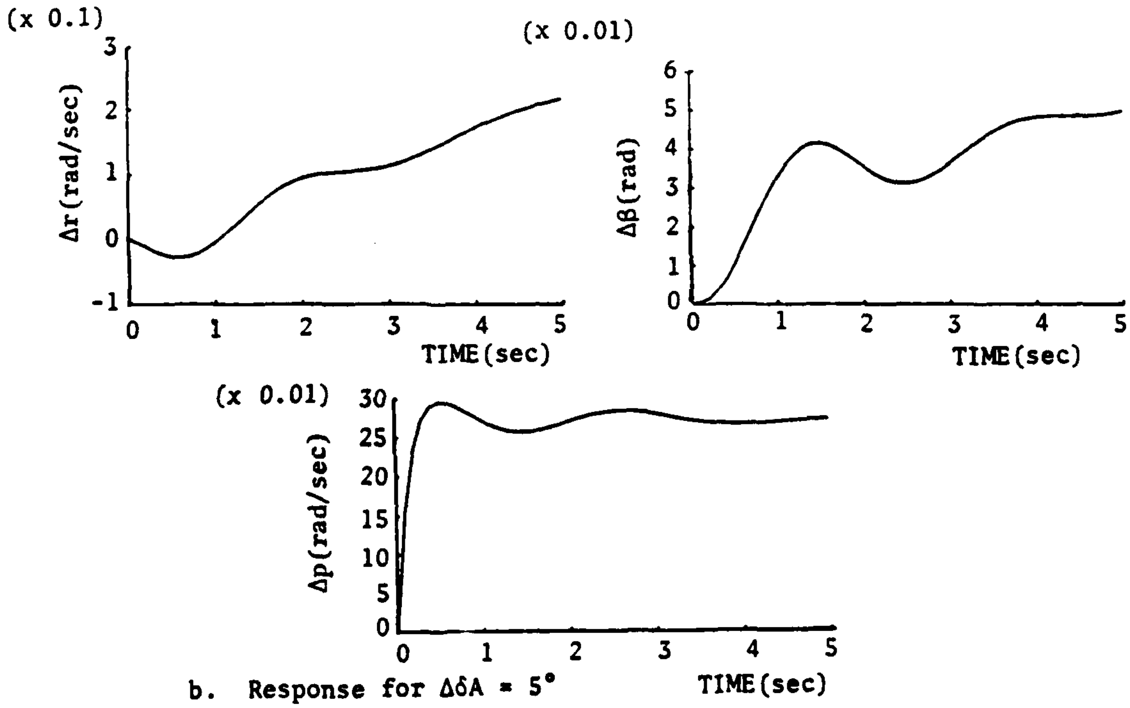

b. Response for ΔδA = 5°

Figure 2-4. Step Response Characteristics for Unaugmented VRA.

Table 2-2 Eigenvalues of the VRA Linear Model

$\omega_{n_{DR}}$, rad/sec	ζ_{DR}	λ_R, sec^{-1}	λ_S, sec^{-1}
2.63	.203	-6.575	-.0071

Table 2-3 Eigenvectors of the VRA Linear Model

	Dutch Roll	Rolling Convergence	Spiral
Δr, rad/sec	2.47	3.4	8.14
$\Delta\beta$, rad	1.	1.	1.0
Δp, rad/sec	1.79	98.65	0.33
$\Delta\phi$, rad	0.68	15.	47.71

for the rapid acquisition of roll rate following an aileron input, as shown in Figure 2-4b. The spiral mode, having large components of both yaw rate and roll angle, is, in this case, a very slow convergent mode, almost neutrally stable. The Dutch roll mode, with a period of about 2.4 seconds, is very evident in the step responses shown in Figure 2-4. It is in this mode that the lateral-directional coupling is most evident, as seen in the eigenvectors; the degree of coupling is normally expressed in the flying qualities parameter ϕ/β, which is the ratio of the roll angle and sideslip angle eigenvector magnitudes in the Dutch roll mode. These eigenvalues and eigenvectors, especially of the Dutch roll mode, will be used as a basis of comparison and evaluation of the command augmentation control laws.

In addition to providing the basic framework for designing advanced control laws, knowledge of the system dynamics matrix, F, is used to compute the rate of error build-up between samples, by equation 2.3-14. This allows one to determine whether a specified sampling rate will maintain the error buildup within specified bounds. In this investigation, a nominal sampling rate of 10 samples per second will be used, based on the results of previous investigation [19]. Assuming that disturbances enter the system dynamics in the same manner as sideslip angle,

and assuming a moderate turbulence, e.g., sideslip angle gusts with an rms value of 2 degrees and correlation time of 1 second, Figure 2-5 shows the propagation of the state covariances with time. If an rms error of 5 degrees per second for angular rates and 1 degree for angles are to be tolerated, then a sampling rate of 10 samples per second will be sufficient under the above conditions.

This section has presented the basic characteristics of the VRA to be used as the basis for design and evaluation of the command augmentation control laws. These laws are now presented.

2.5.1 Roll Rate/Sideslip Angle Command

Roll rate and sideslip angle represent perhaps the most obvious pair of control variables for a lateral-directional CAS; roll provides the only feasible method of control about the longitudinal axis, while sideslip angle is normally adjusted to maintain coordinated flight and directional alignment. *In this investigation*, Type 0 controllers with rate restraint, derived using a first difference approximation for control rate, and an equivalent Type 1 controller in these two command variables are derived. The development proceeds as shown in Figure 2-3.

Because the dynamics governing these two command vectors are already contained in F and G, the first step in the design process is to choose observation matrices, H_x and H_u, which define the command vector,

$$\Delta \underline{y}^T = [\Delta\beta \quad \Delta p] \tag{2.5-3}$$

In this case:

$$H_x = \begin{bmatrix} 0 & 1 & 0 & 0 \\ 0 & 0 & 1 & 0 \end{bmatrix} \tag{2.5-4}$$

$$H_u = \begin{bmatrix} 0 & 0 \\ 0 & 0 \end{bmatrix} \tag{2.5-5}$$

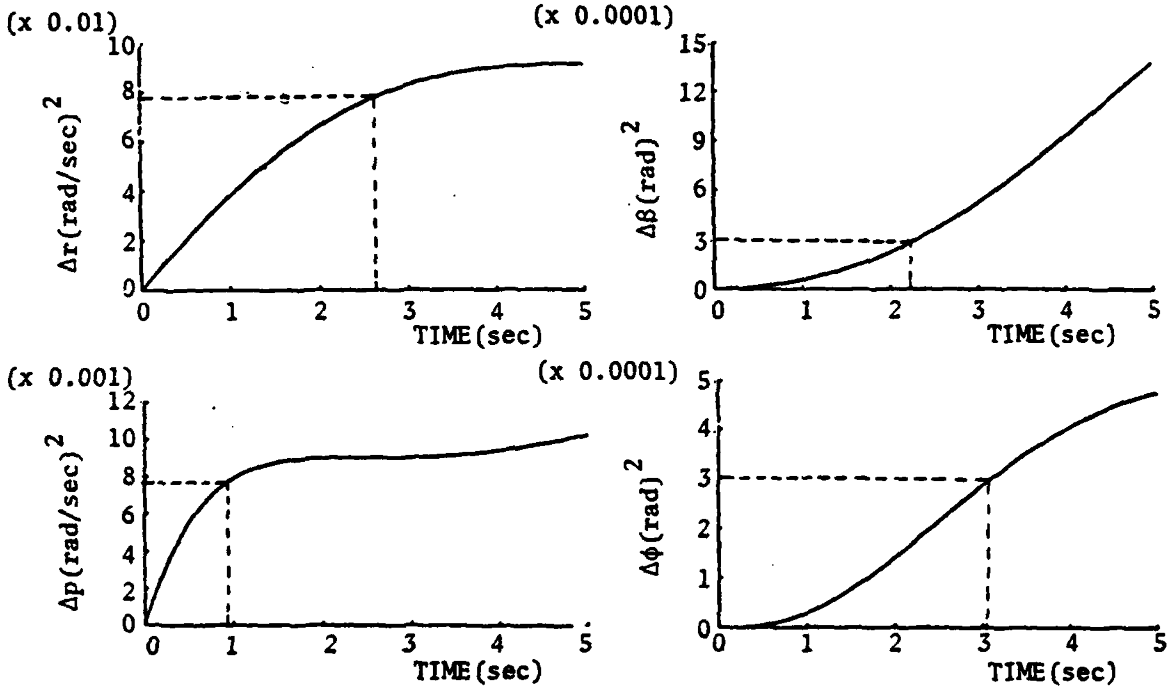

Figure 2-5. Propagation of the State Covariances.

Next, the steady-state relationships between state and control and pilot commands must be established. (Normally, the sampling rate is chosen next, but it already has been stated to be 10 samples per second). It should be remembered that when roll rate is commanded, the compound matrix of Equation 2.3-23 is singular, and the reduced-order state vector must be used to calculate steady-state relationships. The reduced-order matrices governing the equations of motion are given by

$$F' = \begin{bmatrix} -.75 & 5.9 & 0.26 \\ -1. & -.40 & 0 \\ 1.16 & -11.5 & -6.5 \end{bmatrix} \quad ; \quad G' = \begin{bmatrix} -6.1 & -.252 \\ -.07 & 0 \\ .58 & 21. \end{bmatrix}$$

$$L = \begin{bmatrix} 0 \\ 0.181 \\ 0 \end{bmatrix} \tag{2.5-6}$$

Using these values, Φ', Γ', and Λ are calculated using Equations 2.3-5, 2.3-6 and 2.3-29, and steady-state relationships S'_{11}, S'_{12}, S'_{21}, S'_{22} can be found using Equation 2.3-34. For the roll rate/sideslip angle controller, the steady-state relationships are found to be

$$\begin{bmatrix} \Delta r^* \\ \Delta \beta^* \\ \Delta p^* \end{bmatrix} = \begin{bmatrix} 0.183 \\ 0 \\ 0 \end{bmatrix} \Delta\phi^* + \begin{bmatrix} -.470 & .0039 \\ 1.0 & 0 \\ 0 & 1.0 \end{bmatrix} \Delta \underline{y}_d \tag{2.5-7}$$

$$\begin{bmatrix} \Delta\delta R^* \\ \Delta\delta A^* \end{bmatrix} = \begin{bmatrix} -.0221 \\ -.0095 \end{bmatrix} \Delta\phi^* + \begin{bmatrix} 1.002 & -.0559 \\ .5459 & .3109 \end{bmatrix} \Delta \underline{y}_d \tag{2.5-8}$$

Note that yaw rate is the only state variable affected by a steady-state value of roll angle. This is because yaw rate must be present when bank is established in order to maintain the desired rate of coordinated turn, even in the absence of any other command inputs.

Once the relationships have been established, the iterative process of choosing weighting matrices Q and R to achieve the desired step response characteristics remains. As a starting point, the square of the inverse of the maximum allowable state, control, and control rate perturbations can be used. These can be adjusted up or down as necessary, or state-rate weightings can be added, to provide various step response characteristics. While there are no specific relationships between weightings and step responses, past research indicates that state weighting controls rise time (time to 95 percent amplitude), while state-rate weighting controls overshoot and modal damping. In this investigation, four sets of weightings are used to provide the pilot with various response characteristics. These sets of weightings, along with the step response characteristics, are given in Table 2-4, while Table 2-5 presents the optimal feedback gains for the various modes.

The step response characteristics of the roll rate/sideslip angle control laws are displayed in Figures 2-6 through 2-9. Several characteristics of the control law are readily apparent in these graphs. Most notable of these is the absence of the Dutch roll oscillations; this is due to the high Dutch roll damping of the closed-loop system, as will be seen in the eigenvalues of the closed-loop system. Also noticeable are two characteristics inherent in the nature of the control law. As was mentioned earlier, when the first-difference approximation for control rate is used to generate the control law, the initial control response depends entirely upon the steady-state value. This characteristic is seen best in the sideslip angle command responses; regardless of the weighting matrices chosen, the initial control responses are identical. In addition, the Type 0 property of not nulling steady-state error is evident in the time histories. This characteristic is best seen in the roll response histories, where sideslip angle reaches a steady-state hang-off error which goes uncorrected by the control law.

An examination of the control response time histories provides some insight as to how the controller provides improved command response

Table 2-4 Weightings and Step Response Characteristics for β, p CAS

		Mode A	Mode B	Mode C	Mode D
	Δr	250	30	25	10
State	$\Delta\beta$	5000	250	30	10
Weightings	Δp	100	30	10	0
	$\Delta\phi$	25	15	.5	0
Control	$\Delta\delta R$	15	33	15	15
Weightings	$\Delta\delta A$	15	33	15	15
Control Rate	$\Delta\dot{\delta} R$	1	1	1	1
Weightings	$\Delta\dot{\delta} A$	1	1	1	1
	$\Delta\dot{r}$	0	0	0	0
State Rate	$\Delta\dot{\beta}$	0	0	0	20
Weightings	$\Delta\dot{p}$	0	0	0	.25
	$\Delta\dot{\phi}$	0	0	0	0
Roll Rate	Rise Time	.20 sec	.25 sec	.37 sec	.96 sec
Command	% Overshoot	7.4%	7.4%	3.6%	2.8%
Sideslip	Rise Time	.82 sec	1.00 sec	1.83 sec	2.37 sec
Angle Command	% Overshoot	.06%	.21%	.80%	1.20%

Table 2-5 Optimal Gains for β, p CAS

Mode	K_1				K_2	
A	-10.48	11.21	.40	1.704	14.25	1.01
	.626	-3.34	1.45	2.60	0.02	11.93
B	-3.63	-.44	1.48	.36	8.83	.42
	.68	-3.29	.89	2.17	-.145	9.35
C	-2.23	-3.48	.10	.15	7.07	.36
	.43	-2.21	.43	.66	-.045	6.68
D	-2.00	-4.70	.19	.26	6.97	.71
	.25	-1.95	-.63	.30	.147	5.38

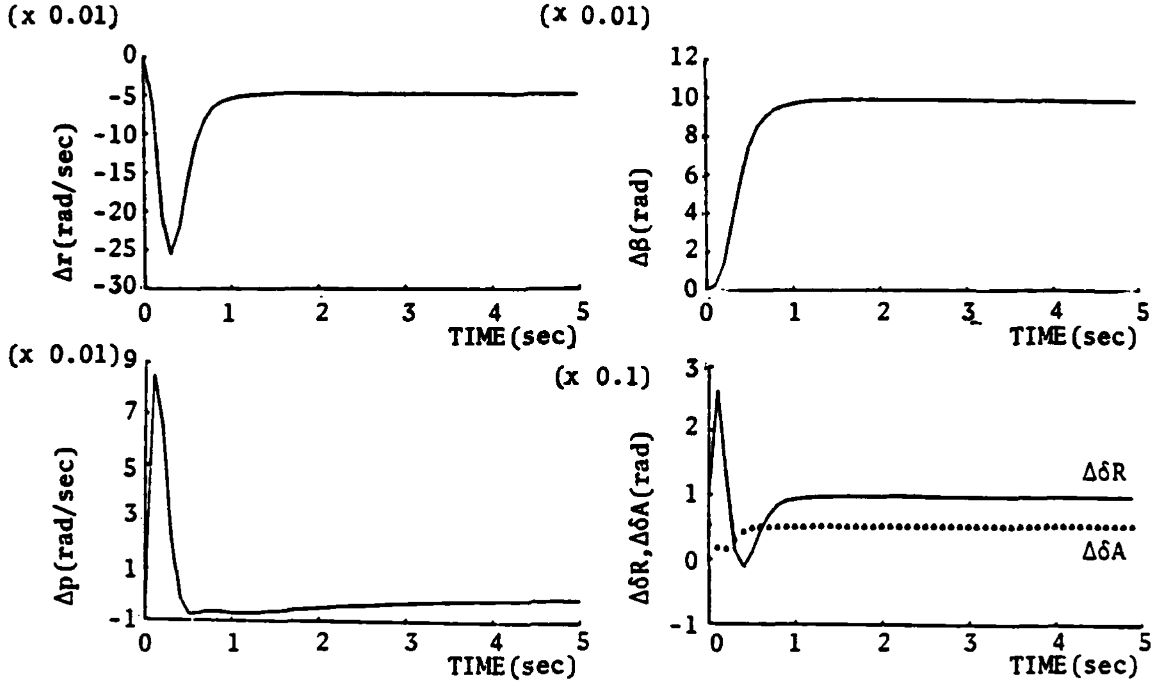

a. Response for Commanded Sideslip Angle, y_d = .1 RAD.

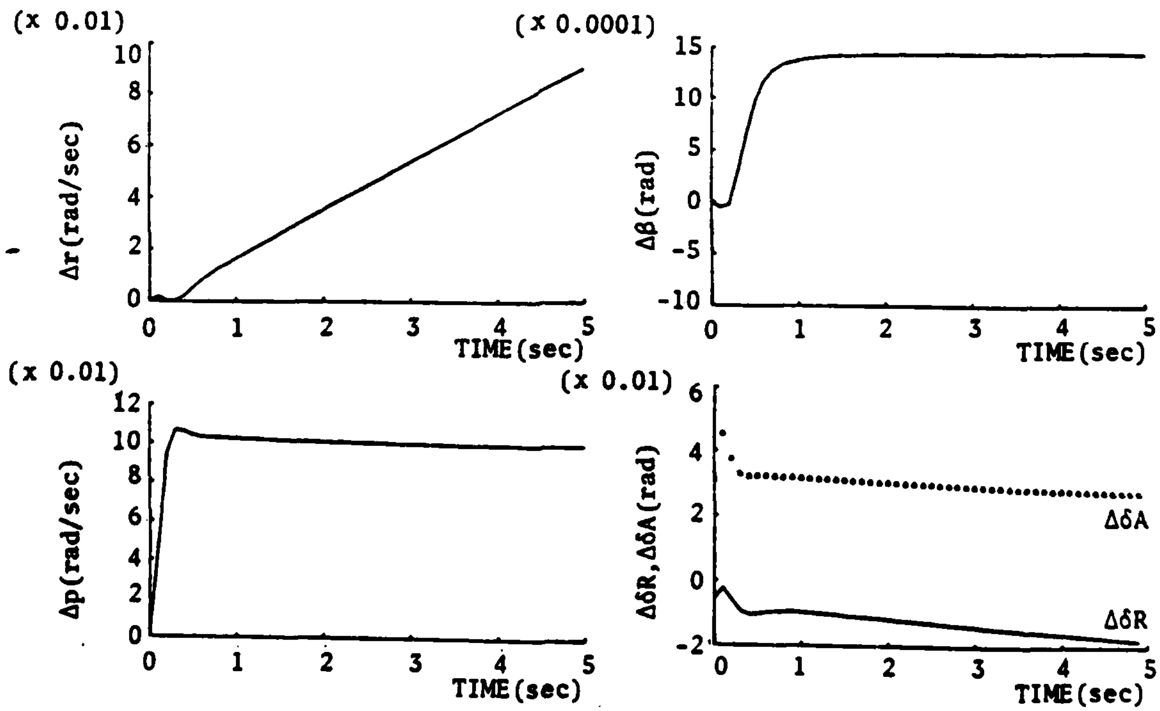

b. Response for Commanded Roll Rate, y_d = .1 rad/sec.

Figure 2-6. Step Responses for β,p Mode A.

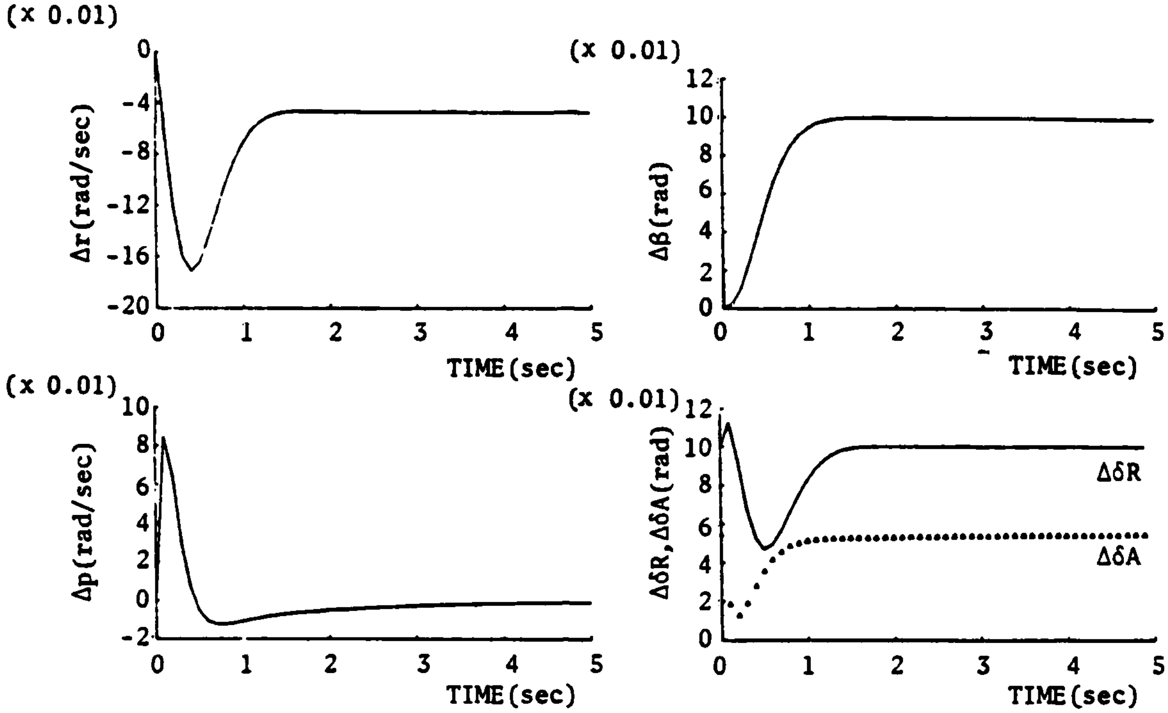

a. Response for Sideslip Angle Command, y_d = .1 RAD.

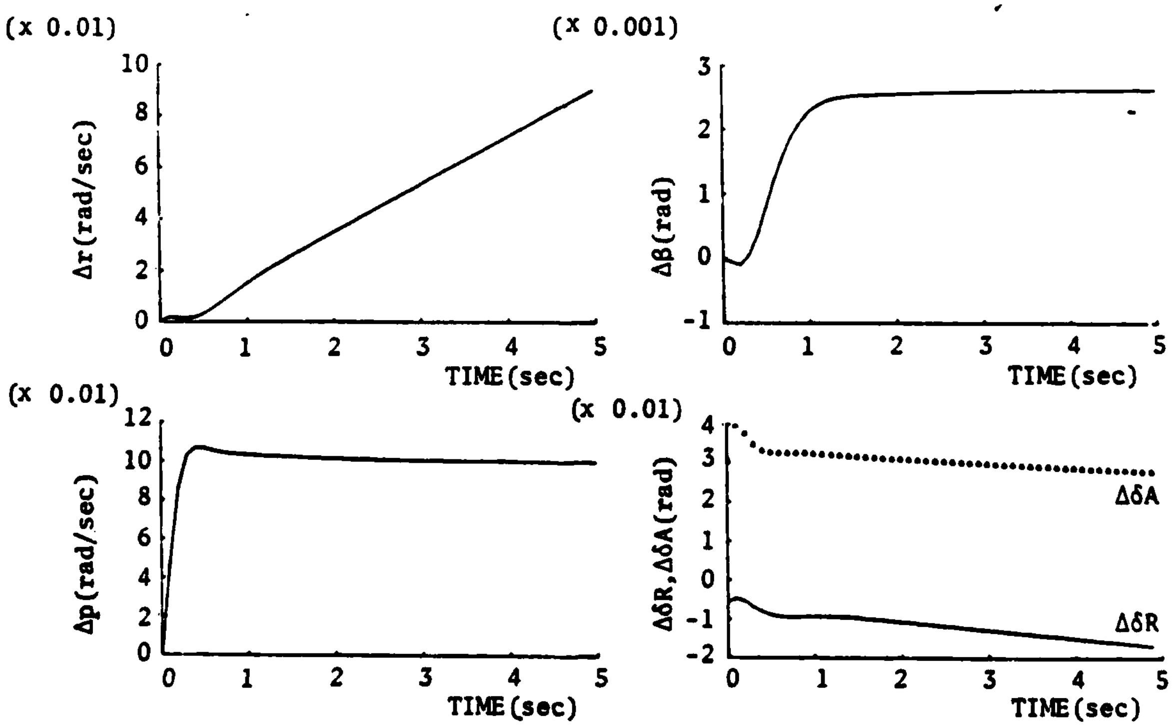

b. Response for Roll Rate Command, y_d = .1 rad/sec.

Figure 2-7. Step Responses for β,p Mode B.

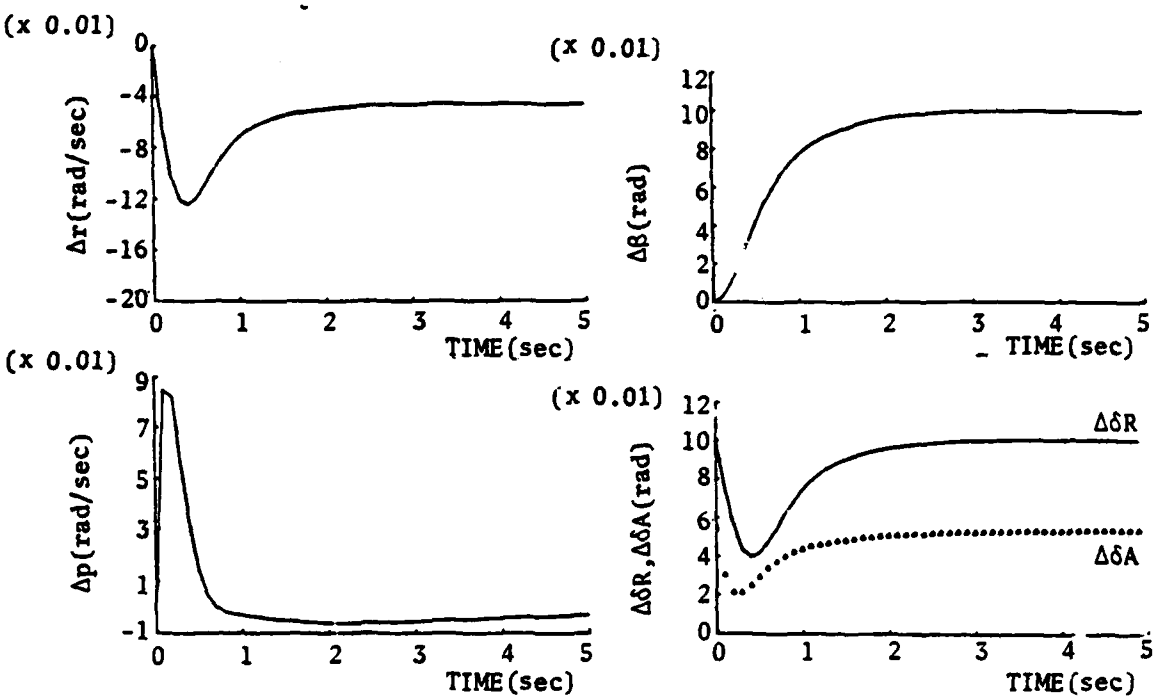

a. *Response for Sideslip Angle Command, y_d = .1 RAD.*

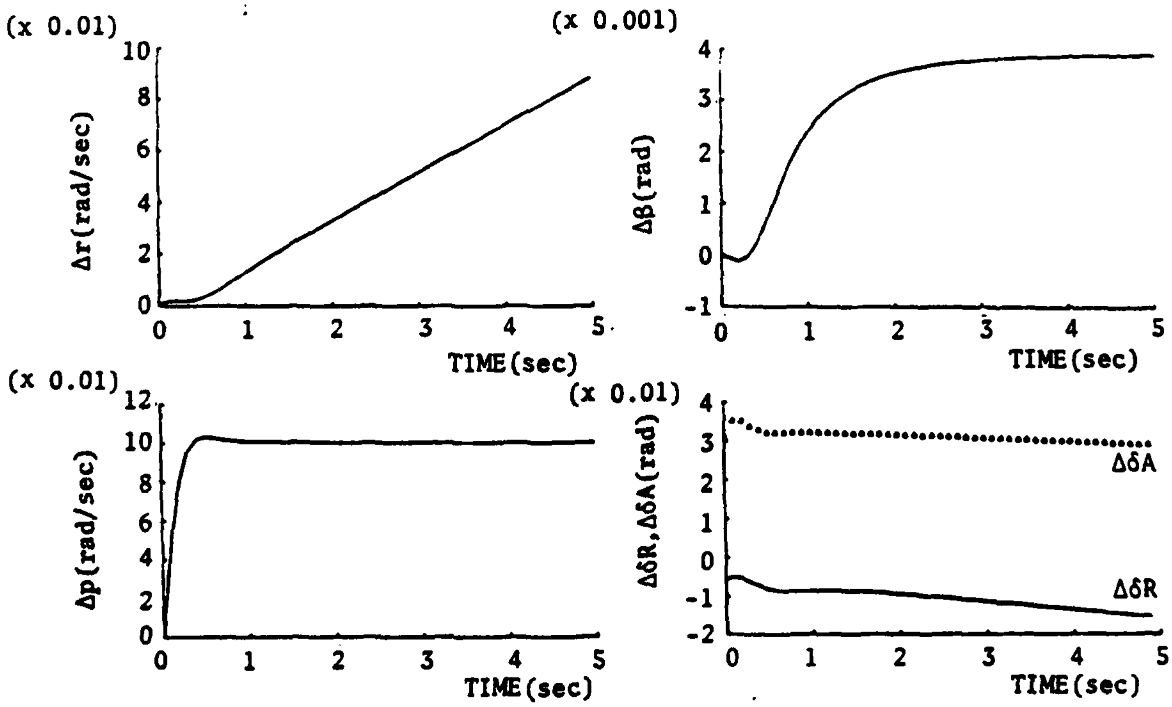

b. Response for Roll Rate Command, y_d = .1 rad/sec.

Figure 2-8. Step Responses for β,p Mode C.

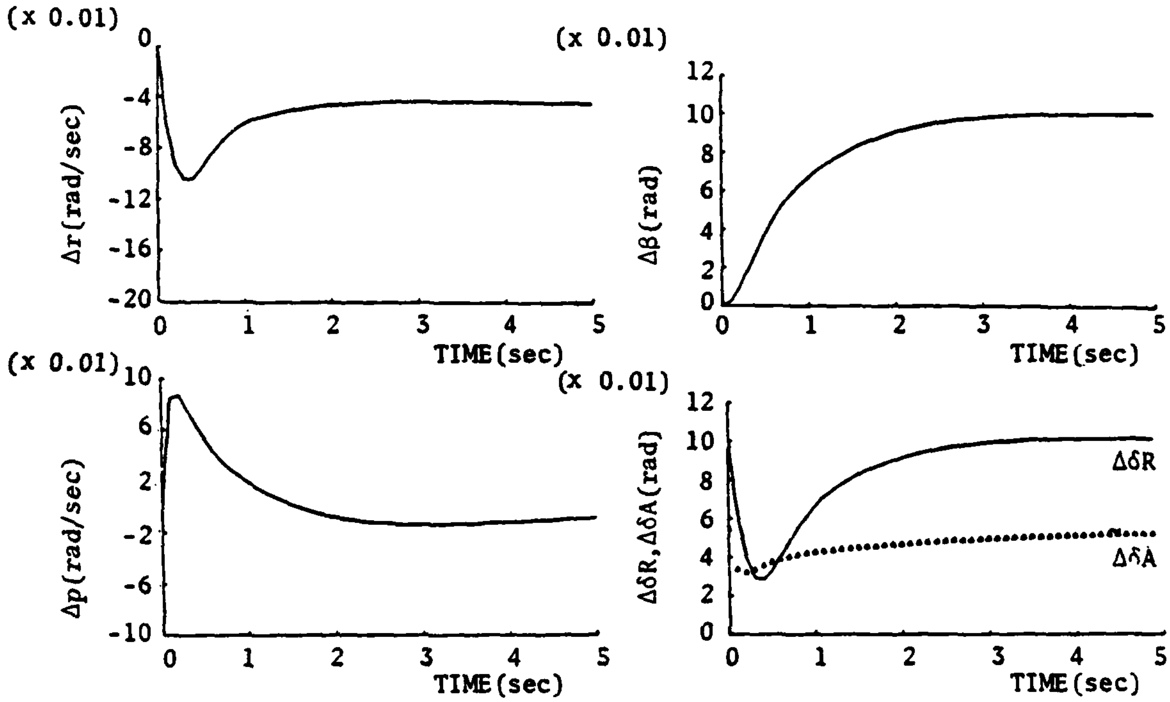

a. Response for Sideslip Angle Command, y_d = .1 rad/sec.

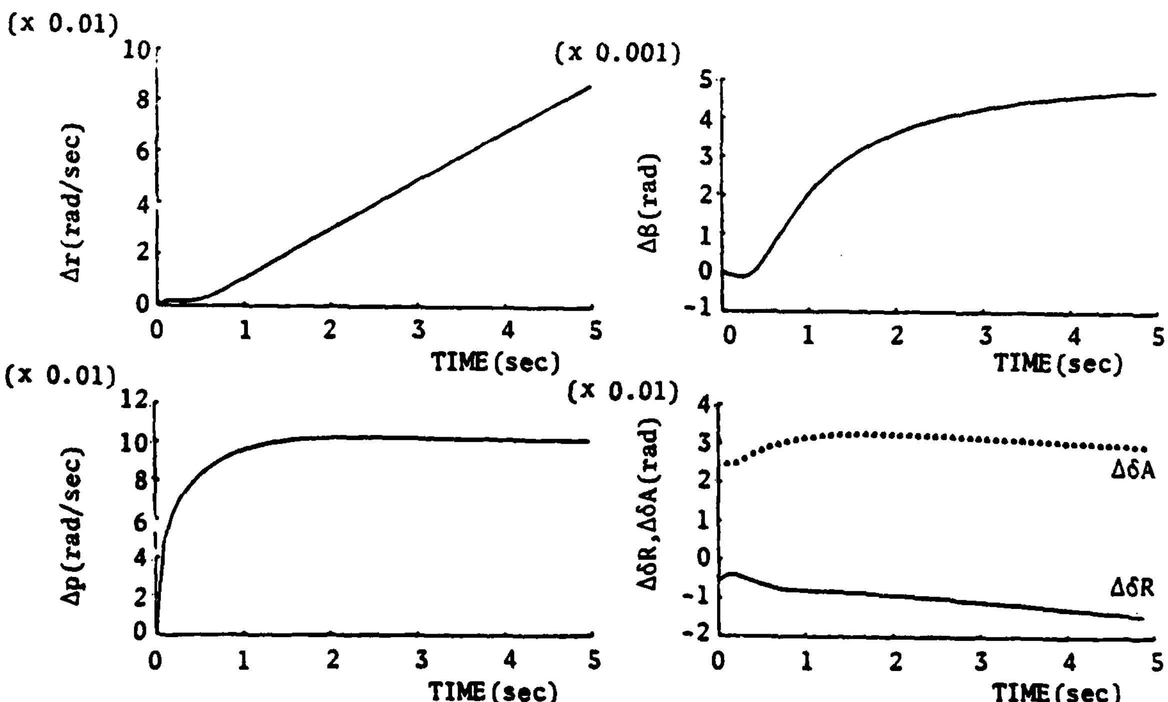

b. Response for Roll Rate Command, y_d = .1 rad/sec.

Figure 2-9. Step Responses for β,p Mode D.

with basically uncoupled lateral and directional dynamics. For a command in sideslip angle, the rudder primarily shapes the step response, while the aileron acts to counter the dihedral effect of the aircraft. Roll rate/sideslip angle control mode A presents a vivid example of how the rudder shapes the command response: following the initial steady-state deflection, rudder deflection immediately increases to provide rapid control response, then decreases rapidly to control the overshoot. Rudder deflection then increases to its steady-state position as the desired sideslip angle is attained. This same pattern is exhibited in all the various control modes, except that the slower modes are characterized by an immediate decrease in the control surface deflection to provide a slower acquisition of the commanded value. This mode also presents a good example of how aileron deflection is used to counter the rolling caused by the dihedral effect. Positive aileron is used to produce positive roll rate in order to counter the negative rolling tendency of the aircraft, as is seen in the open-loop response. Because the buildup of negative roll rate is slow, however, the initial positive aileron deflection produces the roll rate transient exhibited in all the time histories. The control law recognizes this transient and immediately reduces the aileron deflection until the dihedral effect builds up. Aileron deflection is then increased to provide the desired balancing effect.

Similar characteristics are demonstrated in the time histories for roll rate command responses; aileron deflection is used to shape the command response, while rudder acts to provide good turn coordination and to eliminate the adverse yaw characteristics. Note that for a commanded right roll (positive aileron), the control law produces right (negative) rudder to provide turn coordination, just as the pilot would do in the absence of command augmentation. The yaw rate time histories show the absence of the adverse yaw exhibited by the open-loop responses, even though a finite lag is evident before the nose of the aircraft begins tracking in the desired direction of turn.

The classical response modes of the lateral-directional dynamics are greatly affected by augmenting the state vector to include control dynamics; the eigenvectors of the closed-loop system cannot be neatly categorized into Dutch roll, roll, and spiral modes. Table 2-6, for example, presents the eigenvalues, and the three largest components of the corresponding eigenvector, of the roll rate/sideslip angle Command Mode A.

Table 2-6 β, p Mode A Eigenvalues and Eigenvectors

$\omega_n(\lambda)$ rad/sec	ζ, --	Largest Component	Second Largest Component	Third Largest Component
14.558	.751	Roll Rate	Aileron	Roll Angle
9.903	.681	Rudder	Yaw Rate	Roll Rate
(-4.412)	--	Yaw Rate	Rudder	Sideslip Angle
(-0.573)	--	Roll Angle	Roll Rate	Yaw Rate

The last mode is easily identified as the spiral mode, while the second-to-last mode can be identified as being associated with the rudder dynamics. The second mode can be identified as the Dutch roll mode, while the first mode appears to be a coupled roll-aileron mode.

The Dutch roll mode is easily identified by examining the eigenvectors of the closed-loop system. The characteristics of this mode represent an important means of evaluating control laws; the Dutch roll frequency and damping coefficient show the characteristics of the dominant oscillatory response mode, while the parameter ϕ/β gives a measure of the degree of coupling of lateral and directional dynamics. These parameters for both the open- and closed-loop systems are presented in Table 2-7. These characteristics show the improvement in command response for the augmented system; the increased frequency and damping of the Dutch roll are responsible for its absence in the time histories presented, while ϕ/β shows the marked decrease in lateral-directional coupling expected of the CAS.

Table 2-7 Dutch Roll Mode Characteristics

Mode	ω_n (rad/sec)	ζ	ϕ/β
Open Loop	2.627	.203	.68
Mode A	9.903	.681	.19
Mode B	5.186	.755	.097
Mode C	5.386	.719	.244
Mode D	5.608	.727	.224

Examination of the coefficients of F_{CL}, i.e., the equivalent stability derivatives, shows how the stability derivatives have been augmented to provide the command responses shown. The open-loop and closed-loop stability derivatives are summarized in Table 2-8. Examination of these stability derivatives reveals information about the effects of the command augmentation system. The closed-loop control effectiveness stability derivatives, $N_{\delta R}$ and $L_{\delta A}$, are seen to be greatly increased over the unaugmented VRA, with the greatest increase shown for the fastest modes. Examination of the damping terms, N_r (yaw rate damping) and L_p (roll damping), reveals that in all cases except one, the modal damping has been decreased in the augmented system, with the fastest modes corresponding to the most lightly damped systems. It is interesting to note that the only exception in which one of the closed-loop damping coefficients is greater than the unaugmented VRA is an increased roll damping term in Mode D; this corresponds to the case in which state-rate weighting is used in the cost function.

In addition to the four modes of the Type 0 CAS for roll rate and sideslip angle control, a Type 1 controller for these same variables was derived. As presented in Section 2.3.4, Type 1 proportional-integral control can be attained from a Type 0 controller by transforming the gains. Because roll rate/sideslip angle control Mode C was designed to be the "average" case, it was chosen to be the basis for designing an equivalent Type 1 control law.

Table 2-8 Closed-Loop Stability Derivatives for β, p Control Modes

	Basic VRA	Mode A	Mode B	Mode C	Mode D
N_r	-.75	9.43	1.65	.62	.544
N_β	5.90	-10.64	5.18	7.27	8.0
N_p	-.26	-.67	-.37	-.32	-.33
$N_{\delta R}$	-6.10	-15.77	-10.62	-9.31	-9.30
$N_{\delta A}$	-.252	-1.25	-.57	-.47	-.69
Y_β/V	-.40	-1.03	-.43	-.36	-.34
L_r	1.16	-2.0	1.79	1.42	1.12
L_β	-11.5	-14.24	-19.93	-15.82	-19.03
L_p	-6.5	1.75	-3.07	-5.19	-9.03
$L_{\delta R}$	.58	4.09	1.52	1.32	2.25
$L_{\delta A}$	21	56.52	42.23	33.10	37.35

Following the derivation of the Type 1 controller presented in Section 2.3.4, the Type 0 gains are transformed to Type 1 gains by taking into account the system dynamics. Because the compound matrix used in this transformation is non-invertible, the second method of finding the optimal gains applies, and the Type 1 gains are found using Equation 2.3-69 and 2.3-70. Using the gains from the Type 0 Control Mode C as the basis for the transformation, the Type 1 gains are found to be

$$C_1 = \begin{bmatrix} -1.075 & 3.532 & -.014 \\ .018 & .099 & .433 \end{bmatrix} \qquad (2.5\text{-}9)$$

$$C_2 = \begin{bmatrix} .486 & -.044 \\ .118 & .250 \end{bmatrix} \qquad (2.5\text{-}10)$$

Note that only a third-order state vector is used to provide Type 1 control for a fourth-order system (See Appendix B for the derivation of this transformation and control law). Using these gains and the Type 1 control law presented in Equation 2.3-75, the command response characteristics of this controller were computed, and its time histories

are presented in Figure 2-10. Note the very nearly identical command responses as compared with Mode C, and the nearly identical rise times: approximately 0.4 seconds for both roll rate commands, and about 2.1 seconds for the Type 1 sideslip angle response, as opposed to 1.8 seconds for Mode C.

The Type 1 properties of this control law are evident in the time histories. As opposed to the Type 0 controllers, where the control law did not act to null the steady-state errors, here no hang-off error exists. In the case of a commanded step in sideslip angle, the roll transient still occurs due to the positive aileron input, but now the error is nulled. Similarly, for a roll rate command, a sideslip angle transient occurs, but this error also is nulled by the system. Here, all adverse yaw characteristics are eliminated, and, as noted by the linear response in yaw rate, the nose of the aircraft immediately begins tracking in the desired direction of turn. Other properties of this Type 1 control law will be presented later in this report.

2.5.2 Roll Rate/Lateral Acceleration Command

The second choice of command variables for the lateral-directional CAS includes lateral acceleration control rather than sideslip angle control. Following the development presented in Figure 2-3, there are two methods of providing these command variables. The first option is to use the F and G matrices presented earlier, but to command lateral acceleration and roll rate by a suitable choice of observation matrices H_x and H_u. Using the relationship for lateral acceleration given earlier,

$$\Delta a_y = Y_\beta \Delta_\beta + Y_{\delta R} \Delta_{\delta R} \qquad (2.4\text{-}33)$$

such a suitable choice would be,

$$H_x = \begin{bmatrix} 0 & Y_\beta & 0 & 0 \\ 0 & 0 & 1 & 0 \end{bmatrix} \; ; \; H_u = \begin{bmatrix} Y_{\delta R} & 0 \\ 0 & 0 \end{bmatrix} \qquad (2.5\text{-}11)$$

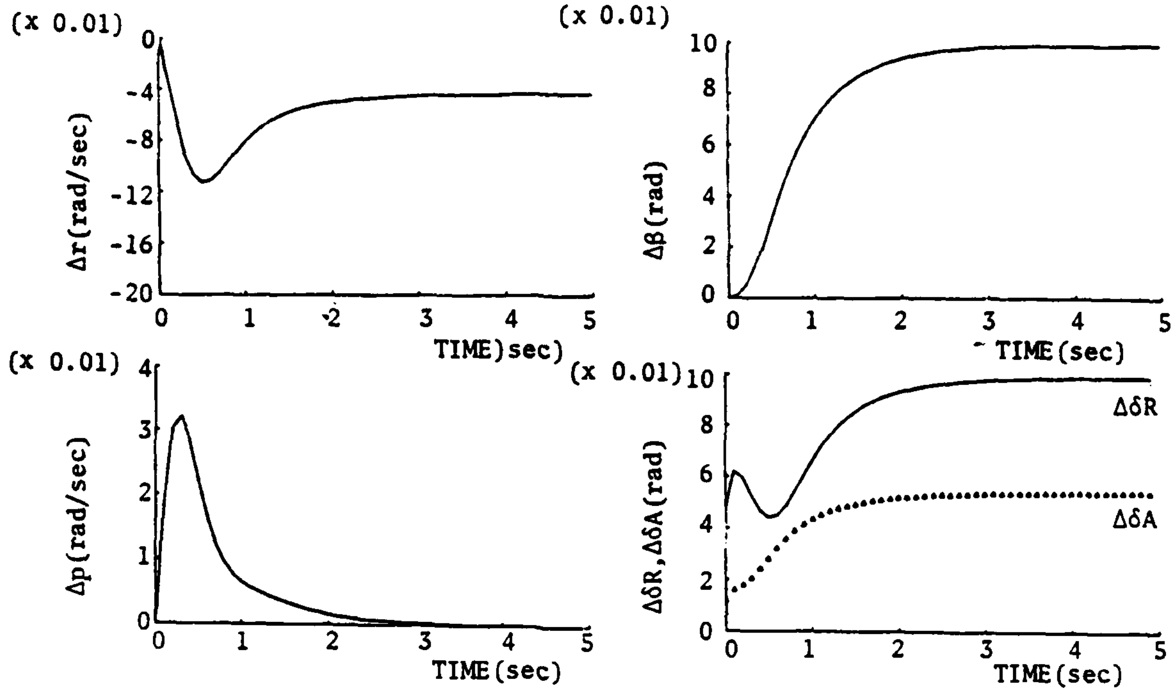

a. Response for Sideslip Angle Command, y_d = .1 RAD.

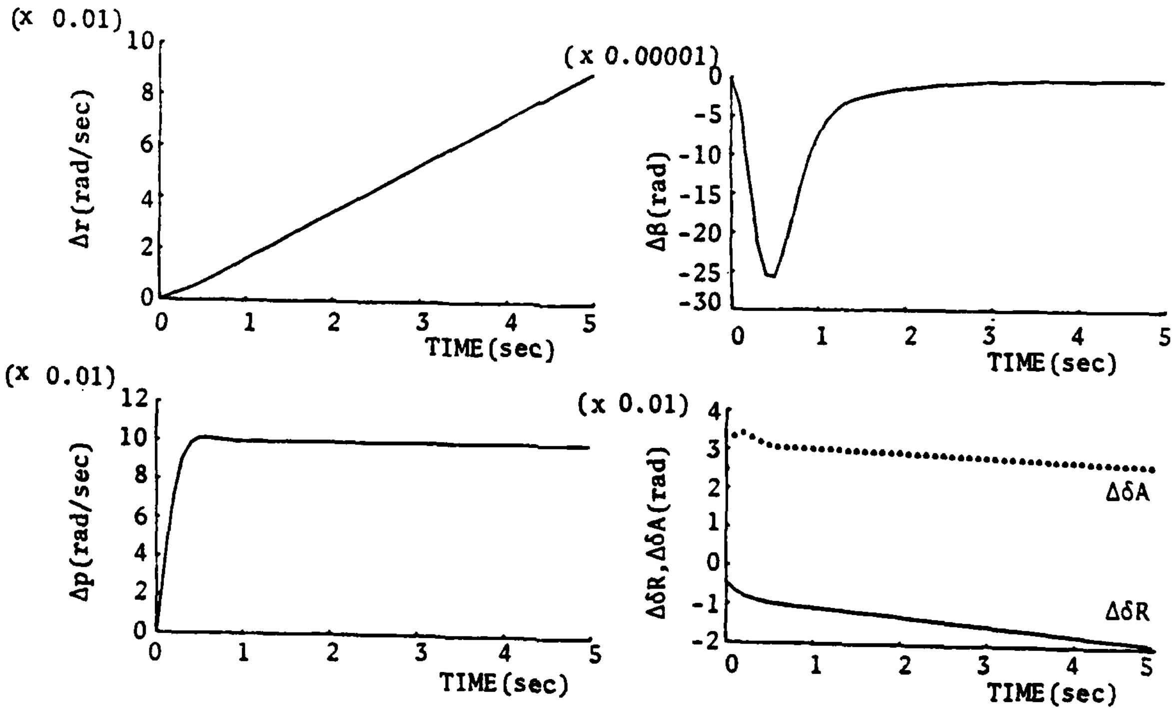

b. Response for Roll Command, y_d = .1 rad/sec.

Figure 2-10. TYPE 1 Command Augmentation System.

Using this approach, lateral acceleration would be controlled by feeding back yaw rate, sideslip angle, roll rate, and roll angle.

An alternative approach, and the approach that is used in this investigation, is to replace sideslip angle in the state vector with lateral acceleration, redefining matrices F and G to reflect this change. This approach is advocated for one reason: most aircraft have the capability to measure acceleration, whereas sideslip angle is difficult to measure; by designing the control laws in this fashion, the need to measure sideslip angle is eliminated, as is the need to provide an accurate estimate of sideslip angle based on other measurements. Using this approach, the control law development proceeds as follows.

Matrices F and G are transformed to contain lateral acceleration dynamics. Using the expression for lateral acceleration given by Equation 2.4-33, the resulting matrices are given by

$$F = \begin{bmatrix} N_r & N_\beta/Y_\beta & N_p & 0 \\ Y_\beta(Y_r/v-1) & Y_\beta/V & Y_p Y_\beta/V & Y_\beta g/V \\ L_r & L_\beta/Y_\beta & L_p & 0 \\ 0 & 0 & 1 & 0 \end{bmatrix} \tag{2.5-12}$$

$$G = \begin{bmatrix} (N_{\delta_R} - N_\beta \frac{Y_{\delta R}}{Y_\beta}) & N_{\delta A} \\ 0 & Y_\beta Y_{\delta A}/V \\ L_{\delta_R} - L_\beta \frac{Y_{\delta R}}{Y_\beta} & L_{\delta A} \\ 0 & 0 \end{bmatrix} \tag{2.5-13}$$

where

$$\underline{x}^T = [\Delta r \quad \Delta a_y \quad \Delta p \quad \Delta\phi] \tag{2.5-14}$$

In straight-and-level flight at 105 KIAS, and normalizing lateral acceleration by the force of gravity,

$$F = \begin{bmatrix} -.75 & -2.67 & -.26 & 0 \\ 2.204 & -.4 & 0 & -.403 \\ 1.16 & 5.216 & -6.5 & 0 \\ 0 & 0 & 1 & 0 \end{bmatrix} \tag{2.5-15}$$

$$G = \begin{bmatrix} -7.13 & -.252 \\ 0 & 0 \\ 2.59 & 21. \\ 0 & 0 \end{bmatrix} \tag{2.5-16}$$

with Δa_y given in units of g's.

With these matrices governing system dynamics, the design proceeds by suitable choice of matrices, H_x and H_u, which define the command vector,

$$\Delta \underline{y}^T = [\Delta a_y \quad \Delta p] \tag{2.5-17}$$

These matrices are given by

$$H_x = \begin{bmatrix} 0 & 1 & 0 & 0 \\ 0 & 0 & 1 & 0 \end{bmatrix} \; ; \; H_u = \begin{bmatrix} 0 & 0 \\ 0 & 0 \end{bmatrix} \tag{2.5-18}$$

Using these values, and using the approach followed in the previous section, steady-state relationships are found to be

$$\begin{bmatrix} \Delta r^* \\ \Delta a_y{}^* \\ \Delta p^* \end{bmatrix} = \begin{bmatrix} .183 \\ 0 \\ 0 \end{bmatrix} \Delta\phi^* + \begin{bmatrix} .181 & 0 \\ 1.0 & 0 \\ 0 & 0.1 \end{bmatrix} \Delta \underline{y}_d \tag{2.5-19}$$

$$\begin{bmatrix} \Delta\delta R^* \\ \Delta\delta A^* \end{bmatrix} = \begin{bmatrix} -.019 \\ -.008 \end{bmatrix} \Delta\phi^* + \begin{bmatrix} -.386 & -.048 \\ -.211 & .315 \end{bmatrix} \Delta \underline{y}_d \tag{2.5-20}$$

As was done for the sideslip angle controller, several sets of weightings are used to present the pilot with several different sets of dynamic characteristics. These weighting factors, along with the associated response characteristics, are presented in Table 2-9. Note the effects of the weighting factors on the step responses: merely including weighting on the rate of change of lateral acceleration significantly increases the acceleration response rise time, while the same effect is derived in the roll response by weighting roll acceleration and by increasing the weightings on aileron control rate. The optimal gains for each of these command modes are presented in Table 2-10, while Figures 2-11 through 2-13 present the time histories for step inputs in each of these modes.

The closed-loop step response characteristics for the lateral acceleration/roll rate command modes shown are nearly identical to the step responses of the sideslip angle/roll rate command modes; additionally, the effects of the controller on the closed-loop stability derivatives, shown in Table 2-11 are very similar to the effects of the sideslip angle control laws. Inasmuch as the control characteristics of the two different command structures are nearly identical, using lateral acceleration control rather than sideslip angle control may prove desirable when sideslip angle measurements are not possible.

2.5.3 Roll Rate/Yaw Rate Command

The combination of roll rate and yaw rate commands provides a third alternative for the digital CAS. Decoupled control of these two variables provides rather unusual control characteristics, with foot pedals producing a flat, or "skid", turn capability and lateral stick producing a "knife-edge" flight condition; in this respect, from an actual design viewpoint, a control law which governs these two variables may not have practical significance. This unusual combination is useful, however, in that it demonstrates some of the problems and capabilities of the control law design process.

Table 2-9 Weighting Factors and Response Characteristics for a_y, p CAS

		Mode A	Mode B	Mode C
	Δr	30	15	15
State	Δa_y	250	15	15
Weightings	Δp	100	15	15
	$\Delta\phi$	25	5	5
Control	$\Delta\delta R$	33	15	15
Weightings	$\Delta\delta A$	33	15	15
Control Rate	$\Delta\dot{\delta}R$	1	1	1
Weightings	$\Delta\dot{\delta}A$	1	1	20
	$\Delta\dot{r}$	0	0	0
State Rate	$\Delta\dot{a}_y$	0	0	5
Weightings	$\Delta\dot{p}$	0	0	1
	$\Delta\dot{\phi}$	0	0	0
Roll	Rise Time	.20 sec	.27 sec	.55 sec
Command	% Overshoot	6.4%	6.3%	3.6%
Lat. Acc.	Rise Time	.68 sec	1.24 sec	1.97 sec
Command	% Overshoot	2.0%	.17%	.09%
$\omega_{n_{DR}}$		6.455 rad/sec	5.107 rad/sec	6.54 rad/sec
ζ_{DR}		0.65	0.70	0.74

Table 2-10 Optimal Gains for a_y, p CAS

Mode	K_1				K_2	
A	-5.68	-2.82	0.31	1.06	11.39	.88
	1.40	2.25	1.36	2.14	-.17	11.80
B	2.34	.63	.14	.27	7.55	.48
	.73	1.16	.61	1.41	-.09	7.62
C	-2.98	1.56	.02	.40	8.82	.81
	.39	.46	-.14	.36	-.23	3.51

Table 2-11 Closed Loop Stability Derivatives for a_y, p Control Modes

	Basic VRA	Mode A	Mode B	Mode C
N_r	-.75	4.12	.88	1.71
N_{a_y}	-2.67	.92	-2.79	-3.45
$N_{\delta R}$	-7.13	-14.75	-11.19	-12.44
L_{a_y}	5.216	10.37	7.60	6.54
L_p	-6.5	1.68	-4.52	-6.92
$L_{\delta A}$	21.	57.53	35.72	27.46

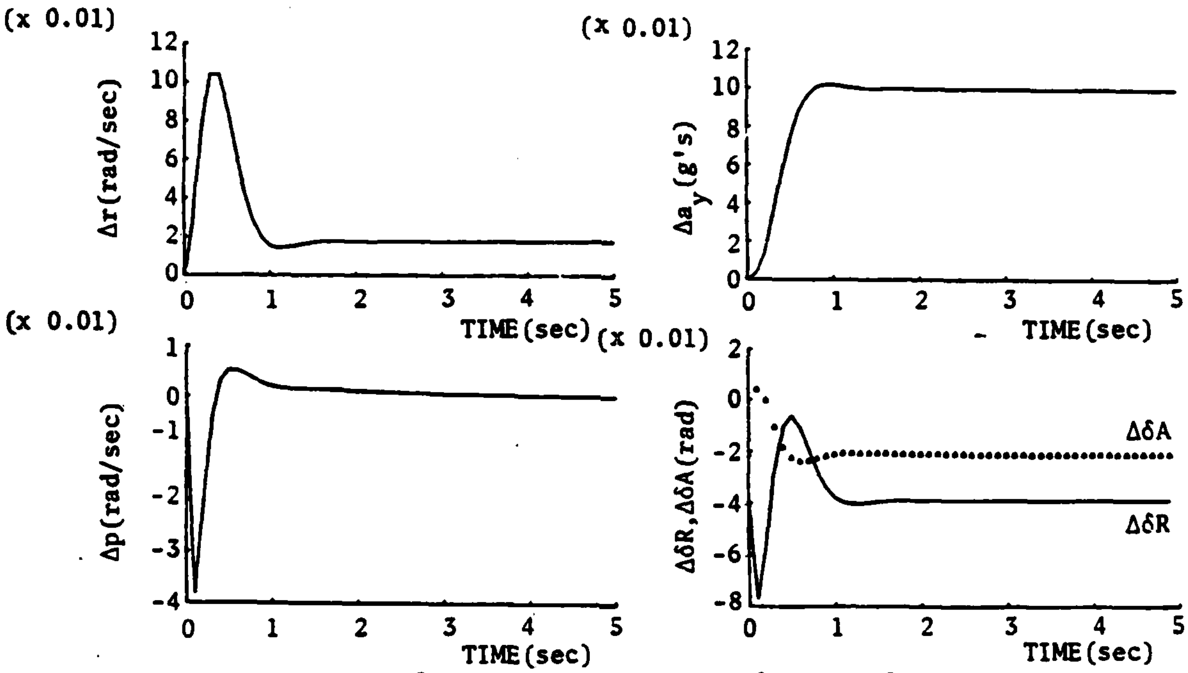

a. Response for Acceleration Command, y_d = .1 g.

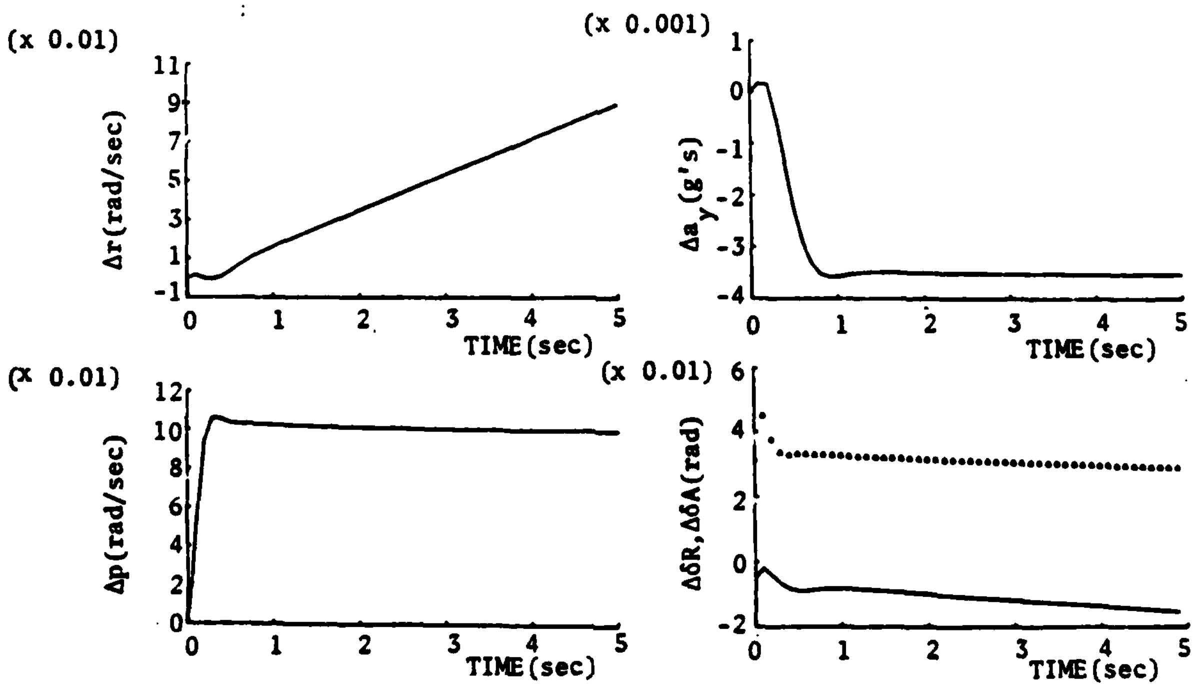

b. Response for Roll Rate Command, y_d = .1 rad/sec.

Figure 2-11. Step Responses for a_y,p Mode A.

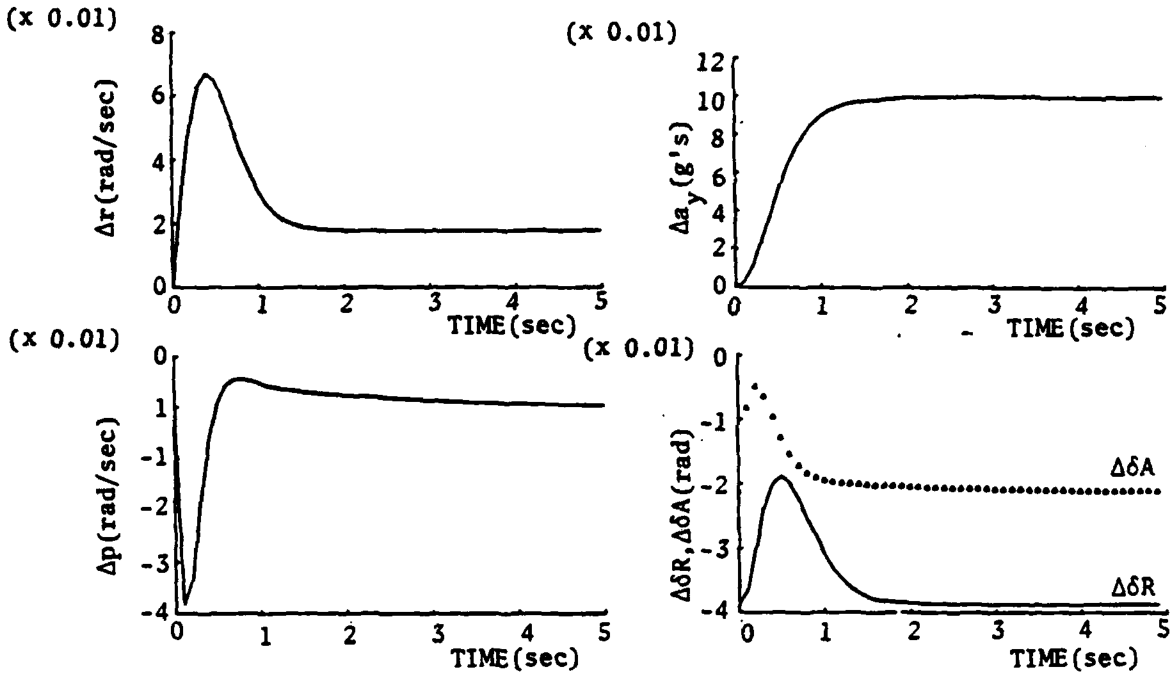

a. Response for Acceleration Command, y_d = .1 g.

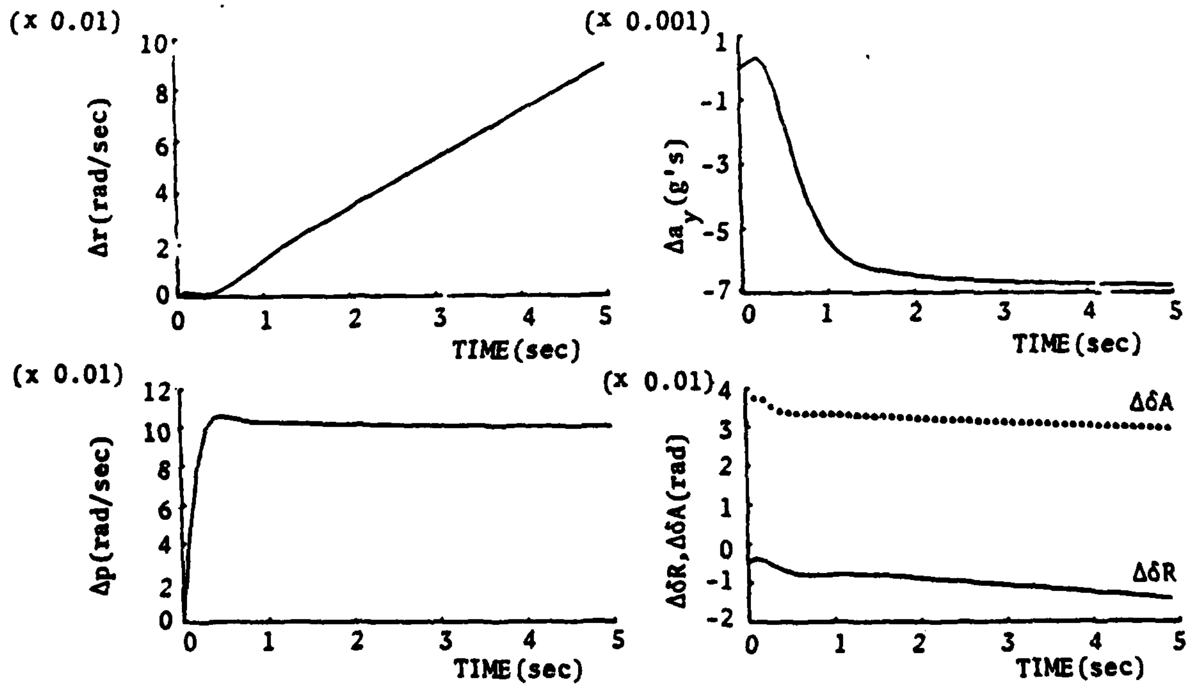

b. Response for Roll Rate Command, y_d = .1 rad/sec.

Figure 2-12. Step Responses for a_y,p Mode B.

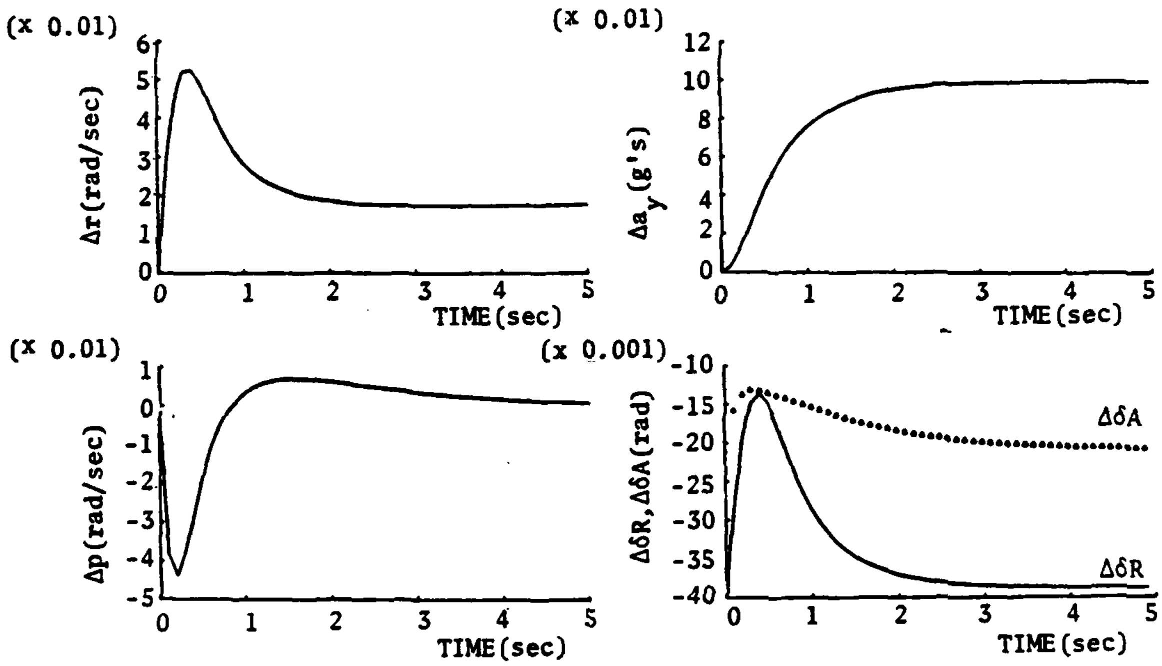

a. Response for Acceleration Command, y_d = .1 g.

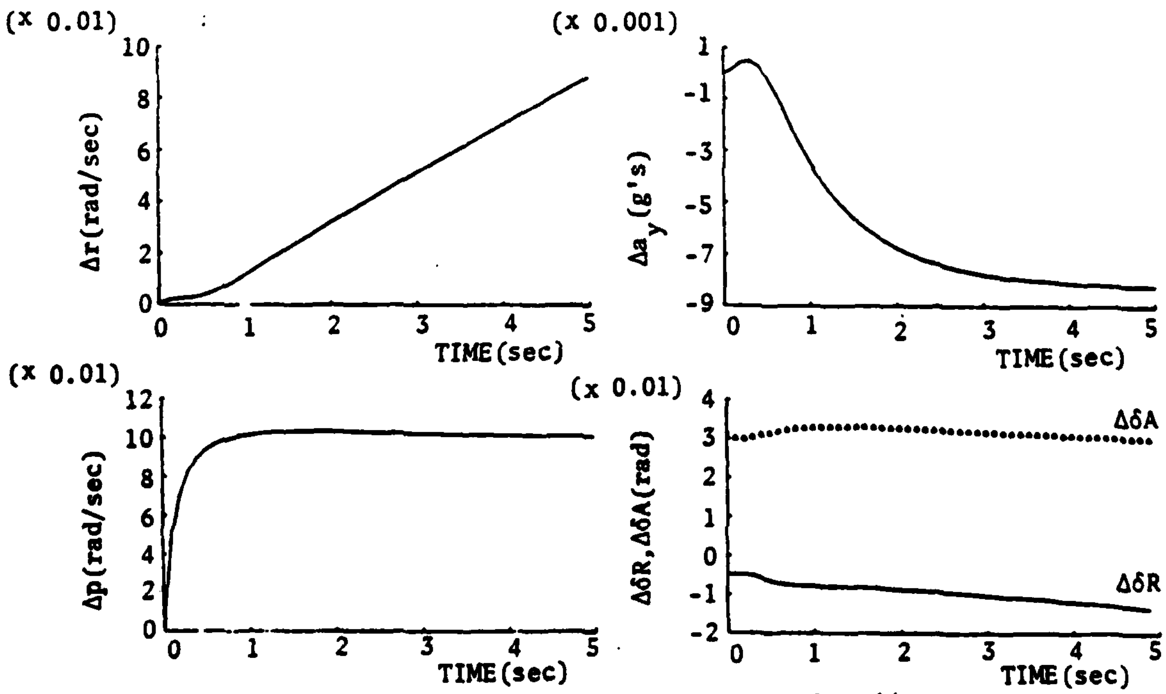

b. *Response for Roll Rate Command, y_d = .1 rad/sec.*

Figure 2-13. Step Responses for a_y,p Mode C.

Using the F and G matrices associated with the roll rate/sideslip angle CAS, the design proceeds by specifying the command vector and its defining observation matrices,

$$\Delta \underline{y}_d = [\Delta r \quad \Delta p] \tag{2.5-21}$$

$$H_x = \begin{bmatrix} 1 & 0 & 0 & 0 \\ 0 & 0 & 1 & 0 \end{bmatrix} \quad ; \quad H_u = \begin{bmatrix} 0 & 0 \\ 0 & 0 \end{bmatrix} \tag{2.5-22}$$

Using these, the steady-state relationships between pilot commands and state and control positions are determined. Again, these are found using the reduced-order state vector, since roll rate is one of the command variables. The relationship of interest here is that between steady-state control deflection and pilot command,

$$S_{22} = \begin{bmatrix} -2.132 & -0.048 \\ -1.161 & 0.315 \end{bmatrix} \tag{2.5-23}$$

When commanding yaw rate, control position is given by

$$\begin{bmatrix} \Delta\delta R^* \\ \Delta\delta A^* \end{bmatrix} = \begin{bmatrix} -2.132 \\ -1.161 \end{bmatrix} \Delta r_c \tag{2.5-24}$$

where the subscript c indicates the command value.

While not immediately apparent, this relationship helps demonstrate some of the limitations of the control law, when the law is derived using a difference approximation for control rate. Using the above relationship, it should be noted that any substantial yaw rate command causes steady-state control positions which are far from the nominal control positions; for example, a commanded turn rate of 5 degrees per second gives a steady-state response of over 10 degrees and 5 degrees for rudder and aileron, respectively. The problems with this are threefold: first, the control law specifies that the initial control positions are identically the steady-state values; second, this large

initial control deflection produces correspondingly large transients in the response characteristics; and, third, rudder deflection produces immediate yaw rate response, as evident in all of the step responses presented thus far. The combination of these effects produces a significant problem for the control law: the transient overshoot in the yaw rate command initial response cannot be corrected by adjusting this control law's weighting matrices. Indeed, in time histories generated, overshoots in the yaw rate command response of over 300 percent existed regardless of the weightings chosen.

It was this situation that dictated the necessity of finding a different approach to generate control position output from a control rate command structure, leading to the Tustin Transform approach presented in Section 2.3.3. Using the Tustin Transform, the control law is

$$\Delta \underline{u}_K = \left(\frac{2}{\Delta t} I + K_2\right)^{-1}\left[\left(\frac{2}{\Delta t} I - K_2\right)\Delta \underline{u}_{K-1} - K_1(\Delta \underline{\tilde{x}}_K - \Delta \underline{\tilde{x}}_{K-1}) + K_2(\Delta \underline{u}^*_K - \Delta \underline{u}^*_{K-1})\right] \tag{2.3-59}$$

This control law structure has an obvious advantage: the initial response depends upon the optimal gains. The dramatic effect of this is seen in the three yaw rate command responses shown in Figure 2-14, for the weightings presented in Table 2-12. All responses are for a command in yaw rate of 0.1 radian per second. The effect of state rate weightings also is dramatic when the control law is allowed to temper the initial command response.

Because this control law structure was derived late in the investigation, and because of the unusual aircraft response characteristics associated with these two command variables, an in-depth evaluation of the closed-loop control characteristics was not conducted, nor was this form of the control law further developed for actual implementation in the VRA. A representative set of command responses for both yaw rate and roll rate command, however, is presented in Figure 2-15; these time histories show how such a CAS would affect the aircraft's command response characteristics. Figure 2-15a presents the response to foot

Table 2-12 Weightings and Step Response Characteristics for Yaw Rate Commands

Weightings	Case 1	Case 2	Case 3
Δr	25	25	25
$\Delta\beta$	30	30	30
Δp	10	10	10
$\Delta\phi$	0.5	0.5	0.5
$\Delta\delta R$	15	15	15
$\Delta\delta A$	15	15	15
$\Delta\dot{\delta R}$	0.9	0.9	0.9
$\Delta\dot{\delta A}$	0.9	0.9	0.9
$\Delta\dot{r}$	0	20	40
$\Delta\dot{\beta}$	0	0	40
$\Delta\dot{p}$	0	0	0
$\Delta\dot{\phi}$	0	0	0
Rise Time (sec)	0.23	0.5	0.75
% Overshoot	129%	39%	13%

pedal inputs: flat, uncoordinated skid turns, characterized by near-zero roll rate and large sideslip angle. Figure 2-15b represents the aircraft's response to lateral stick inputs: knife-edge flight, characterized by near-zero yaw rate, and a sideslip angle proportional to roll angle which produces the nose-up attitude necessary for level flight.

This is the last of the command combinations to be evaluated for the lateral-directional CAS. The remaining two sections of this chapter deal with the remaining subjects of this investigation, the design and evaluation of a sideslip angle estimator, and a comparison of Type 0 and Type 1 control structures under less than ideal conditions.

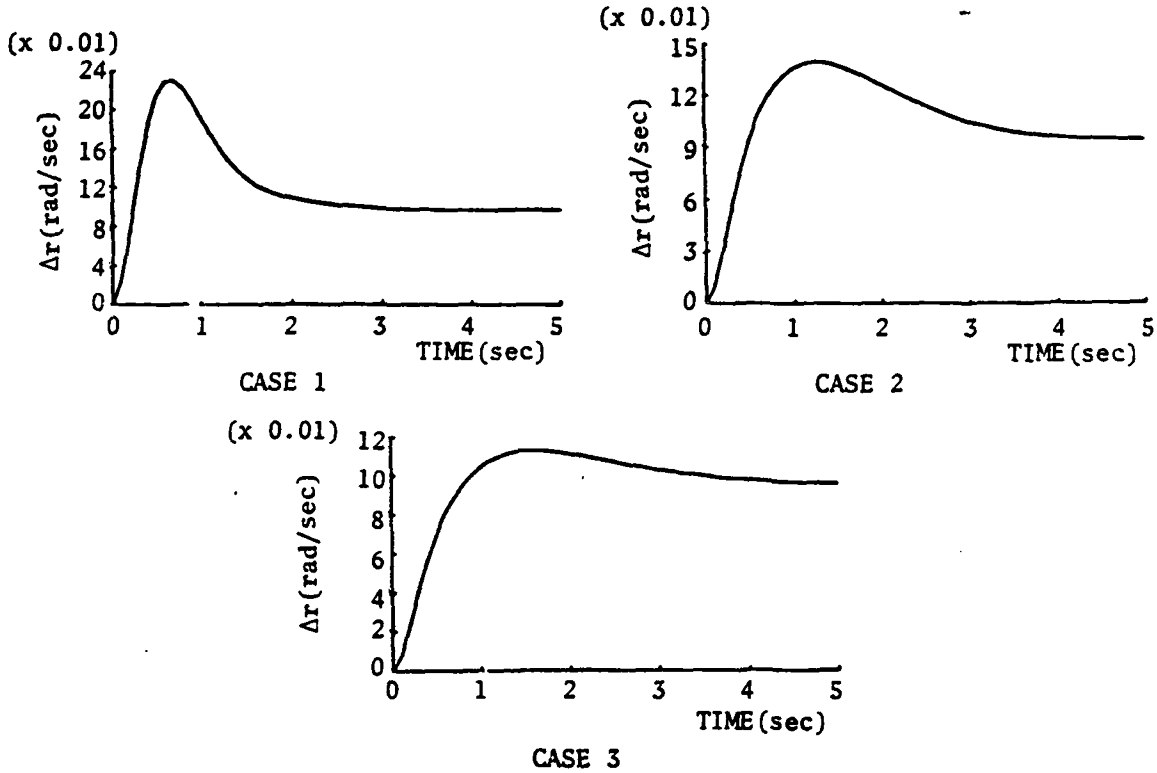

Figure 2-14. *Weighting Effects Using Tustin Transform Approach.*

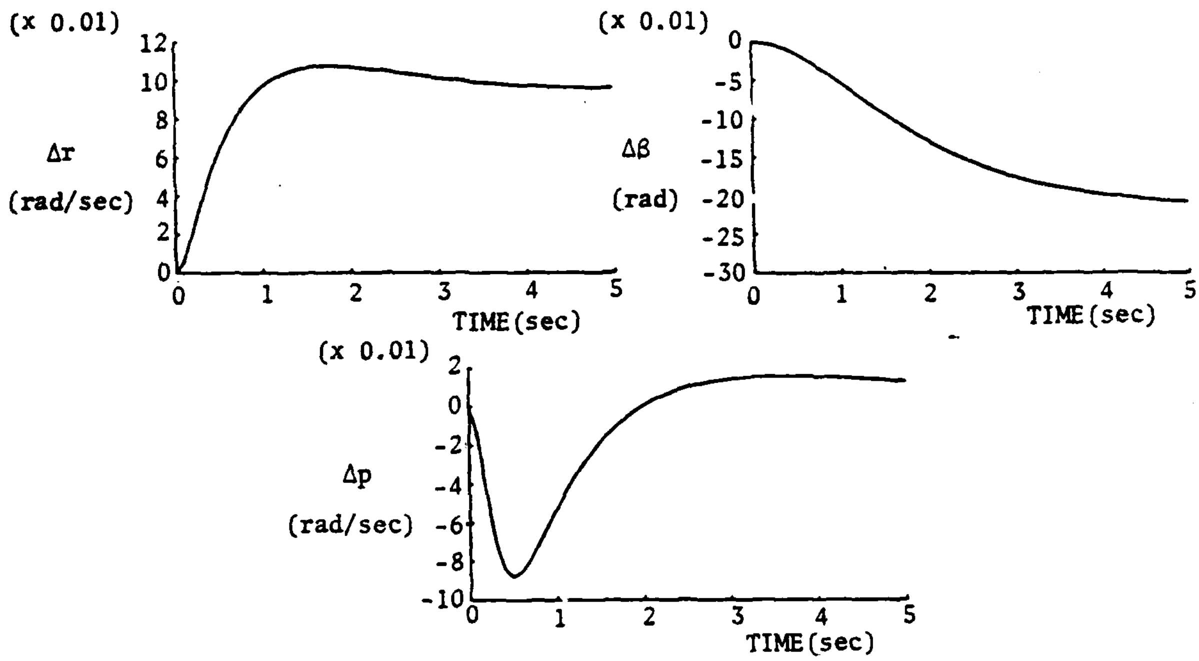

a. Response for Yaw Rate Command, Δr_d = .1 rad/sec.

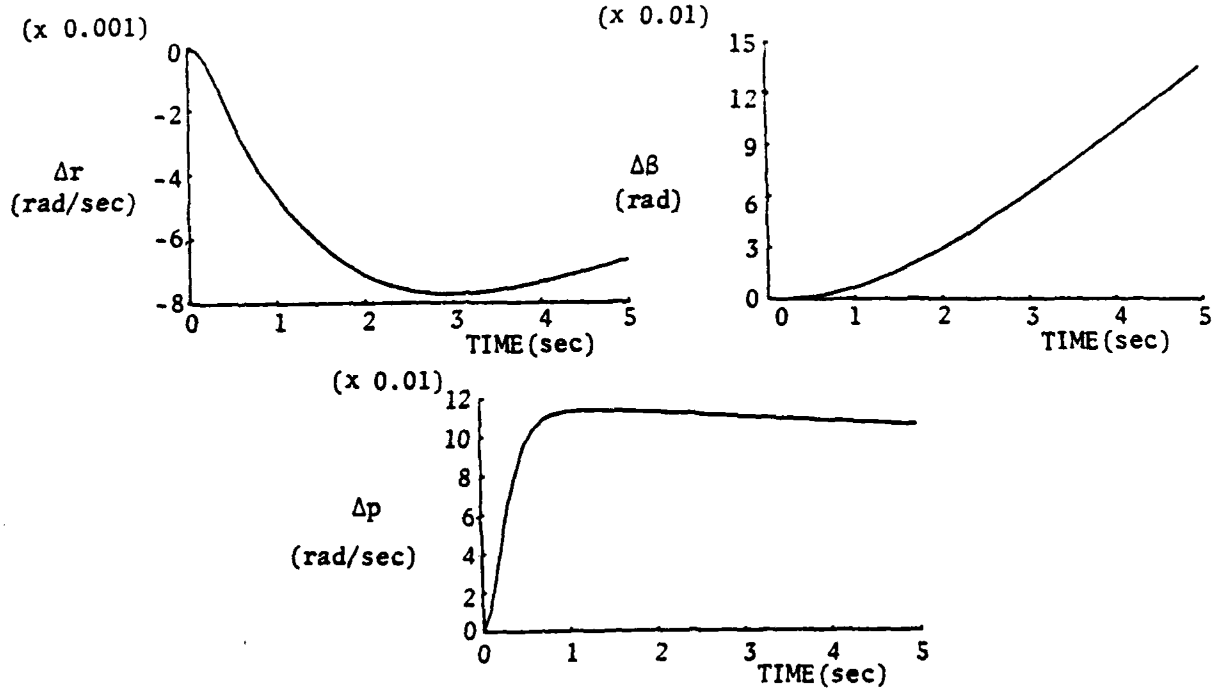

b. Response for Roll Command, Δp_d = .1 rad/sec.

Figure 2-15. Step Responses for r, p Command Mode.

AD-A110 274 PRINCETON UNIV NJ DEPT OF MECHANICAL AND AEROSPACE --ETC F/6 1/2
DIGITAL COMMAND AUGMENTATION FOR LATERAL-DIRECTIONAL AIRCRAFT D--ETC(U)
MAY 81 D ATZHORN N00014-78-C-0257
UNCLASSIFIED MAE-1511 ONR-CR-300-003-2 NL

2 of 3

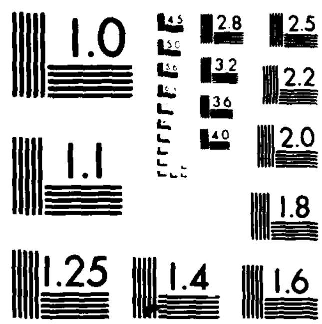

MICROCOPY RESOLUTION TEST CHART

2.5.4 Comparison of Sideslip Angle Estimators

This section presents the actual design of reduced-order sideslip angle estimators based on the Kalman Filter algorithms presented in Section 2.4-1 and based on the reduced-order models presented in Sections 2.4.2 and 2.4.3.

The first step in the design of a reduced-order estimator is to establish the validity of the truncated and residualized models presented earlier. The eigenvalues of these different models are presented in Table 2-13.

Table 2-13 Eigenvalues of Reduced-Order Models

Case	$\omega_{n_{DR}}$	δ_{DR}	λ_R	λ_S
1) Full 4th Order Model	2.627	.203	-6.575	-.0071
2) Fast Roll Mode, Neutral Spiral, Slow Dutch Roll	2.584	.23	-6.5	0
3) Fast Roll Mode, Slow Spiral, Slow Dutch Roll	2.644	.225	-6.5	-.0071
4) Fast Dutch Roll, Slow Roll, Slow Spiral	2.490	.231	-6.994	-.0074
5) Truncated 2nd Order Model	2.490	.231	-6.5	0

Based on these eigenvalues, three reduced-order models are investigated. These include the third-order model based on a fast roll mode, slow spiral and slow Dutch roll modes (Case 3); the second-order truncated model (Case 5); and the first-order model based on the equation for lateral acceleration, Equation 2.4-33.

Once the appropriate reduced-order model has been established, the sequence for finding the optimal estimator gains follows that shown in Figure 2-16. After defining the continuous-time system dynamics, control effects,and disturbance effects matrices, their discrete-time equivalents are found using Equation 2.3-5, 2.3-6,and 2.3-29. These matrices define the linear difference equations of motion which take into account disturbance inputs. Next, the measurement vector is defined by choice of H_x and H_u, where $\Delta \underline{z}_K$, the measurement vector, is given as

$$\Delta \underline{z}_K = H_{x_K} \Delta \underline{x}_K + H_{u_K} \Delta \underline{u}_K + \underline{v}_K \tag{2.5-25}$$

since measurements will include both state and control.

Defining the statistics of both the measurement noise and disturbance inputs follows next; continuous-time random disturbance are converted to their discrete-time equivalents using Equations 2.4-15 and 2.4-16. When these have been defined, the Kalman filter gains are computed using Equations 2.4-35 and 2.4-36. This algorithm is followed below in deriving third-order, second-order, and first-order sideslip angle estimators.

The third-order residualized model of sideslip angle dynamics presented in Section 2.4.2 is governed by

$$F = \begin{bmatrix} -.796 & 6.36 & 0 \\ -1. & -.4 & .181 \\ .178 & -1.769 & 0 \end{bmatrix} \; ; \; G = \begin{bmatrix} -6.123 & -1.092 \\ -.07 & 0 \\ .089 & -3.23 \end{bmatrix} \; ;$$

$$L = \begin{bmatrix} 6.36 \\ -.4 \\ -1.769 \end{bmatrix} \tag{2.5-26}$$

where

$$\Delta \underline{x}^T = [\Delta r \quad \Delta\beta \quad \Delta\phi] \tag{2.5-27}$$

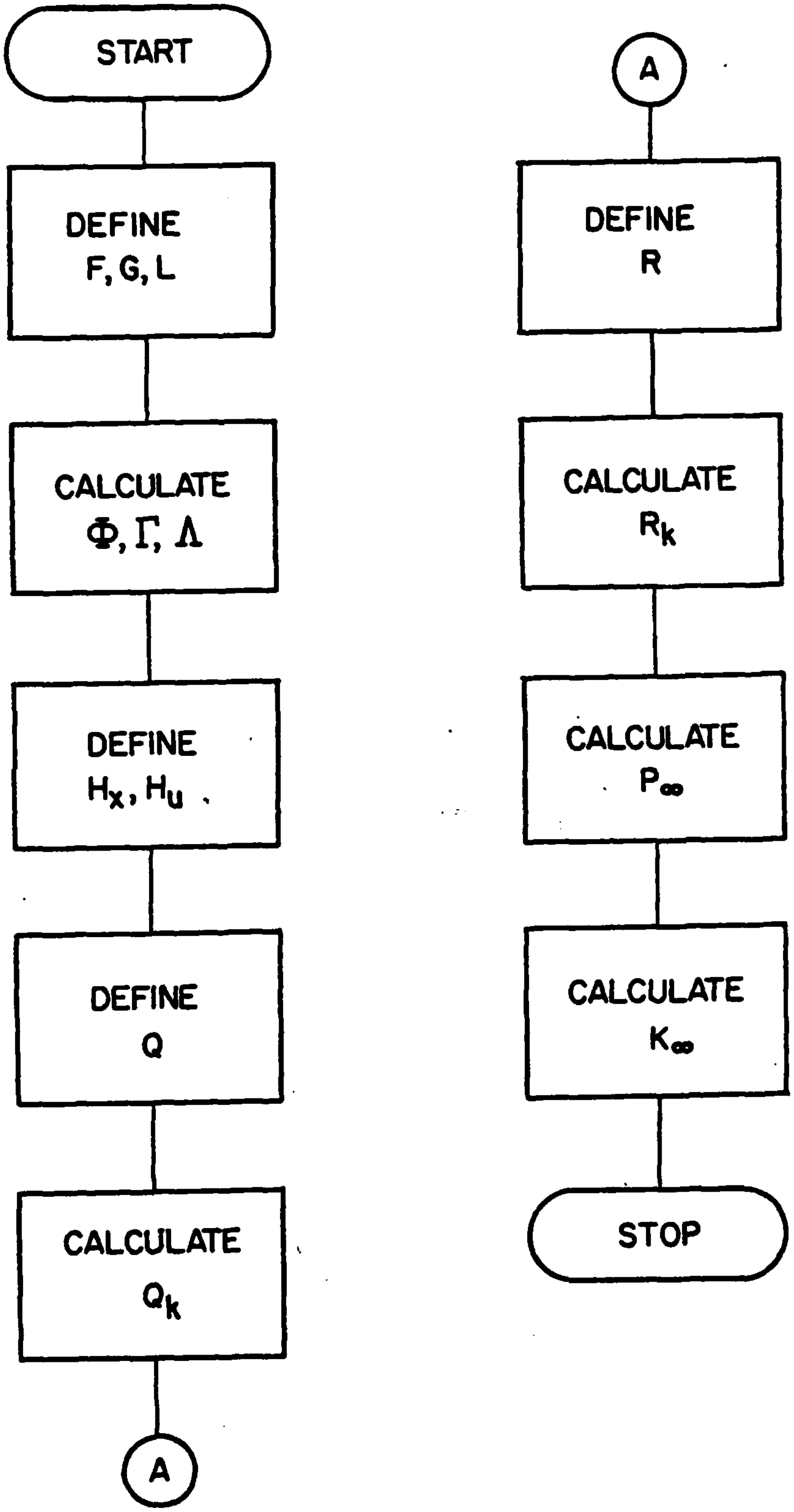

Figure 2-16. Sequence for Finding Kalman Filter Gains.

Since the estimate of sideslip angle will be based on measurements of yaw rate, lateral acceleration, and roll angle, the measurement vector is defined by

$$H_x = \begin{bmatrix} 1 & 0 & 0 \\ 0 & -2.204 & 0 \\ 0 & 0 & 1 \end{bmatrix} \; ; \; H_u = \begin{bmatrix} 0 & 0 \\ -.3858 & 0 \\ 0 & 0 \end{bmatrix} \tag{2.5-28}$$

For the purpose of this investigation, it was assumed that the disturbance input magnitude was large when compared with the measurement error magnitudes; the actual values used to describe the random noise are given in Table 2-14.

Table 2-14 Disturbance Input Intensities

Quantity	Intensity
Sideslip Angle Random Disturbance	5 deg
Yaw Rate Measurement Error	.15 deg/sec
Lat Acc Measurement Error	.003 g
Roll Angle Measurement Error	.05 deg

Using these values as the continuous-time noise descriptions, discrete-time covariance matrices are found, the steady-state covariance matrix, P_∞, is determined, and the steady-state Kalman filter gains for the third-order model are found to be

$$K_\infty = \begin{bmatrix} .643 & .023 & -1.25 \\ -.014 & -.313 & .079 \\ -.178 & -.019 & .346 \end{bmatrix} \tag{2.5-29}$$

The truncated model which governs sideslip angle dynamics is given by

$$F = \begin{bmatrix} -.75 & 5.9 \\ -1 & -.4 \end{bmatrix} \; ; \; G = \begin{bmatrix} -6.1 \\ -.07 \end{bmatrix} \; ; \; L = \begin{bmatrix} 5.9 \\ -.4 \end{bmatrix} \tag{2.5-30}$$

Using measurements of yaw rate and lateral acceleration, the measurement vector is defined by

$$H_x = \begin{bmatrix} 1 & 0 \\ 0 & -2.204 \end{bmatrix} \quad ; \quad H_u = \begin{bmatrix} 0 \\ -.3858 \end{bmatrix} \tag{2.5-31}$$

and using the same values for disturbance intensities, the second-order Kalman filter steady-state gains are found to be

$$K_\infty = \begin{bmatrix} .979 & .068 \\ -.039 & -.305 \end{bmatrix} \tag{2.5-32}$$

The first-order model of sideslip angle dynamics contains only sideslip angle in the state vector; its dynamics are governed by

$$F = [-.4] \quad ; \quad G = [-.07] \quad ; \quad L = [-.4] \tag{2.5-33}$$

Using only a measurement of lateral acceleration,

$$H_x = [-2.204] \quad ; \quad H_u = [-.3858] \tag{2.5-34}$$

and the steady-state Kalman filter gain is

$$K_\infty = [-.398] \tag{2.5-35}$$

These gains are used in the Kalman filter estimate equation, which is found by combining the state estimate extrapolation equation, Equation 2.4-12, and the state estimate update equation, Equation 2.4-7:

$$\Delta\hat{\underline{x}}_K = \Phi\Delta\hat{\underline{x}}_{K-1} + \Gamma\Delta\underline{u}_{K-1} + K_\infty[\Delta\underline{z}_K - H_x(\Phi\Delta\hat{\underline{x}}_{K-1} + \Gamma\Delta\underline{u}_{K-1}) - H_u\Delta\underline{u}_K] \tag{2.5-36}$$

The actual estimators are compared by giving the system a step rudder input, by generating time histories of each of the estimators based on actual knowledge of the system states, and by comparing the estimator responses to the actual sideslip angle response. These time histories are presented in Figure 2-17.

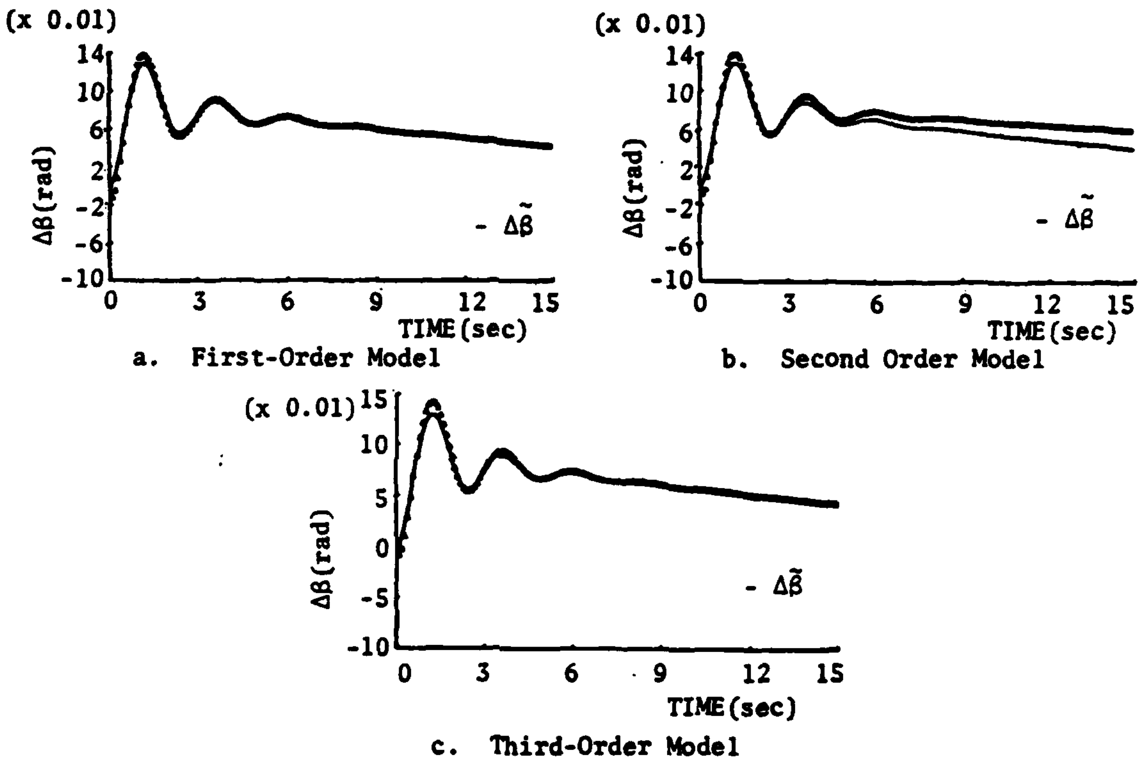

Figure 2-17. Sideslip Angle Estimator Responses.

It seems that the responses shown are inconsistent; the first-order model, while being the most inexact dynamic model, produces an estimator response which is very similar to the good estimation of the third-order model, while the second-order model diverges from the actual value. The explanation is important. The second-order model estimator diverges from the actual sideslip angle response because it does not take into account the convergent spiral mode dynamics as does the convergent third-order estimator. The first-order estimator converges because it takes into account only the linear relationship between sideslip angle and lateral acceleration. This can be seen by expanding Equation 2.5-36 for the first-order model,

$$\Delta\hat{\beta}_K = (\Phi - KY_\beta\Phi)\Delta\hat{\beta}_{K-1} + (\Gamma - KY_\beta\Gamma)\Delta\underline{u}_{K-1} - KY_{\delta R}\,\Delta\delta R_K + K\,\Delta a_{y_{m_K}} \tag{2.5-37}$$

Note that when K_∞ is approximately equal to $1/Y_\beta$, as is true in this case, the following approximations can be made:

$$(\Phi - KY_\beta\Phi) \simeq 0 \tag{2.5-38}$$

$$(\Gamma - KY_\beta\Gamma) \simeq 0 \tag{2.5-39}$$

$$\Delta\hat{\beta} \simeq K\,\Delta a_{y_K} - KY_{\delta R}\,\Delta\delta R_K \tag{2.5-40}$$

In this case, the estimator does not actually update the previous estimate, as do the other two cases; it derives an estimate based only on a knowledge of the current value of lateral acceleration and rudder position, and on the linear relationship between sideslip angle and lateral acceleration. Because the first-order estimator appeared to produce as good an estimate as the third-order estimator while minimizing necessary control computations, the first-order estimator was chosen for implementation in the lateral-directional CAS for the VRA.

2.5.5 Effects of Parameter Variations

As was mentioned earlier, the Type 0 control laws do not null steady-state errors under all conditions. Of specific interest in this investigation is how the Type 0 command response differs from Type 1 command response under these conditions: first, when disturbances are present, and, second, when the model used in the design process is different from the actual aircraft model. The disturbance response characteristics of the two control structures will be dealt with in the next chapter; this section presents the response characteristics of the two structures when the aircraft parameters are varied.

This comparison was made using the Type 0 controller governing roll rate and sideslip angle, Mode C, and its equivalent Type 1 structure. The model used to compute steady-state values of state, control, and optimal gains was identical in each case; however, stability derivatives were selectively changed in the model used to generate the time histories. In this manner, the response of the control laws to a design model mismatch in each stability derivative i.e., the control laws' "robustness" could be computed. The most dramatic of these responses are illustrated in Figure 2.18.

Figure 2.18a shows both responses to a roll command when the roll damping coefficient, L_p, is reduced by 25 percent in the actual model. The Type 0 response is seen to overshoot dramatically, because it depends upon the actual roll damping of the aircraft to control roll response. On the other hand, the Type 1 response also overshoots slightly because of the decreased damping, but immediately responds to produce the desired result. Figure 2-18b shows the sideslip angle command responses when the dihedral effect is increased by 25 percent. Again, the Type 0 controller fails to correct the increased rolling of the aircraft due to the sideslip angle, and settles at the wrong values of both sideslip angle and roll rate. The Type 1 controller exhibits no such hangoff error. The same characteristics are evident in Figure 2-18c. where the weathercock stability of the aircraft is decreased by 25 percent.

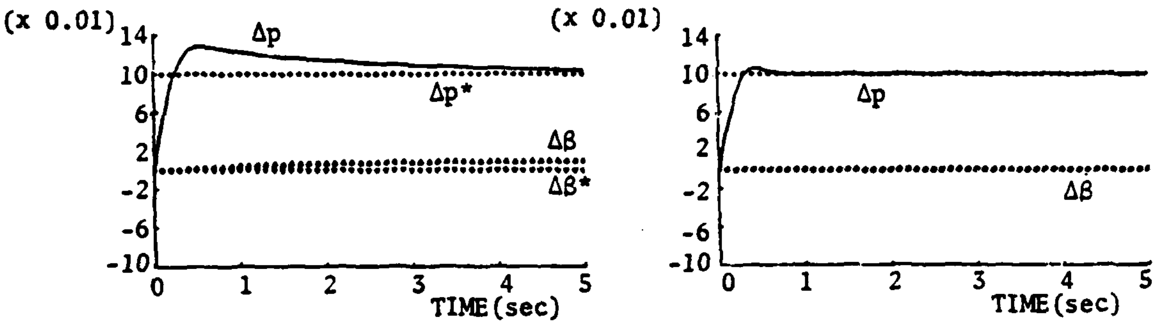

a. L_p Reduced by 25%, Δp_c = .1 rad/sec.

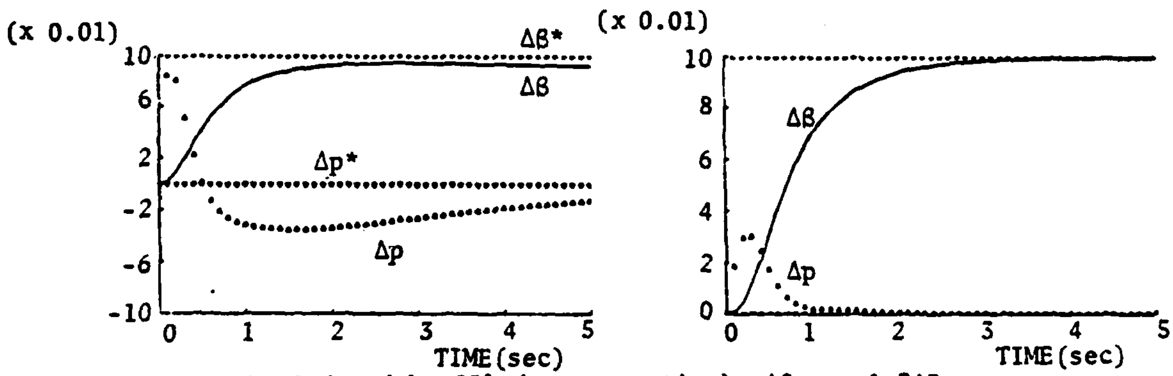

b. L_β Reduced by 25% (more negative), $\Delta\beta_c$ = .1 RAD.

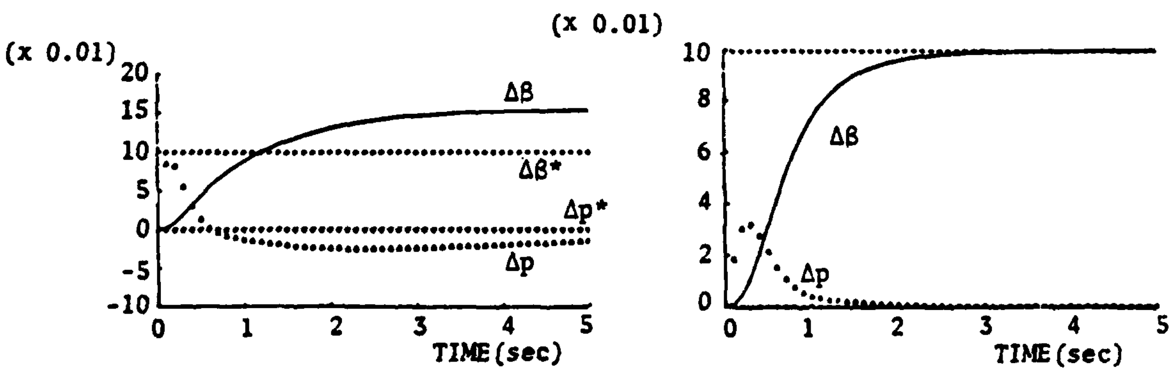

c. N_β Reduced by 25%, $\Delta\beta_c$ = .1 RAD.

Figure 2-18. TYPE 0 vs TYPE 1 Responses for Model Mismatch.

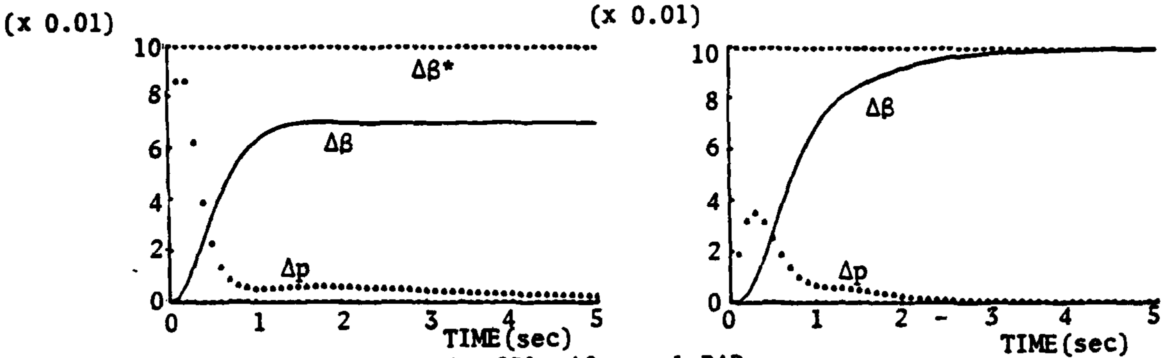

d. $N_{\delta R}$ Reduced by 25%, $\Delta\beta_c$ = .1 RAD.

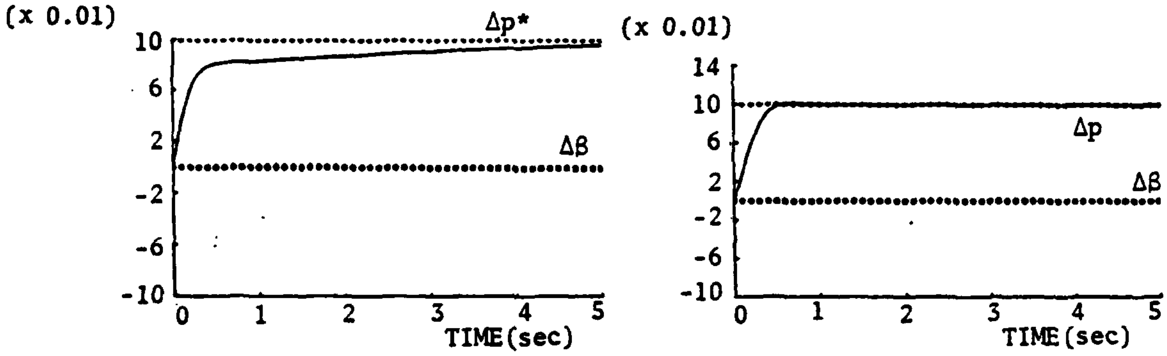

e. $L_{\delta A}$ Reduced by 25%, Δp_c = .1 rad/sec.

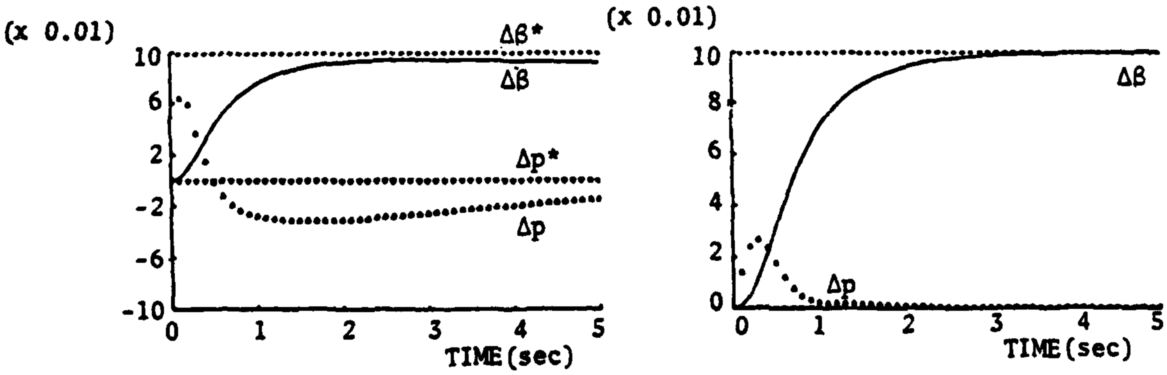

f. $L_{\delta A}$ Reduced by 25%, $\Delta\beta_c$ = .1 RAD.

Figure 2-18. (continued).

Figures 2-18d, e, and f demonstrate the difference between the controllers when the control effectiveness derivatives, $L_{\delta A}$ and $N_{\delta R}$, are reduced by 25 percent. Here again, the results are the same. The Type 0 controller settles at the wrong values of Δp^* and $\Delta\beta^*$, while the only differences in the Type 1 responses are a slight increase in the rise time due to the decreased control effectiveness.

It appears that the Type 0 controller relies heavily upon the natural stability and response characteristics of the system to produce the desired response; it does not force the system to the commanded values, as does the Type 1 control law. Under these conditions, the Type 1 system is clearly superior to the Type 0 system because it actively pursues the commanded input value; however, as will be seen later, this Type 1 control law has extremely undesirable response to disturbances.

The next chapter describes how the control laws presented in this chapter actually are implemented in the Micro-DFCS. It describes the hardware and software aspects of the DFCS, and presents pre-flight test results in the form of hybrid simulation.

3. OPERATIONAL DIGITAL CONTROL LAW STRUCTURE

The control laws presented in the last chapter are transformed into control programs which operate within the microprocessor-based digital flight control system. The type of equipment used to implement the Micro-DFCS, in addition to the control laws themselves, dictates the structure of these control programs. This chapter details these specific aspects of this investigation; a description of the equipment used in the actual flight control computer unit (FCCU) and of the operational control programs used is presented here. Results of control system validation testing using hybrid simulation of the VRA also are presented.

3.1 MICROPROCESSOR-BASED DIGITAL FLIGHT CONTROL SYSTEM

The primary task of the Micro-DFCS FCCU is to accept analog information from aircraft sensors, to calculate the control laws, and to provide analog commands to the aircraft controls at periodic instants in time. This definition suggests several necessary characteristics for the hardware to possess. In order to minimize error in control law calculations, the computations must not only be fast, as determined by the instruction cycle time, data and bit length, and the speed of the mathematical operations themselves, but the computations must have precision at least as great as the resolution of the digital data words generated by the analog-to-digital (A/D) converter. Resolution of the A/D and digital-to-analog (D/A) converters should be consistent with the measurable resolution of the sensors and control actuators. In addition, a computer with at least one interrupt that can be triggered by a resetable timer is needed to initiate the control law calculation at precise instants in time. The description of the FCCU used in this investigation will be based on these quantities. Additional descriptions of the Micro-DFCS hardware can be found in References [19] and [30].

The Model 1 Micro-DFCS FCCU is based on the Intel Single Board Computer (iSBC) using the Intel 8085 Central Processing Unit (CPU). The main functions of the FCCU are executed on separate circuit boards. Figure 3-1 displays the organization of the Micro-DFCS FCCU; the iSBC 80/05 central processing board is supported by a high-speed mathematics unit, random-access and programmable read-only memory (RAM and PROM), A/D and D/A conversion boards, and a hand-held control-display unit (CDU). The CPU has an eight-bit data word length and uses a set of 80 machine instructions, with instruction cycle times ranging from 2 to 6.1 μsec. The CPU board has 22 parallel lines of input and output (I/O), 4.5K of memory, and one hardware interval timer which may be wired to an interrupt line of the 8085 and which may be preset by software to vary the interrupt time interval.

The mathematics unit performs fixed-point and floating-point operations, where the typical time needed to do one 32-bit floating-point operation (including time to pass arguments to the unit) is 137 μsec. This unit provides the operational speed necessary to compute the control law in the required time interval. The main memory provides 24K words of RAM and PROM and also interfaces with the CDU. The battery-back-up board stores data and programs with power off for up to 96 hours, and is used to transfer the control programs from the software development system to the FCCU mounted in the VRA. The analog I/O boards provide 16 differential or 32 single-ended input channels and 6 output channels, each with 12 bit resolution. The A/D has a conversion rate of 28 KHz and can be interrupt- or software-driven [18]. The Termiflex HT/4 hand-held CDU provides double-stroke (keypad plus shift key) input and 2-line, 12-character LED display of ASCII characters. Although it has a limited display and requires multiple key strokes, it is functionally equivalent to a conventional 1200-baud keyboard/display terminal; it allows the pilot to monitor and command the Micro-DFCS.

The FCCU is housed in an RF-shielded, shock-mounted aluminum box. The 6 computer boards identified in Figure 3-1 plug into two 4-board cages, which allows the addition of additional boards without hardware

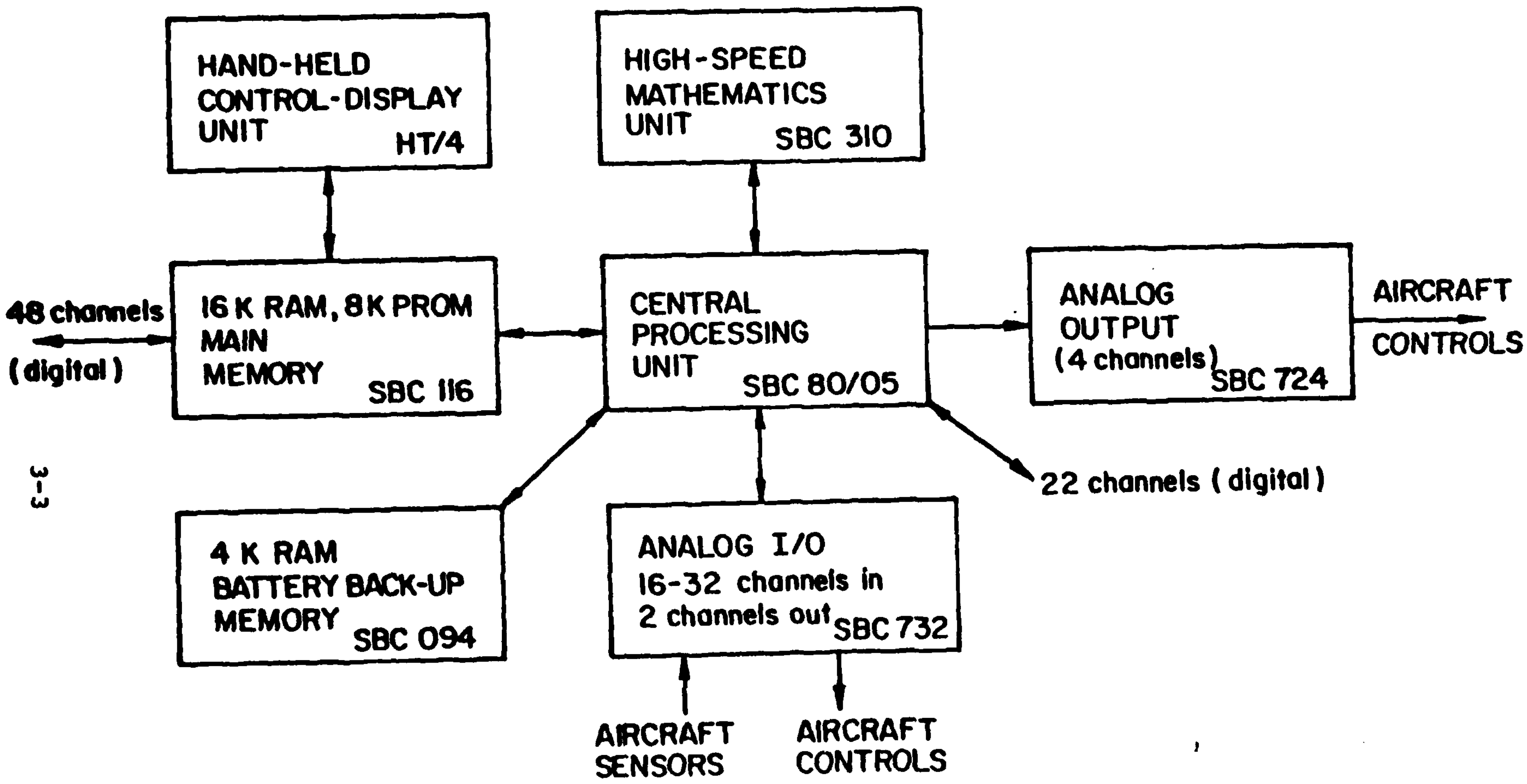

Figure 3-1. Microprocessor Digital Flight Control System (Micro-DFCS), Model 1

modification. FCCU power (±5, ±12) is obtained by regulating the VRA's primary 28vdc.

3.2 CONTROL PROGRAM DEVELOPMENT

The Intel 8085 CPU operates as the data bus control unit, coordinating information flow among the supporting elements of the FCCU. It does so according to control programs which have been coded in machine language for the CDU. These programs provide initialization, CDU interface, control law calculation, and self-test capability; the development of these routines is the subject of this section.

3.2.1 Development System

The FCCU and CDU are shown with components of the control program development system in Figure 3-2; shown are the FCCU and CDU resting upon the ground chassis/power supply, a keyboard-CRT terminal, an acoustic coupler, and a telephone extension. Not pictured is a keyboard-printer unit. These components provide for an efficient and flexible method of coding Micro-DFCS control programs; a schematic depicting the overall development system is shown in Figure 3-3.

The ground chassis holds and powers the microcomputer boards identified in Figure 3-1 during the development phase. The keyboard-CRT terminal serves multiple purposes during program development. It provides a direct communications link with the microcomputer; it allows programs, when first coded in assembly language, to be entered into the microcomputer, and it provides a rudimentary text editing capability before the programs are sent to Princeton University's IBM 370/158 computer via the acoustic coupler and telephone link. The CRT terminal provides system monitoring capability, as well as communciation with the IBM computer over the telephone link. The computer allows more sophisticated text editing, cross-assembly of the Micro-DFCS code, and permanent storage of all programs. During latter stages of program development, the assembled routines can be loaded into the Micro-DFCS from the computer and

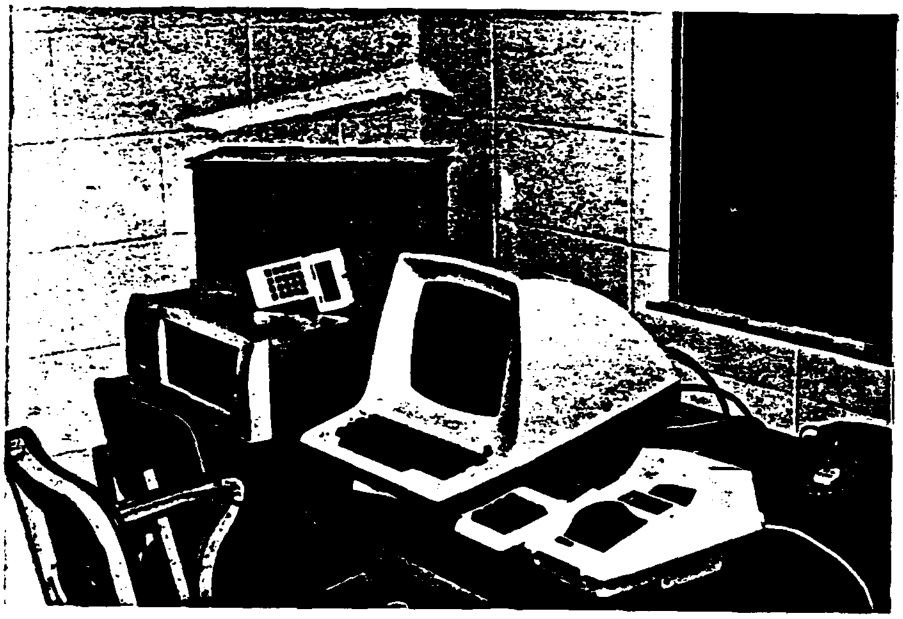

Figure 3-2. Components of the Micro-DFCS and Software Development System.

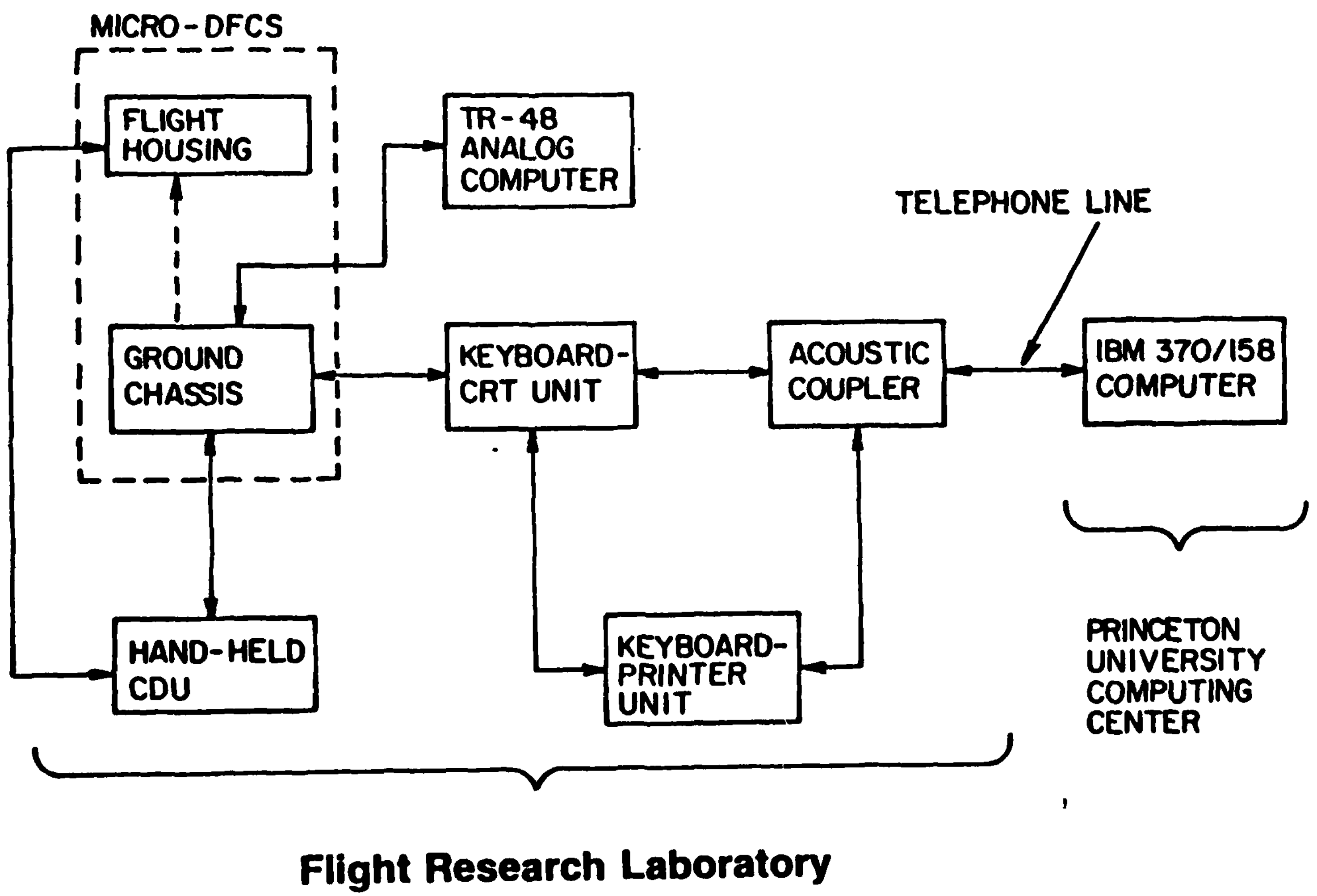

Figure 3-3. Equipment Layout for Micro-DFCS Development.

debugged using the keyboard-CRT unit. The keyboard-printer provides the same functions as the CRT unit, but it provides printed copies of program listings as well.

3.2.2 Control Program Considerations

Prior to actual control program development, consideration must be given to several factors. Among those to be considered are speed of the control calculations, computational delays, and memory space requirements.

The most important consideration in the design process is the speed of the computation. It is important to minimize the computational delay in the control law, that is, to minimize the time between the actual pilot command and the actual control response. This can be done in two manners. First, as noted in Chapter 2, the subscripts in the control laws indicate that the command value at any instant in time depends upon values taken during the previous sample. Therefore, by precomputing values to be used in the next control calculations, computational delay time can be reduced. Using this approach, the following should be the sequence of the control law algorithm:

1. Sample the aircraft states and pilot commands
2. Compute portions of control laws based on current sample
3. Add portion of control law based on previous sample
4. Send control law commands to control surfaces
5. Compute values to be used in the next control law calculation

A second method of minimizing computation time is to make the control program specific to the task. By avoiding the use of generalized subroutines, the actual execution duty cycle of the control law can be minimized. This can be accomplished only when a large memory capability is available. Because of the limited memory available during this investigation, some tradeoffs must be made between the use of specific task control programs to minimize control execution times, and

the use of subroutines to minimize memory requirements. This tradeoff can be accomplished efficiently in the following way. The part of the control program between the sampling of the aircraft states and pilot commands and the generation of Micro-DFCS command values should be specifically coded to minimize computational delay. The remaining portion of the control program, that part associated with computing values for the next control calculation, may use subroutines to minimize the memory requirements. By doing this, the time critical part of the routine can be optimized with respect to time, while the remaining part can be optimized with respect to memory space.

Other factors to be considered in the control program development include design flexibility, system interfaces, and an error detection capability. These factors will be discussed in more detail in the following section.

3.2.3 Control Program Implementation

The actual implementation of the control laws presented for the Micro-DFCS is accomplished using three sets of control routines. These sets, entitled the Flight Control, Executive, and Utility Routines [19], together make up the control program entitled CAS-4 [30]. The routines of CAS-4, arranged in chapter format, are listed with memory requirements in Table 3-1.

The Flight Control Routines are responsible for performing the actual control law calculations at each timed interrupt. The selected control mode (Direct, Roll Rate-Sideslip Angle, or Roll Rate-Lateral Acceleration) determines which control law will be executed at each sampling instant. Because these calculations must be accomplished at precise time intervals, the control law execution takes priority over all other control programs.

Supporting the Flight Control Routines are the Executive and Utility Routines. The Executive Routines provide for initialization of all

Table 3-1 CAS-4 Table of Contents and Memory Requirements

	Memory Words
Executive Routines	
Initialization	120
CDU Interface and Command Recognition	89
Memory Check	154
Utility Routines	
Analog-to-Digital Conversion	19
Entry Error	68
Blink	24
Clear Line	24
Console Output	11
Count-Up Display	76
Decimal to Hex Conversion	25
Erase Block Memory	8
Math Error Processor	112
Hex-to-Decimal Conversion	61
Numeric Input	67
Interrupt Count	20
Limit Analog Output	46
Math Unit Driver	47
Mode Change	143
Mode 4 Words	13
Serial Output	13
Calibrated Step Input	295
Set Delay	274
Hex Input	76
Timer	137
Console In	12
16 Bit Decimal-to-Hex Conversion	75
Delay	143
Slow	24
Resolution	126
Flight Control Routines	
Direct Mode Set Up Routine	97
Type 1 Control Law Set Up Routine	59
Lateral Acceleration, Roll Rate Command Set Up (Mode A)	227
Lateral Acceleration, Roll Rate Command Set Up (Modes B, C)	232
Sideslip Angle, Roll Rate Command Set Up (Mode A)	272
Sideslip Angle, Roll Rate Command Set Up (Modes B, C, D)	348
Sideslip Angle, Roll Rate Command Set Up (Modes 15, 16, 17, 18)	480
Direct Mode Interrupt Service Routine	158
Type 1 Control Interrupt Service Routine	813
Lateral Acceleration, Roll Rate Command Interrupt Service Routine	34
Sideslip Angle, Roll Rate Command Interrupt Service Routine	1657
Sideslip Angle Estimator Routine	172
TOTAL	6851

user defined parameters, CDU interface, and one of three error detection methods. This error detection routine checks the contents of memory every 50 samples to ensure that the coding of CAS-4 has not changed (the other error detection methods include checking for mathematical errors on each operation and a steady blinking light on the pilot's panel which indicates the Flight Control Routines are operating properly [19]). The Utility Routines comprise major and often performed tasks which are written as general subroutines.

These supporting sets of routines are responsible for the flexibility of the control program. New flight control programs can be developed quickly and efficiently using these existing routines. A brief description of these subroutines which make up the Executive, Utility, and Flight Control Routines can be found in Appendix D.

3.3 CONTROL SYSTEM VALIDATION USING HYBRID SIMULATION

Prior to actual flight test, the flight control program is examined in a hybrid simulation of the VRA/Micro-DFCS combination. The VRA's lateral-directional dynamics are modeled on an EAI TR-48 analog computer, allowing a "real-time" simulation of the Micro-DFCS performance to be generated prior to flight. By comparing the hybrid simulation test results with the computer generated results presented in Chapter 2, the Micro-DFCS control program can be tested and validated prior to installation in the VRA. The results of the hybrid simulation tests are presented here. In addition, response characteristics of the various command structures in the presence of both step and random sideslip angle gust inputs are examined under hybrid simulation; these results are presented as well.

Based on the fourth-order model of lateral-directional dynamics presented in Chapter 2, Figure 3-4 depicts the analog computer schematic used to represent the VRA during hybrid simulation testing. The potentiometer settings for the test flight condition are given in Table 3-2. Roll rate, yaw rate, roll angle, and sideslip angle (lateral acceleration) signals generated by the analog simulator are sent to the Micro-

Table 3-2 Computer Potentiometer Settings for VRA Lateral-Directional Model

Pot	Parameter	Scaling	Setting
00	$L_{\delta A}$	$L_{\delta A}/100$	.210
01	L_p	$L_p/10$	.650
02	L_β	$L_\beta/100$	.115
03	L_r	$L_r/10$	.116
05	$N_{\delta R}$	$N_{\delta R}/10$	.610
07	N_β	$N_\beta/10$	.590
08	N_r	N_r	.750
10	Y_β/V	Y_β/V	.400
11	g/V	g/V	.181
12	$N_{\delta A}$	$N_{\delta A}$	.252
13	$L_{\delta R}$	$L_{\delta R}$	.058
15	V_o/g	$V_o/g \times \frac{1}{57.3}$	.096
18	rad/deg	10/57.3	.175
20	N_p	N_p	.260
30	NYCON	.5/NYCON	
45	RRCON	.087/RRCON	.112
46	YRCON	.087/YRCON	.136
47	BCONV	.087/BCONV	.840
50	FICON	.087/FICON	.416
52	AICON	1/.087 x AICON	.386
53	RUCON	1/.087 x RUCON	.386

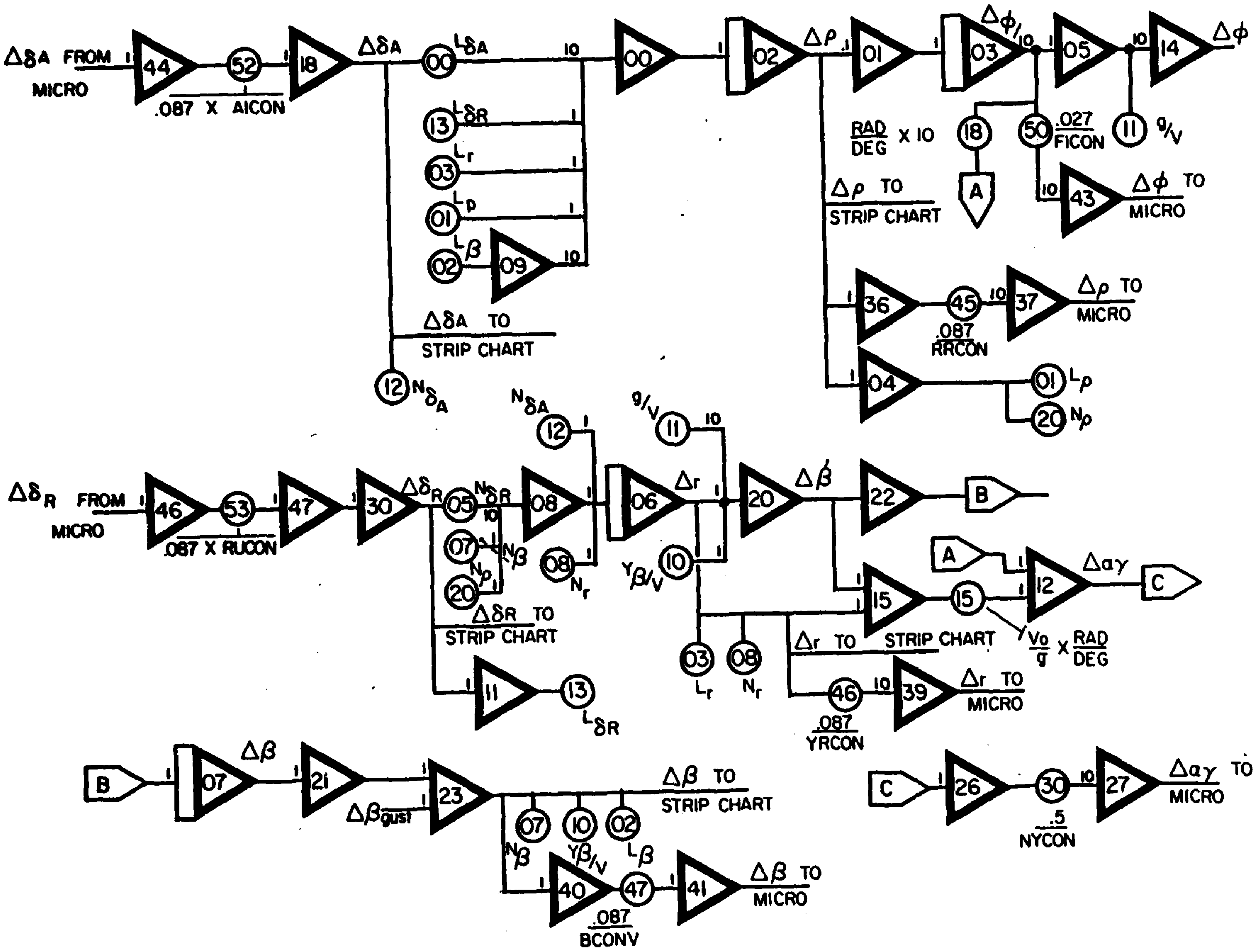

Figure 3-4. Analog Computer Schematic Used in Hybrid Simulation.

DFCS, which in turn provides rudder and aileron commands to the analog computer, based on the control program in effect. Inputs to the A/D converters and outputs of the D/A converters of the Micro-DFCS are scaled for a specific reason: the voltage levels of incoming and outgoing signals must duplicate the voltage levels produced by the actual sensors of the VRA. This ensures that all gains and scaling factors within the control programs can be verified on the ground.

All of the control law combinations presented in Chapter 2--Direct, Type 0 and Type 1 roll rate, sideslip angle, and Type 0 roll rate, lateral acceleration command structures--were tested on the analog computer. The same quadratic weighting factors used in the computer generated responses were used in the hybrid simulations (mode designations for these tests are identical to those used earlier)*. In addition, different sampling rates were tested on the analog simulator, with the linear-optimal gains used in the control laws reflecting the different sampling intervals. Each mode was tested by generating step commands in lateral stick and foot pedals; these commands were generated internally in the Micro-DFCS using the calibrated step routine explained in Appendix D. The lateral-directional responses of the VRA, and stick and pedal command outputs were recorded on a strip chart recorder.

It was during this series of tests that the actual control program execution times were investigated. It was found that the direct mode control program takes 8 msec to run, while the Type 0 command law takes 37 msec to run. By taking advantage of the control law structure--that is, by using precomputed values in executing the control law--the actual time between the sampling of the aircraft states and the command output from the Micro-DFCS was reduced to 12 msec for the Type 0 control law. The remaining 25 msec of the execution time was devoted to computing values for use in the next sampling instant and control calculation. No such investigation was made of the Type 1 control law.

Figures 3-5 and 3-6 present some of the results of these validation tests. Figure 3-5 presents the responses of the Micro-DFCS to roll

*See Tables 2-4 to 2-11 for mode descriptions.

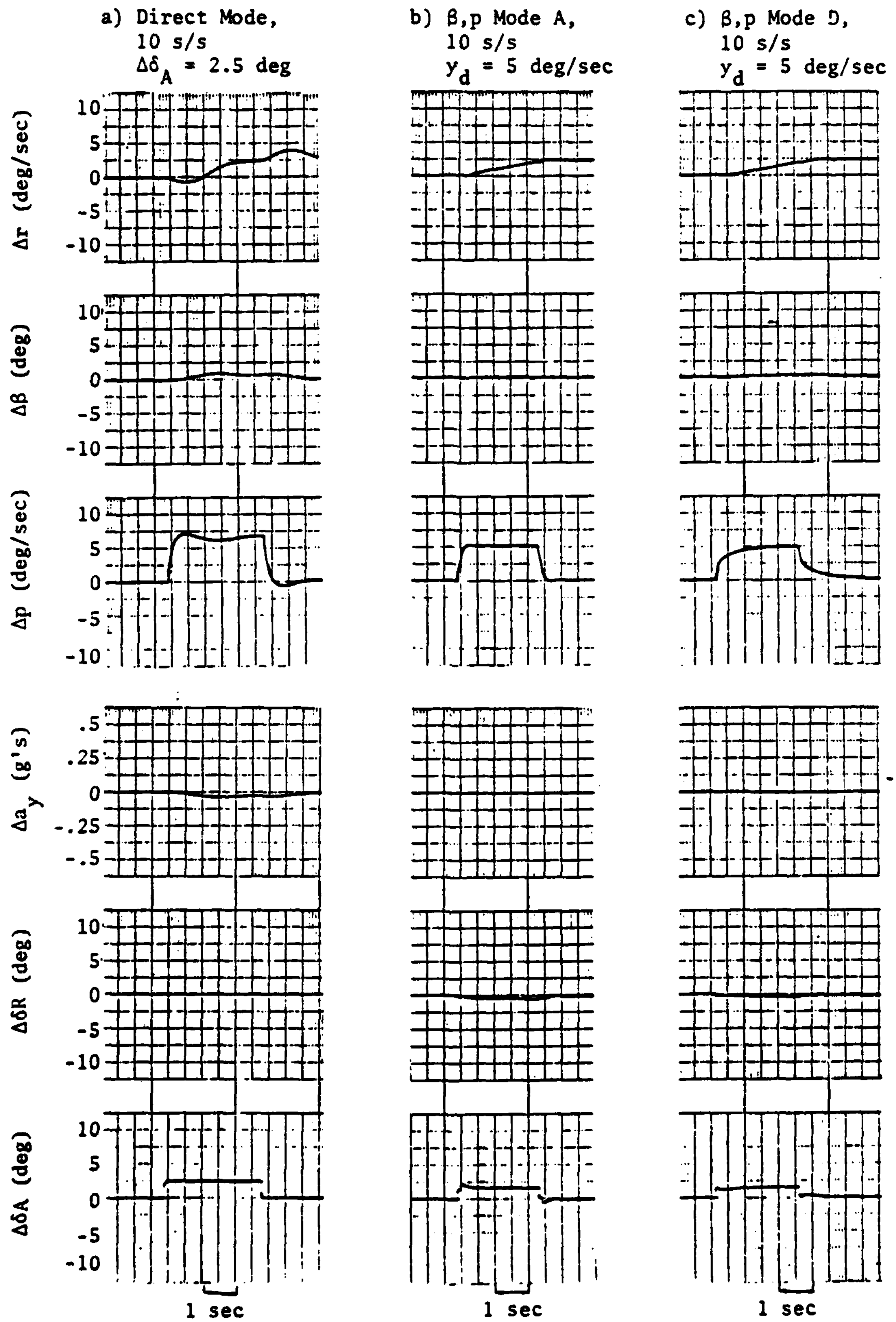

Figure 3-5. CAS-4 Roll Rate Command Response.

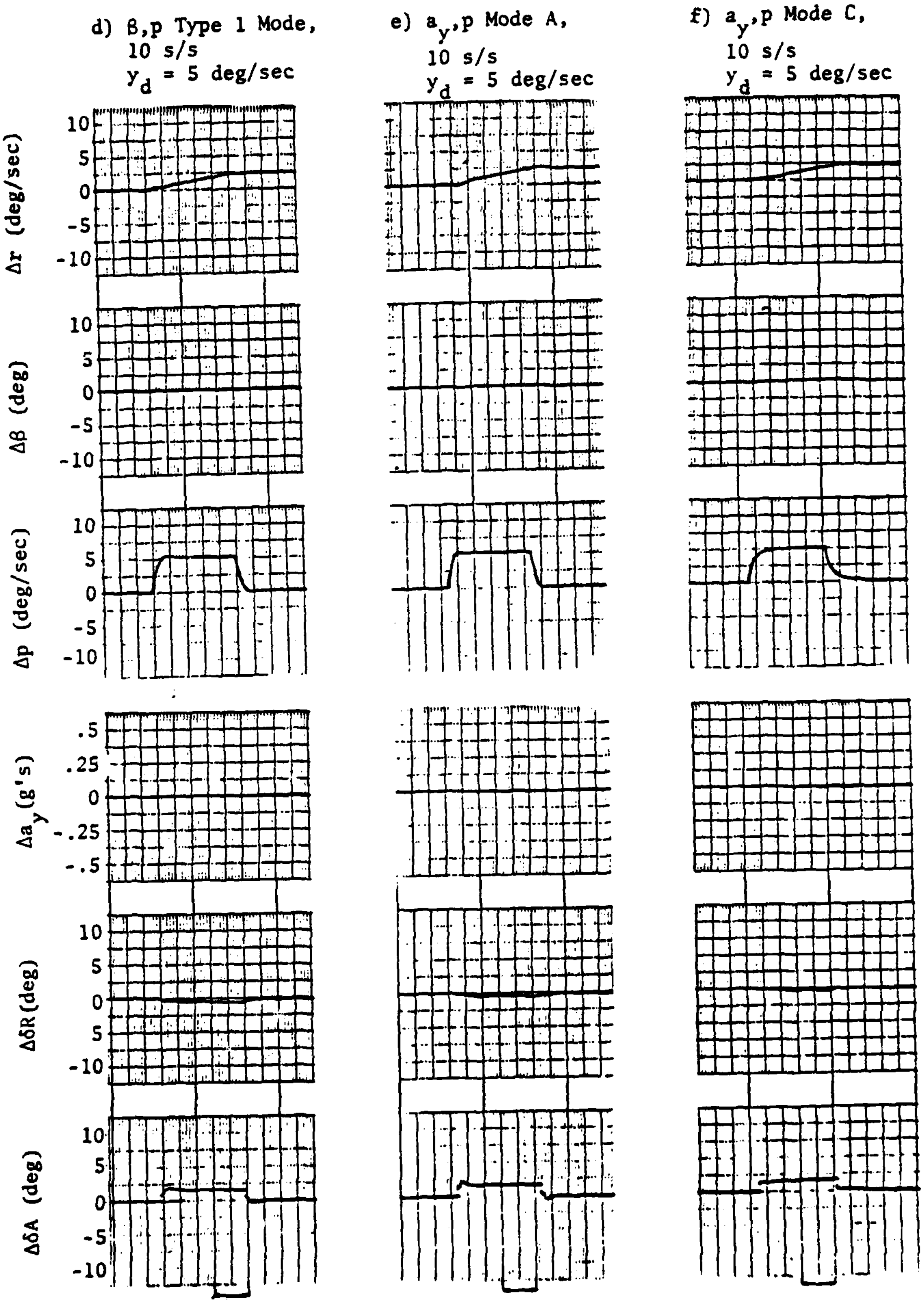

Figure 3-5. CAS-4 Roll Rate Command Response. (continued)

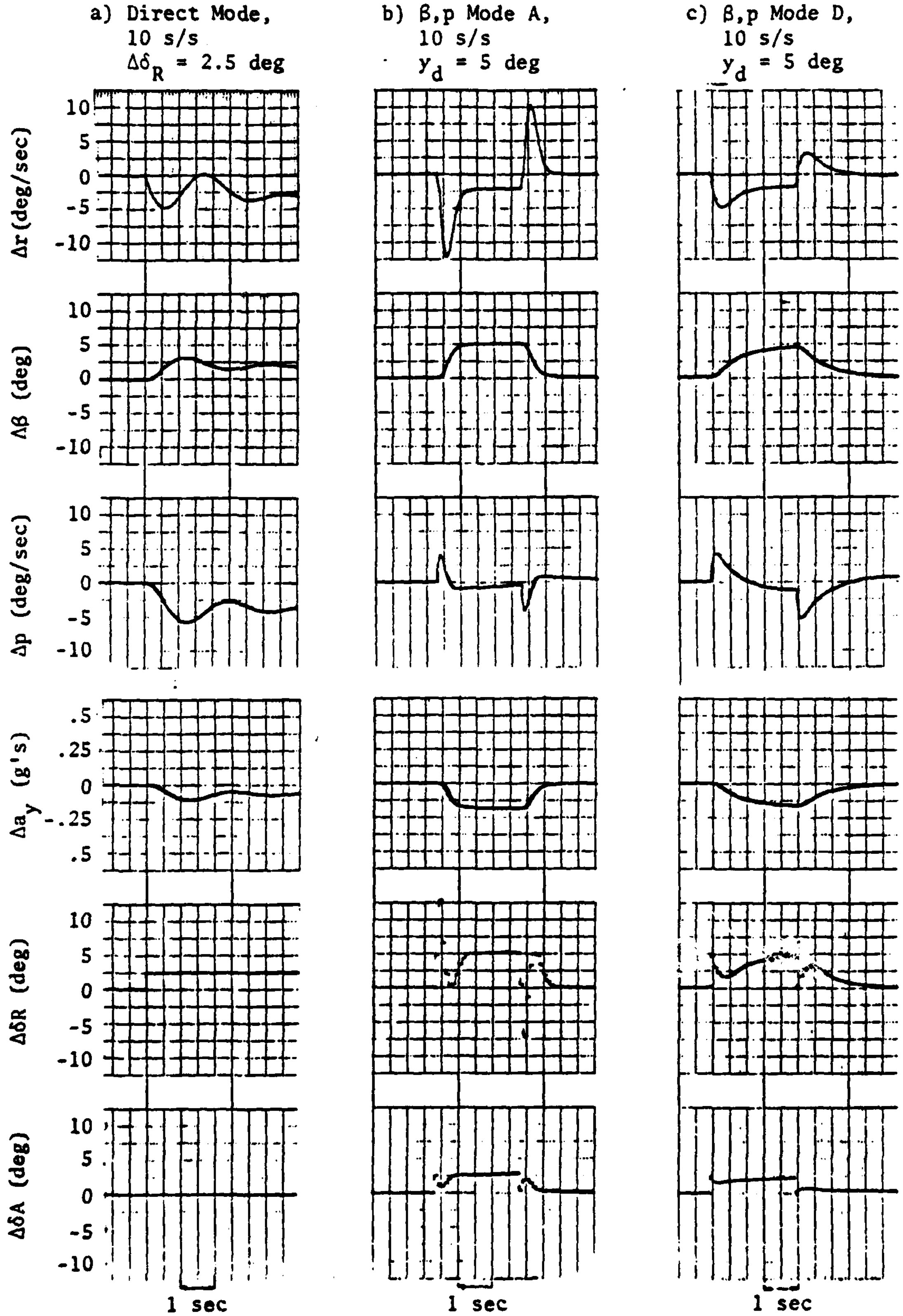

Figure 3-6. CAS-4 Sideslip Angle (Lateral Acceleration) Response.

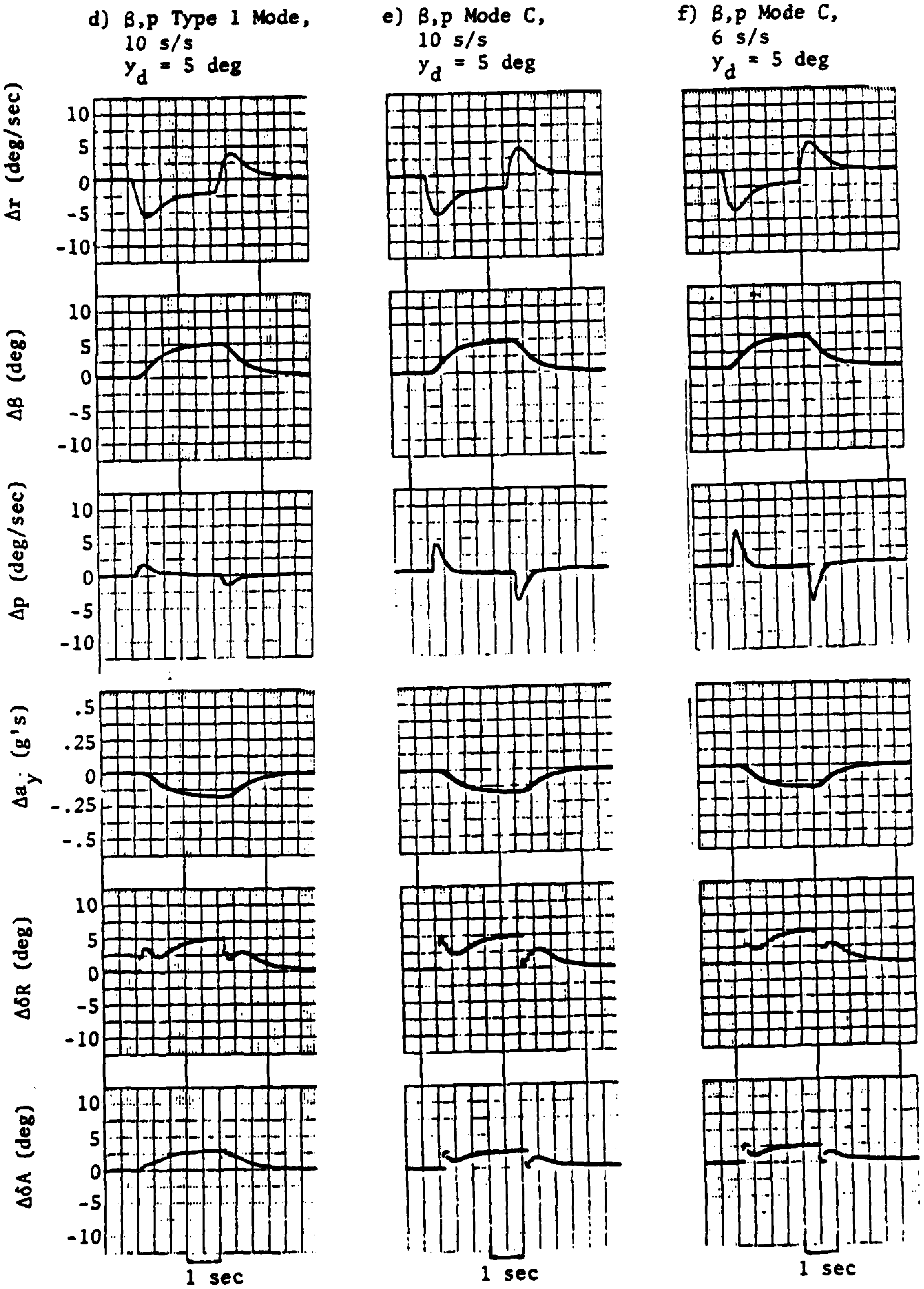

Figure 3-6. CAS-4 Sideslip Angle (Lateral Acceleration) Response. (continued).

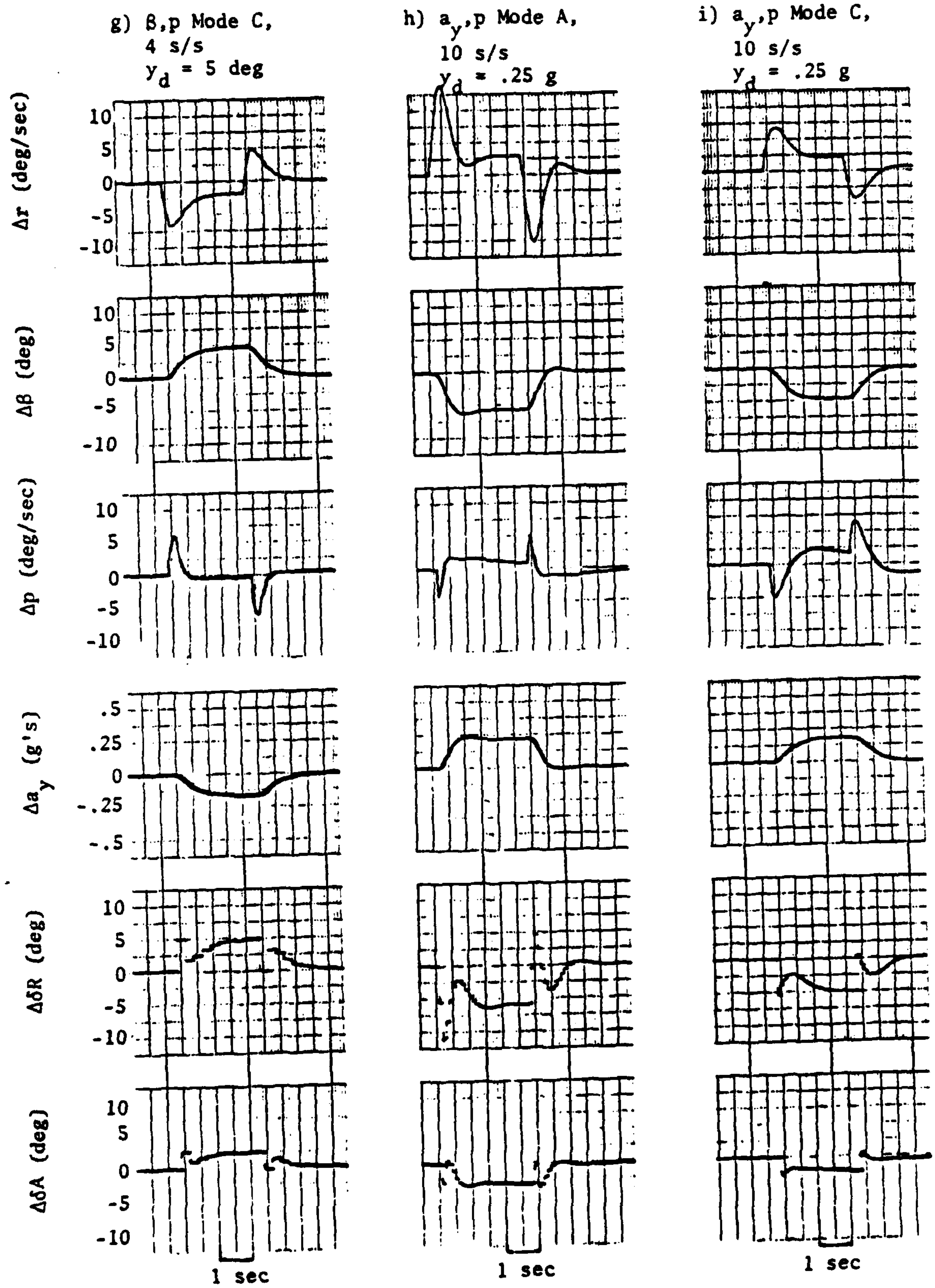

Figure 3-6. CAS-4 Sideslip Angle (Lateral Acceleration) Response. (continued)

commands, while Figure 3-6 represents the sideslip angle (lateral acceleration) command responses. Each column represents one test run, with each column labeled by the flight control mode operating and the desired command value. Responses are shown for yaw rate, sideslip angle, roll rate, lateral acceleration, and pedal and stick commands.

Examination of these responses reveals that the Micro-DFCS operates as desired. A comparison of these responses with the computer generated responses presented in Chapter 2 reveals identical command response characteristics, with one exception. The lateral acceleration command response in Figure 3-6, while exhibiting the desired response shapes, reaches a steady-state condition at less than the commanded value, i.e., a non-zero hangoff error. There are two possible explanations for this apparent system error. One is that one or more of the linear-optimal gains used in the control law was miscoded in the control program. A second possibility is model mismatch, as explained in the previous chapter. During control law development, lateral acceleration control laws were derived based on a fourth-order model using lateral acceleration, yaw rate, roll rate, and roll angle. The analog model of the VRA, however, was based on a fourth-order model using sideslip angle rather than lateral acceleration, with lateral acceleration calculated from the other four lateral-directional states. While the two models should have been the same, model mismatch could have provided the non-zero hangoff error exhibited by the hybrid simulation response. In view of the other results presented, however, no further investigation was made of this anomaly.

Several characteristics of the control laws designed using sampled data regulator theory are evident in the hybrid simulation results. First, the effects of the zero-order hold can be readily seen in the rudder and aileron control time histories. In addition, the effects of decreasing the sampling rate on the command responses can be seen in Figure 3-6. Sideslip angle command response is shown for sampling rates of 10, 6, and 4 samples per second, with identical command response in each case. It should be noted that these responses are characteristic only of an environment with zero disturbance; with large disturbance

inputs, the responses with the lower sampling rate may have been degraded to some extent. The results tend to show, however, that the design process and the optimal gains take into account the longer sampling interval; practically speaking, lower limits on the sampling rate may be bounded by disturbance inputs, as explained in Chapter 2, or by pilot preference.

In addition to providing Micro-DFCS and control program validation, the hybrid simulation of the VRA offered a second opportunity: to compare the basic aircraft response with the Type 0 and Type 1 control response in the presence of controlled disturbance inputs. For this investigation, disturbances in sideslip angle were introduced to the system, and the Micro-DFCS response in three modes of operation were recorded. Step inputs were used to simulate a steady crosswind field, while random inputs were used to determine turbulent gust response.

Direct mode and Type 0 and Type 1 proportional-integral control responses for a constant sideslip angle disturbance are shown in Figure 3-7. The direct mode exhibits the characteristic aircraft response: excitation of the Dutch roll mode, with the natural weathercock stability reducing the sideslip angle to zero. The Type 0 control mode shows a greatly improved disturbance response: a well-damped Dutch roll mode (as evidenced by the eigenvalues presented in Chapter 2) and a smooth return to the steady-state conditions. Because it is a Type 0 system, however, steady-state errors are not necessarily nulled. Except for the hangoff error in the roll rate (p) response, this may not be apparent from the figure. In contrast to the Type 0 response, the Type 1 system attempts to rapidly return the aircraft to the steady state-conditions, which results in overshoots and large transient response characteristics. It does, however, null steady-state errors. The same response characteristics can be seen in each mode for a random gust input. Figure 3-8 presents time histories for the gust response of each mode to the same history of random inputs.

The differences between the Type 0 and Type 1 system responses to the disturbances are functions of the structures of the control laws.

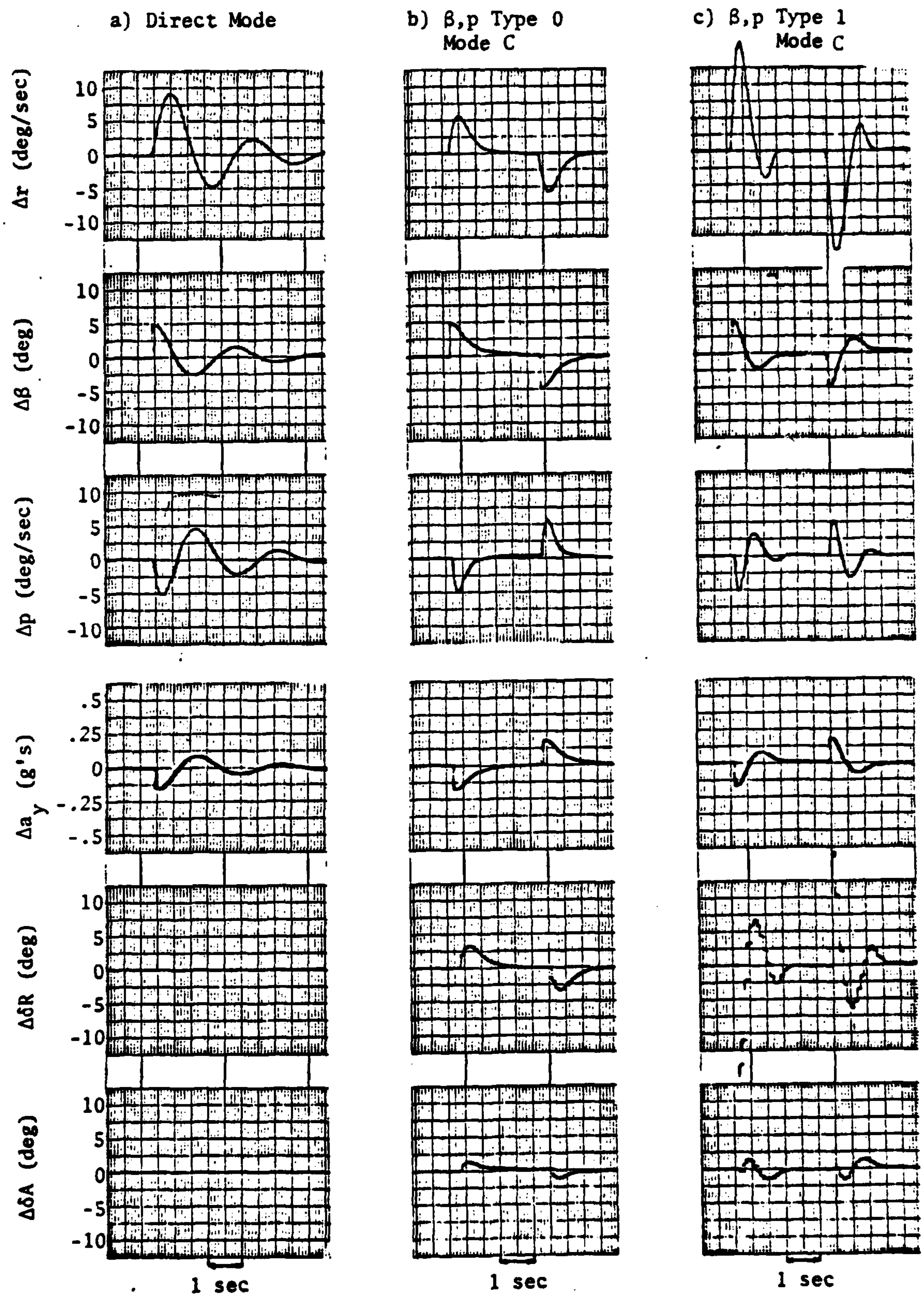

Figure 3-7. Step Sideslip Angle Gust Response.

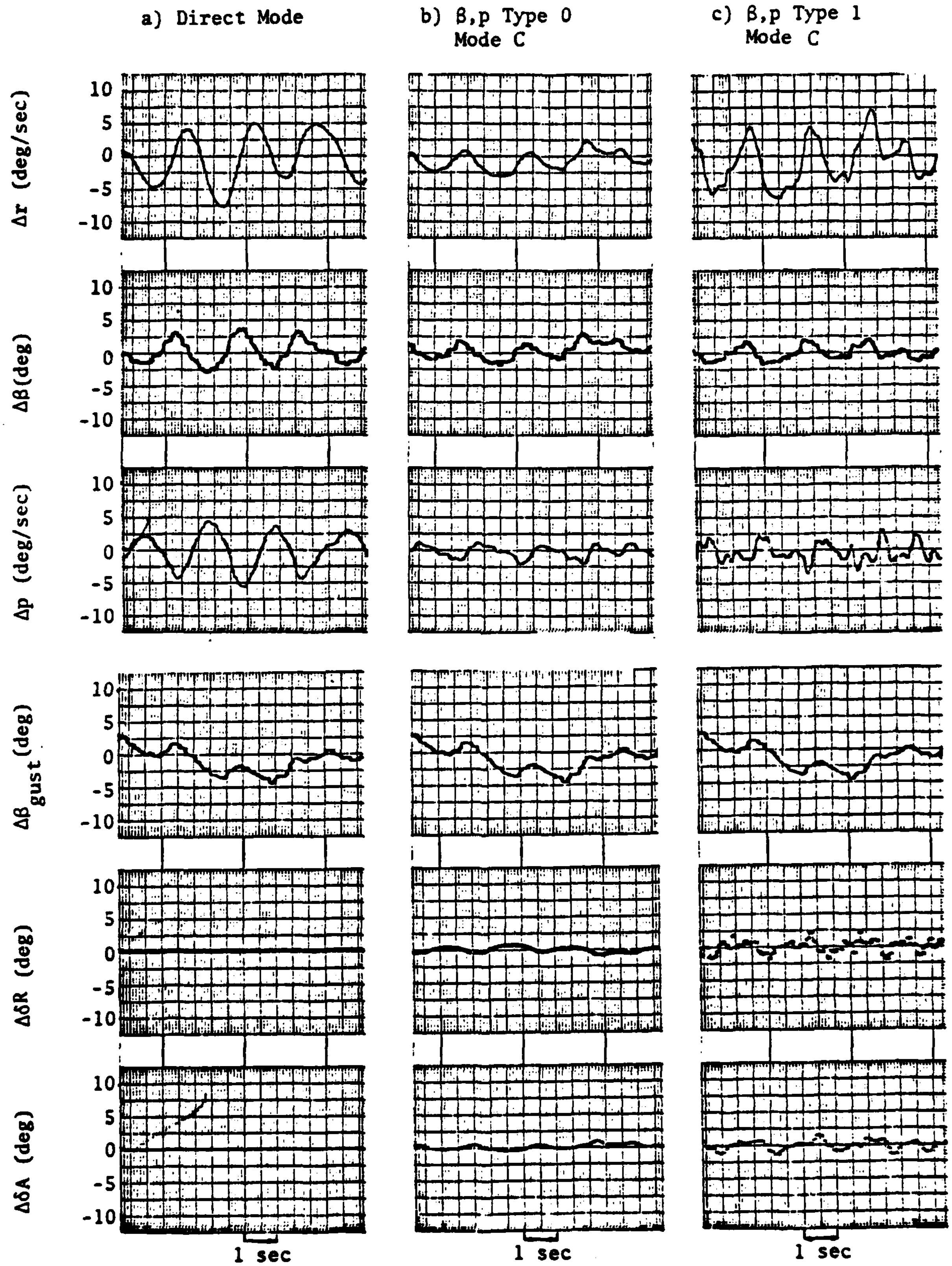

Figure 3-8. Random Sideslip Angle Gust Response Histories.

It was mentioned earlier that the Type 0 system acts as a low-pass filter rather than a pure integration due to the multiplication of several terms by Δt and due to the $(I - \Delta tK)$ term (Chapter 2). No such filtering effect is seen in the Type 1 system. The Type 0 system recognizes not the initial error, but the aircraft response to that error, and consequently uses the controls to damp the aircraft's natural stability and provide a smooth return to steady-state conditions. On the other hand, the Type 1 system recognizes the initial error, and applies controls to correct back. This adds to the naturally stable movement of the aircraft to produce the transient response behavior exhibited in the time histories.

In neither case was the actual knowledge of disturbances used in the design process; the $L\Delta\underline{w}$ term in the linear equations of motion was assumed negligible in the calculation of steady-state values of state and control. It seems possible, then, that some improvement over the uncompensated proportional-integral controller could be achieved by compensating for disturbances in the design process and by using disturbance estimators. A comparison between these two methods is presented in [31]. It was found that, while Type 1 integral control nulls steady-state errors even in the presence of modeling errors, the transient response may be more severe because no use is made of assumed knowledge of the disturbance as in the conventional estimator. The same characteristics of integral control mentioned in [31] appear in the disturbance response time histories presented here.

The hybrid simulation test results presented in this section provide the validation of the Micro-DFCS operation necessary prior to the conduct of actual flight testing. The actual flight test procedures, analysis, and results are presented in the following chapter.

4. FLIGHT TESTING OF THE DIGITAL CONTROL SYSTEM

Actual in-flight testing of the Micro-DFCS is the most important aspect of this investigation. Testing in an operational system such as the VRA is necessary to provide information which will help bring modern control theory and the actual practice of digital flight control closer together. These flight tests are the subject of this chapter; flight test objectives, configuration, and both qualitative and quantitative test results are presented here.

4.1 FLIGHT TEST OBJECTIVES

Specific flight test objectives for the Micro-DFCS can be categorized under two major areas of investigation:

- To identify the problem areas and characteristics of a digital flight control system, especially one which is operating at low sampling rates;
- To provide actual operational verification of control laws designed using modern control theory techniques.

The first major area of investigation deals primarily with hardware-related problems. Those areas of particular concern in this investigation include:

- The effects of radio-frequency noise
- The effects of channel and sensor noise
- The effects of low sampling rates, especially with respect to control surface movements, structural vibrations, and general aircraft responsiveness.

High frequency noise signals, such as RF noise from the VRA's telemetry system and communcations radios, pose a particular problem for the Micro-DFCS. The same is true of channel and sensor noise due to structural vibrations (which are not modelled in the design process and are not present in the hybrid simulation). While these higher frequency signals

go undetected by an analog control system, the sampling process causes these signals to be "aliased" or "folded" to low frequency, thereby contaminating the actual low frequency data. The effects of these signals on the operation of the control laws themselves will be examined in this investigation.

In-flight verification of the control law design process is the second major area of concern. The use of weighting factors in the sampled-data design process to vary aircraft response characteristics is evaluated here. Methods of evaluation and verification include:

- Flying qualities criteria
- Pilot opinion of aircraft responsiveness and handling qualitites
- Actual tracking tasks under various configurations
- In-flight step responses recorded via the VRA's telemetry system

The flying qualities criteria from the Military Specification [18] deal primarily with roll response characteristics and with lateral-directional coupling as discussed in Chapter 2. Pilot opinion provided a very subjective evaluation of each of the flight configurations; general responsiveness and aircraft response to specific tracking tasks were evaluated. Step responses of the same nature as those presented in Chapter 3 were generated. These responses were used primarily to validate the design process and computer generated results,in addition to providing actual documentation of the aircraft's response characteristics.

4.2 FLIGHT TEST PROCEDURES

Preparations for each flight test began with a determination of specific goals; these included the control modes to be tested, sampling intervals to be used, and types of testing to be conducted. The control program for the Micro-DFCS did not encompass all possible combinations of control modes and sampling rates; therefore, slight modifications in the control program, such as optimal gain changes, were necessary prior to each flight test. Once the Micro-DFCS control program

was altered according to the specific test objectives, the Micro-DFCS was tested under hybrid simulation to ensure that all gains and control parameters had been set correctly. Only after hybrid verification of the control program was the FCCU transferred to the VRA for the actual flight tests. During this power-off transfer of the FCCU from the ground chassis to the flight housing, part of the control program was stored in the battery-powered RAM while the remainder was stored in PROM (After VRA power was applied to the FCCU, the PROM memory was transferred to RAM for proper program sequencing).

The FCCU was mounted behind the pilot station on a shock-isolated pallet; four cables connected it to the VRA's fly-by-wire system. One cable provided the necessary power for FCCU operation, while a second connected the FCCU to the CDU. A third cable interfaced the VRA fly-by-wire system; it provided inputs from the motion sensors and pilot controls as well as the outputs to the control surfaces. The fourth cable connected the FCCU to a two-position switch and an error detection/program monitor light mounted on the instrument panel. The switch reset the computer's program counter and gave the CPU program control, and the light flashed at a steady rate whenever a control program was operating, indicating that the system was sequencing properly.

During all flight tests, the VRA was flown by a two-man crew, which provides several advantages over single pilot operation with respect to experimental efficiency and flight safety. The arrangement of the VRA system is shown in Figure 4-1. The safety pilot has conventional aircraft controls with mechanical linkages to the control surfaces, while the fly-by-wire system is flown by the evaluation pilot. Included in the safety pilot's station are the two-position switch, program monitor light, and several mechanisms for disengaging the Micro-DFCS in the event of a malfunction. The evaluation pilot's station includes a center control stick, foot pedals, and conventional instruments. During flight, the Micro-DFCS is managed by the safety pilot through the Termiflex HT/4 hand-held CDU (see Ref. 19 for CDU operation). When not in use, the CDU is stored in a side panel pocket; in this position, the display output is still visible to both pilots.

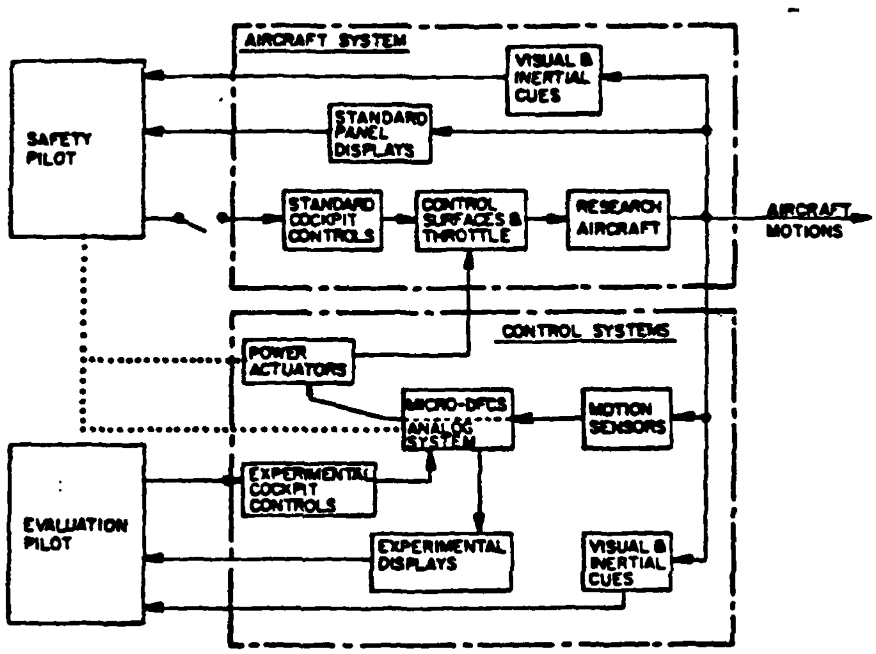

Figure 4-1. Overview of the VRA/Micro-DFCS System.

The actual in-flight testing followed a basic sequence. Once the VRA was airborne and at a sufficient altitude to safely conduct flight tests (usually 5000 feet MSL), the Micro-DFCS was engaged according to the following:

1. Attain desired flight parameters.
2. Choose control configuration.
3. Engage the Micro-DFCS.
4. Conduct flight test maneuver.
5. Disengage Micro-DFCS.
6. Set up for next test.

The first step was necessary for accurate testing, as each control law was designed for a specific point in the flight envelope. Because the control laws designed in this investigation were based on straight-and-level flight at 105 KIAS, most tests were conducted here; however, several tests were conducted at other points in the flight envelope to determine Micro-DFCS performance at other-than-nominal flight conditions. Next, the desired control mode was entered through the CDU. Once the mode was entered and the Micro-DFCS was operating properly, as indicated by the flashing light on the instrument panel, the VRA's FBW system was engaged. Engaging the FBW system allowed the δA and δR commands generated by the Micro-DFCS to be sent to the control surface actuators; the Micro-DFCS biased the computed control perturbation with the actual control surface positions prior to engagement to ensure a smooth transition from the mechanical to the FBW system. Once the system was engaged, the evaluation pilot accomplished a specific test maneuver, the system was disengaged, and the safety pilot maneuvered the VRA for subsequent tests.

Actual flight test maneuvers consisted of both very general and very specific tasks. Initial tests consisted mainly of general observations of the overall performance of the Micro-DFCS and each control configuration. Of these configurations, several configurations were chosen to be evaluated and compared in specific tasks and maneuvers.

These various tasks, as well as the results of each particular flight test, are presented in the following section.

4.3 FLIGHT TEST RESULTS

Several flight tests were conducted during this investigation. The general operation of each control configuration was tested on the first of these flights. No problems were encountered with the Direct Mode of operation, as this mode operated without state feedback. Some problems were encountered with each of the close-loop control modes, due primarily to noise in the unfiltered data.

The lateral acceleration feedback control laws were extremely sensitive to structural vibrations; these vibrations were superimposed on the a_y feedback signal, which resulted in very abrupt and random movements of the rudder. A first-order low-pass analog filter was added to the a_y channel prior to A/D conversion. This filter proved sufficient in eliminating the undesirable effects of the structural vibrations and allowed successful flight testing of lateral acceleration control modes.

A similar problem was noted in the roll axis on the initial flight tests. The closed-loop roll control provided very random movements of the ailerons which, although small enough to cause no actual performance degradation, were very disconcerting to the pilot. This problem was traced to the aircraft sensors and their interfaces with the Micro-DFCS. As was mentioned earlier, signals from the aircraft sensors and pilot inputs have a voltage range of ±10 volts. During initial development, only a portion of this range was actually being used. By recalibrating the sensors and Micro-DFCS control program to equate the full sensor voltage range (±10) with the full range of each particular aircraft state (see Appendix D), the actual signal strength of each particular variable was maximized, thereby reducing the effects of undesirable noise.

While this boosting of the signal strengths minimized the closed-loop control sensitivity in roll, it did not completely eliminate it. The actual roll angle sensor calibration was .0832 volts per degree, allowing a range of ±120 degrees. With such a low signal strength, the closed-loop control law still was susceptible to noise in the roll angle signal; indeed, those control modes with the highest roll angle sensitivity (roll angle feedback gains) demonstrated the random aileron motions most often. Further boosting the sensor signal strengths eliminated the random control movements for all practical purposes, and flight testing was accomplished using this modification.

Following successful completion of the Micro-DFCS checkout flight, several flights were conducted to evaluate each of the control configurations. These tests were evaluated both by the Flight Research Laboratory staff and by test pilots from the Naval Air Test Center. The results of these tests are summarized here.

The first two test flights were conducted by members of Princeton's Flight Research Laboratory. Objectives of these flights included general observations and comparisons of the control modes, comparisons between open- and closed-loop control modes during tracking tasks, and brief evaluations of closed-loop command responsiveness at low sampling rates; these results are presented in Table 4-1. Also as a basis for comparison, Figures 2-1 and 2-2 are reproduced in Figures 4-2 and 4-2 with the unaugmented VRA and β,p control modes marked.

The Direct Mode operating at 10 sps provided the normal open-loop response with no noticeable sampling effects other than the discrete movements of ailerons and rudders. The major improvement gained through the closed-loop control modes was the improved steady-state decoupling of lateral and directional dynamics. This was evident in the pilot comments, where the absence of both dihedral effect and adverse yaw was noted several times, and in Figure 4-2, where sideslip

Table 4-1 Control Mode Response Evaluation

Sampling Rate (sps)	Control Mode	Pilot Comments
10	β,p Mode A	Acceptable response, although yaw is jerky and sensitive to sideslip commands. Roll response good with no adverse yaw. Rate of turn smoothly follows roll rate.
10	β,p Mode B	No difference in roll response from Mode A. Sideslip response better due to perceived lower N_β.
10	β,p Mode C	No noticeable difference in roll response. Sideslip response is softer than Mode B, but very good with no adverse effect in roll. The preferred configuration.
10	β,p Mode D	Roll response considered acceptable, but rated poorer due to slower response time. No noticeable difference in yaw response.
10	Direct Mode	Same response as continuous open-loop response.
10	a_y,p Mode A	Response very similar to β,p Mode B. Good roll and lateral acceleration response. No difference noted between β and a_y control modes.
10	a_y,p Mode B	No differences noted between this mode and β, Mode C.
10	Type 1 β,p	Very jerky hands-off response, especially in yaw. Seems to have a faster yaw response than β,p Mode C. Very sensitive to yaw turbulence in terms of ride quality. No heading changes associated with yaw response, just high frequency aircraft disturbances. Excessive yaw "stiffness". Roll response faster than desired but acceptable. Can't see any control response improvement over Type 0 control that would be a trade-off for jerky inputs and poor turbulence response.
10	β,p Mode C with β Estimator	Response nearly identical with β,p Mode C. Turbulence response identical. Smooth switch-over. Roll response seems the same, with possibly slight favorable yaw as indicated by turn needle. Sideslip response identical, with no roll due to sideslip.
10	β,p Mode A with β Estimator	Identical roll response. Yaw response nearly the same with possible slight improvement in yaw turbulence response over β,p Mode A.

Table 4-1 (continued)

Sampling Rate (sps)	Control Mode	Pilot Comments
10	Type 1 β,p with β Estimator	Estimator engages smoothly, but high-frequency divergent oscillation developed. Pilot disengaged Micro-DFCS each time. Oscillation appeared to be growing rather than reaching limit cycle. Problem confined to yaw.
8	β,p Mode C	No degradation noted in roll or yaw control. Felt slight abruptness in start and stop of roll maneuver.
6	β,p Mode C	Yaw response same as 10 sps. Slight abruptness more noticeable in roll.
5	β,p Mode C	Jerkiness in yaw becoming apparent, but not objectionable. Roll response becoming erratic. Time lag is noticeable, depending upon time of command input.
4	β,p Mode C	Roll objectionable due to ratchet-type control movements and response. Jerky on start and stop. The same is true in yaw response, but not objectionable. Response delay acceptable in yaw, annoying in roll.
4	Direct Mode	Jerkiness of controls main objection. Thumping of control surfaces very apparent. Prefer closed-loop control at low sampling rates due to improved turbulence response.

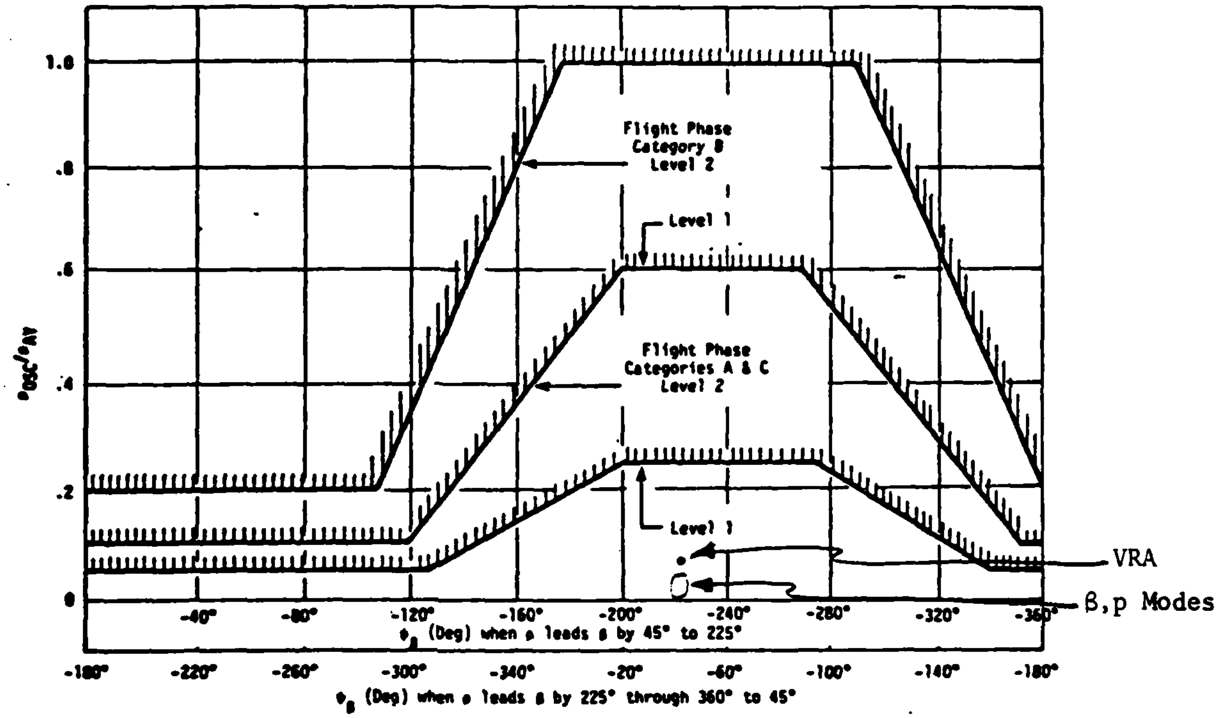

Figure 4-2. Roll Rate Oscillation Limitations.

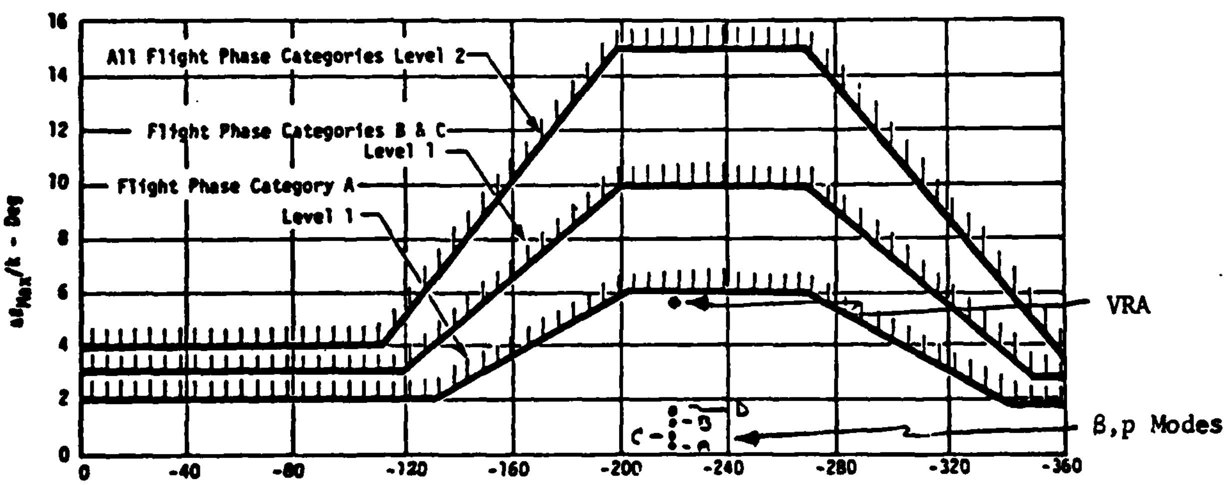

Figure 4-3. Sideslip Angle Excursion Limitations.

excursions during step lateral-stick commands are compared. Differences in the command response times went basically unnoticed by the pilots, except when the responses seemed unnatural, e.g., a slow roll response or a fast sideslip response.

The Type 1 controller was the source of most of the pilots' comments, and based on the results of the hybrid disturbance responses, this reaction was to be expected. This control mode proved to be extremely sensitive to yaw turbulence and sensor noise, confirming the results of the hybrid tests. The pilots reported that both the roll and yaw responses were faster than necessary, although a comparison of the hybrid responses of β,p Mode C and the equivalent Type 1 controller reveals nearly identical command response. It is possible that, in the presence of both a command input and a very sensitive controller, the pilots perceived the abrupt response as an overly responsive controller. Another problem noted with the Type 1 controller was an instability when the sideslip angle estimator was used. The Type 0 controllers provided identical control using the actual and estimated value of sideslip angle, but the Type 1 controller underwent a divergent oscillation. This can be explained with reference to the hybrid disturbance response traces (Fig. 3-8). The Type 0 controller provides lower sensitivity to disturbances that the Type 1 controller, i.e., it uses less high frequency information. Therefore, the Type 0 is likely to be less sensitive to the phase lag introduced by the estimator than the Type 1 controller.

The remaining observations listed in Table 4-1 deal with the Micro-DFCS response at low sampling rates. As the sampling rate is decreased, the control surface deflections become more pronounced, although the pilots mentioned this only in the Direct Mode at 4 sps. The major comment dealt with the inability to control roll and yaw precisely due to the lags in response caused by the long sampling interval. This became increasingly apparent during the actual tracking and maneuvering tasks.

In addition to the results presented in Table 4-1, several other tests were conducted on these flights. The first was to evaluate the Micro-DFCS command response at flight conditions other than the design condition. At airspeeds ranging from 80 to 110 KIAS (design condition 105 KIAS), β,ρ Mode C was engaged. The pilot reported identical command response at all airspeeds within this range. Additionally, comparisons between the open-loop and closed-loop control modes were made during tracking tasks at altitude and on final approach. The closed-loop controller (β,ρ Mode C) provided improved responses over the Direct Mode,in that it had much improved turbulence response in both roll and yaw, allowed deadbeat corrections for runway lineup, and held the trim bank angle (hands-off). The Direct Mode exhibited less yaw damping, larger turbulence upsets, and required more work during flat turn tracking due to lateral-directional coupling.

Additional flight tests were conducted with test pilots from the Naval Air Test Center (NATC) serving as evaluation pilots. These tests were more specific in nature; they included target acquisition and tracking at altitude and Field Carrier Landing Practice (FCLP) tasks. Each pilot rated the various control modes in each task using handling qualities ratings (HQR) on a scale of 1 to 10; these ratings and an explanation of each task are presented in Tables 4-2 and 4-3.

Although few pilot comments are available, and though these ratings are very subjective in nature, several interesting trends can be seen in the handling qualities ratings (HQR). Table 4-2 presents ratings of each control mode evaluated in the first two flights, including the effects of the sampling rates on the pilots' HQR. Task 1 shows steadily decreasing pilot ratings for each increase in the sampling interval. This is to be expected based on the general comments presented in Table 4-1 and on the performed task, where emphasis is placed on quickly establishing the desired bank angle. As the sampling interval is increased, the time lag between pilot command and aircraft response increases, reducing the pilot's ability to start the desired roll rate and to stop the roll at the precise roll angle. This is

Table 4-2 Handling Qualities Ratings of CAS-4 Control Modes
NATC Flights #1 and #2

Mode*	Sampling Rate (sps)	Task Number** 1	2	3
Direct	10	2.5	2.5	6.0
Direct	20	2.0	2.0	
a_y,p Mode A	10	3.5	4.0	4.0
Mode B	10	3.0,2.5	3.0,2.5	3.0
Mode C	10	4.0	4.0	4.0
β,p Mode A	10	4.5	4.0	5.0
Mode B	10	3.0,3.0	3.0,3.5	4.0
Mode D	10	4.5	5.0	
β,p Mode C	10	3.0	3.5	2.5
Mode C	8	4.0	4.0	
Mode C	6	5.0	4.5	
Mode C	5	6.0	4.5	
Mode C	4	7.5	7.0	

* See Tables 2-4 to 2-11 for mode descriptions.

** Task 1 Low-gain lateral maneuvering, 45-degree bank-to-bank turns. Large control inputs with emphasis on quickly establishing the new bank angle.

Task 2 Rapid heading changes of 3 degrees with ±1 degree accuracy. Bank angles of less than 10 degrees. Similar to air-to-air refueling. Foot pedals not used unless required for coordination.

Task 3 Perform 30-degree (or greater) flat turns and stop on heading within ±3 degrees.

Table 4-3 Handling Qualities Ratings of CAS-4 Control Modes
NATC Flights #3 and #4

Mode		Sampling Rate (sps)	Tracking, 105 KIAS* 1	2	FCLP, 86 KIAS** 1	2
Direct		10	3.0	3.0		
a_y,p	Mode A	10	4.0	5.0	-	
	Mode B	10	3.0	3.0		
	Mode C	10	4.0	4.0		
β,p	Mode A	10	5.0	6.0		
	Mode B	10	3.0	3.0		
	Mode D	10	3.0	4.0		
β,p	Mode C	10	3.0	2.5	3.0	3.0
	Mode C	8	2.5	4.0	4.0	5.0
	Mode C	6	2.5	2.0	3.0	3.0
	Mode C	5	4.0	5.0	5.0	6.0
	Mode C	4	4.0	6.0	6.0	7.0
Direct		10	5.0	6.0		
Direct		20	4.0	3.0		

* Task 1 Acquisition: Select target 35 to 45 degrees left or right of aircraft, pull up to 75 KIAS, roll onto target, accelerate to 105 KIAS and maintain airspeed, center target within ±5 mils.

Task 2 Fine tracking: Track target using best combination of stick and pedals,using both conventional and wings-level sidesteps.

**Task 1 FCLP initial: Evaluate last 60 degrees of approach turn, acquisition of centerline. Determine ability to make corrections to aircraft lateral lineup.

Task 2 FCLP final: Evaluate last 10 seconds of approach, line with within ±5 feet, and level wings as required for touchdown.

Note: Control laws of CAS-4 were implemented for operation at 105 KIAS. The FCLP (86 KIAS) and acquisition phase of the tracking task would generally result in a more heavily damped or sluggish response at lower airspeeds.

directly reflected in the HQR of Table 4-2. On the other hand, the ratings for more demanding tasks at different sampling rates reflected not a steadily decreasing rating, but a relatively constant rating leading up to a drastic drop in rating. This trend is noted both in Table 4-2, Task 2, and in the FCLP results presented in Table 4-3, with both pilots' ratings dropping at nearly the same sampling rate. This suggests that a definite lower bound in acceptable sampling rates exists for precise piloting tasks, while there is continual degradation for less precise tasks.

The Task 3 evaluations in Table 4-2 show much poorer ratings for the open-loop controller than for the closed-loop modes. This task was designed to demonstrate the decoupled dynamics; the flat turn task requires precise cross-controlling with the coupled lateral-directional open-loop dynamics, but it can be accomplished using a single control (foot pedals) with the uncoupled closed-loop dynamics. Finally, the results of the tracking tasks presented in Table 4-3 reveal that the ratings for the Direct Mode evaluated before the closed-loop modes are substantially higher than ratings for the same task performed after the evaluation of the closed-loop modes. This could be due to a familiarization with the closed-loop dynamics prior to the pilot's reevaluation of the open-loop dynamics.

One additional documentation flight was conducted to provide the actual VRA step response characteristics; the results, recorded on the strip chart recorder via the VRA's telemetry system (Appendix E), are presented in Figures 4-4, 4-5, and 4-6. The roll rate and side-slip angle command responses, Figures 4-4 and 4-5 respectively, were recorded directly from the VRA. On these figures, the lateral acceleration response is unreadable due to low pen heat on the recorder and the large amount of noise present in the a_y signal (filtered for Micro-DFCS, but not for the telemetry system). The lateral acceleration command responses, Figure 4-6, were first recorded on tape, then sent to the strip chart recorder with the a_y signal filtered using two

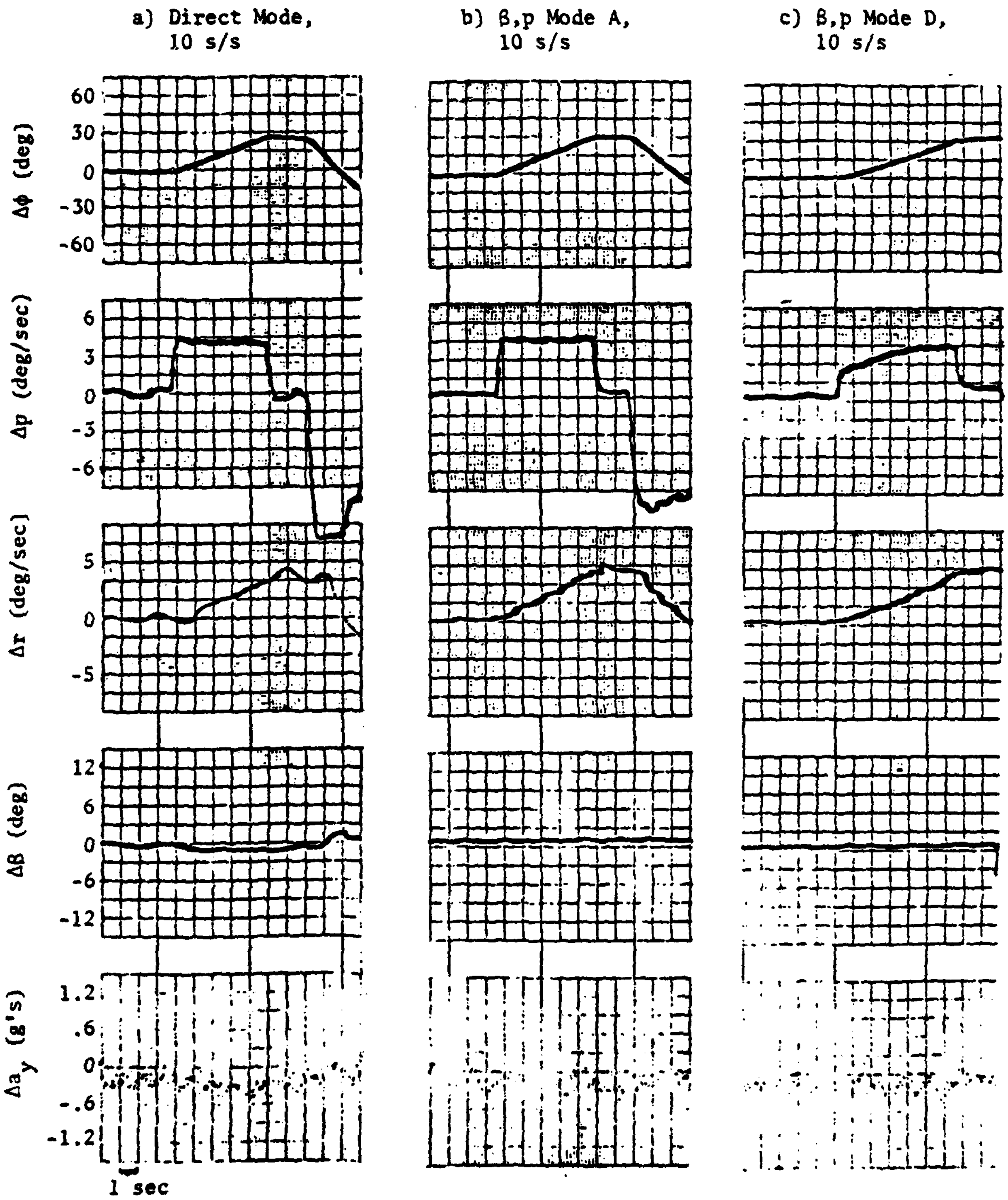

Figure 4-4. VRA Step Responses to Roll Rate Commands.

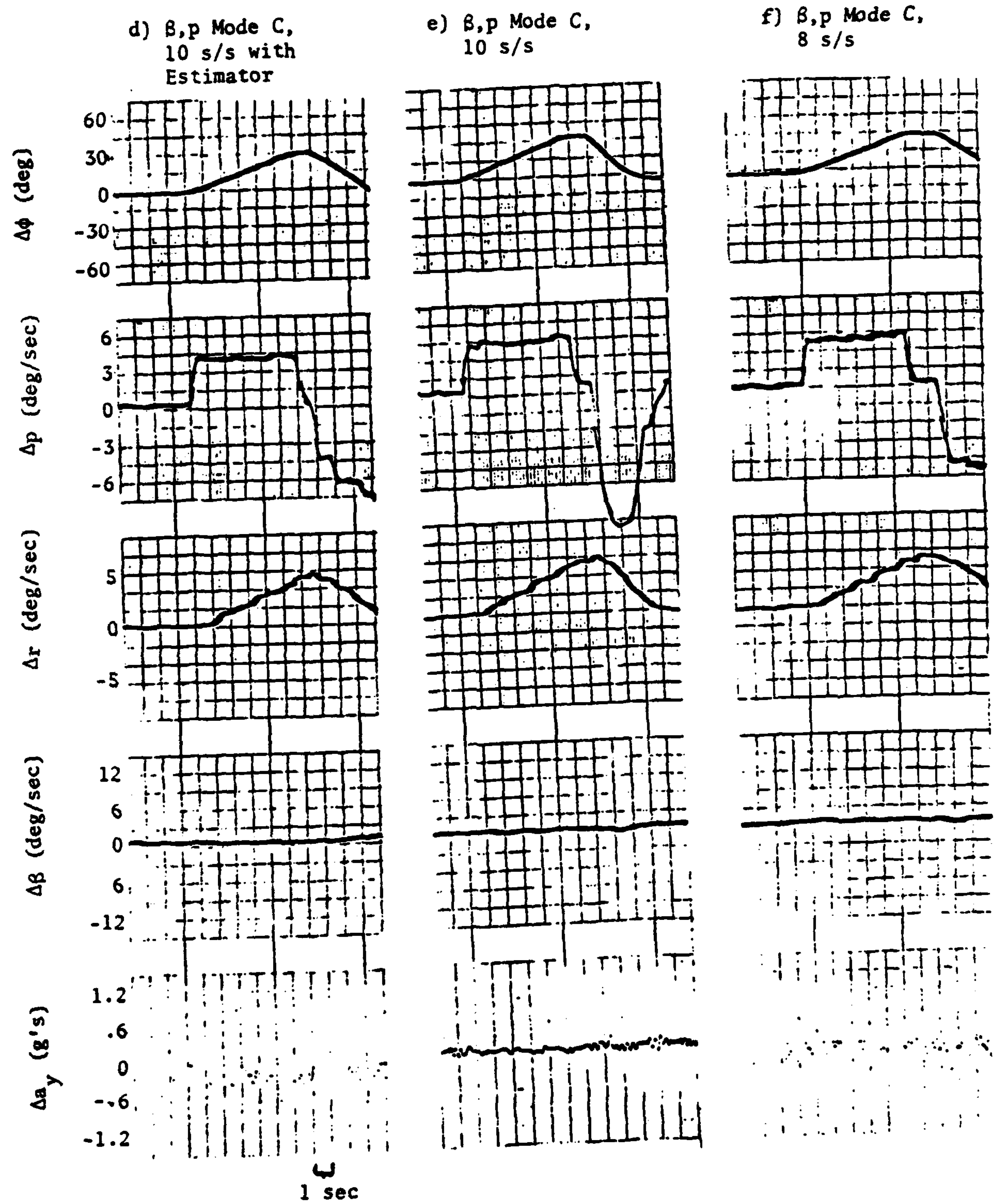

Figure 4-4. VRA Step Responses to Roll Rate Commands. (continued)

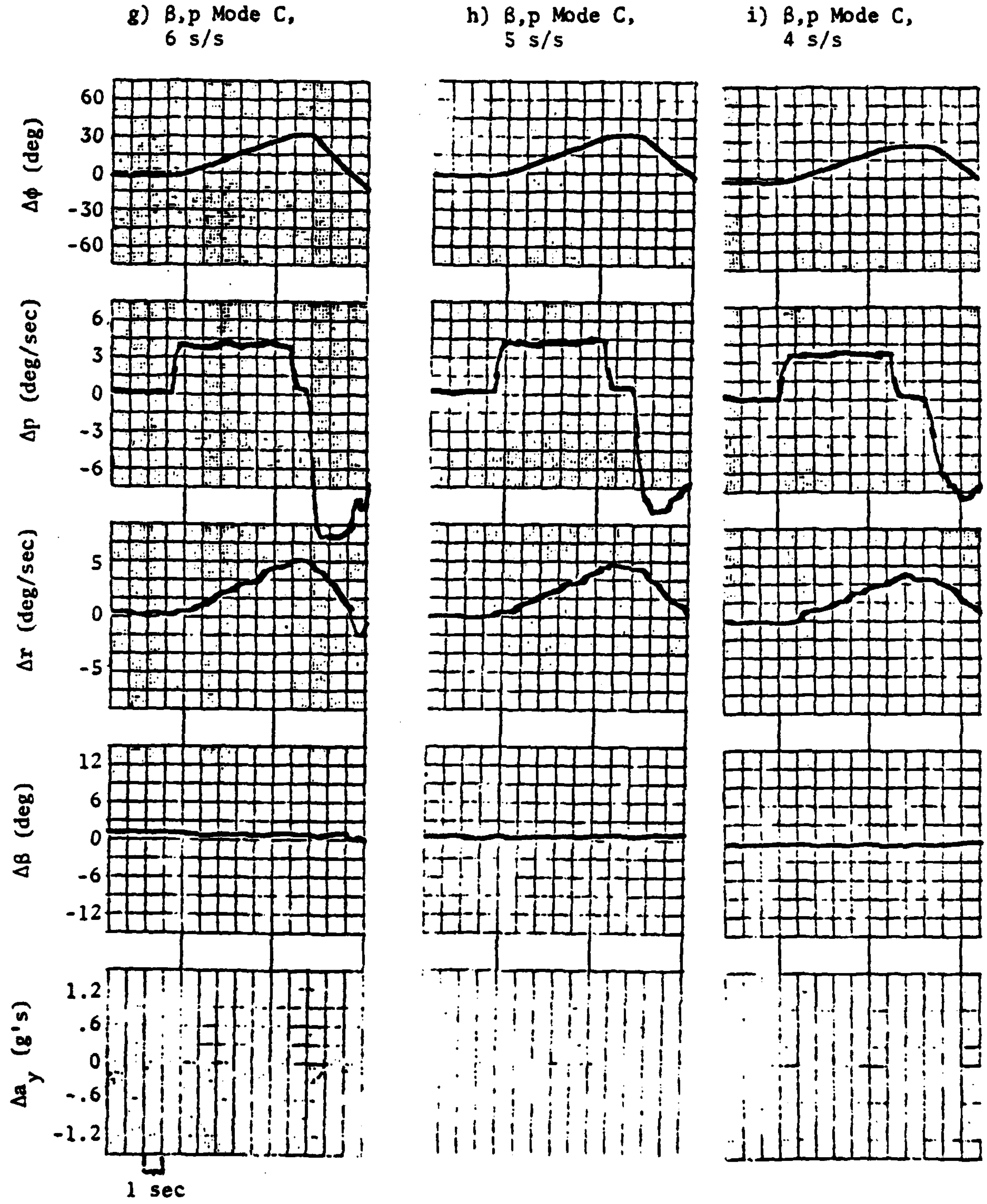

Figure 4-4. VRA Step Responses to Roll Rate Commands. (continued)

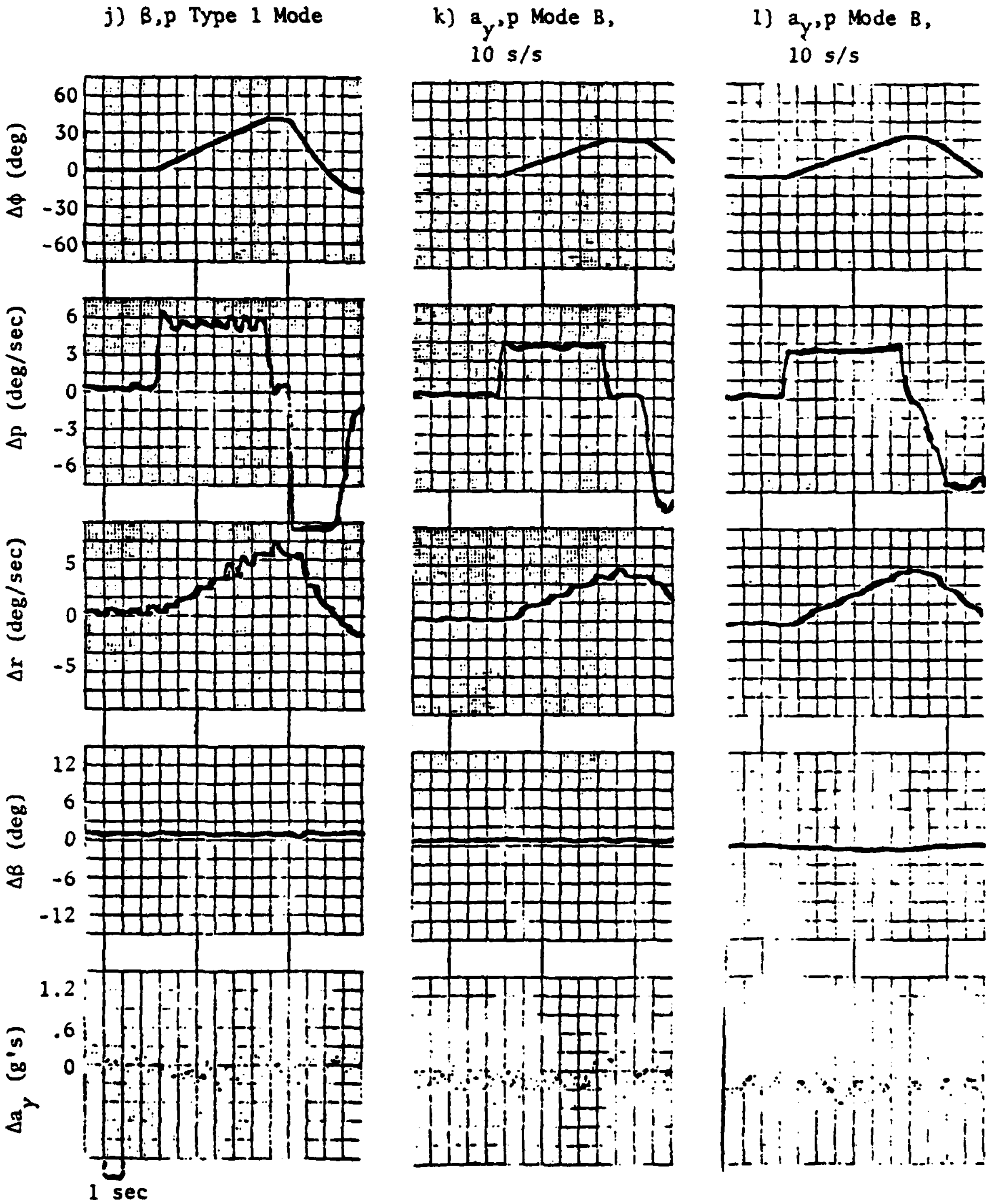

Figure 4-4. VRA Step Responses to Roll Rate Commands. (continued)

m) a_y,p Mode C,
10 s/s

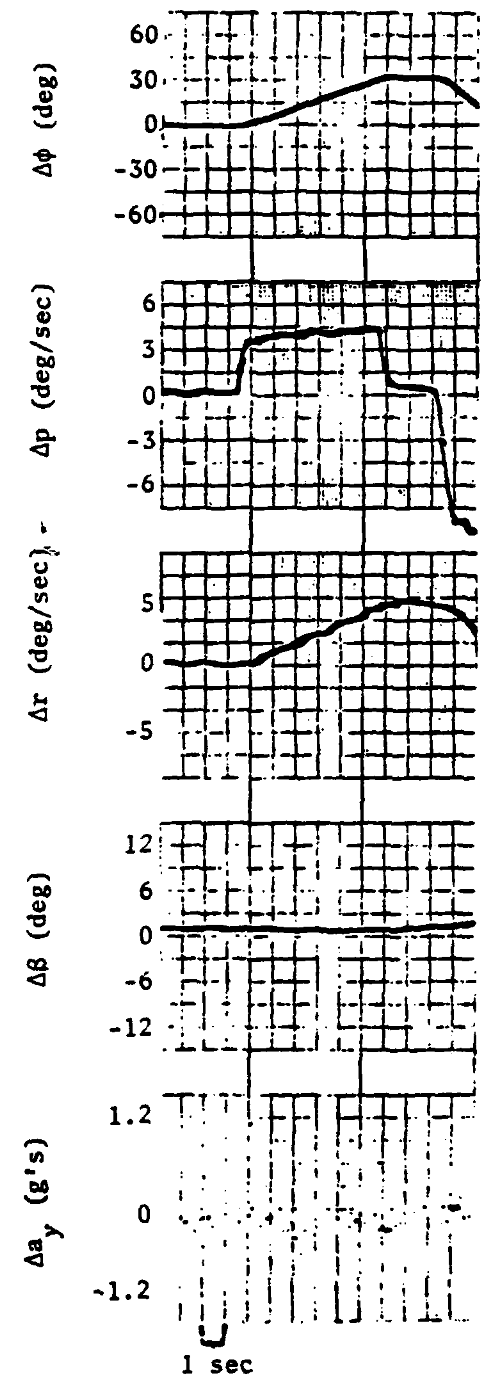

Figure 4-4. VRA Step Responses to Roll Rate Commands. (continued)

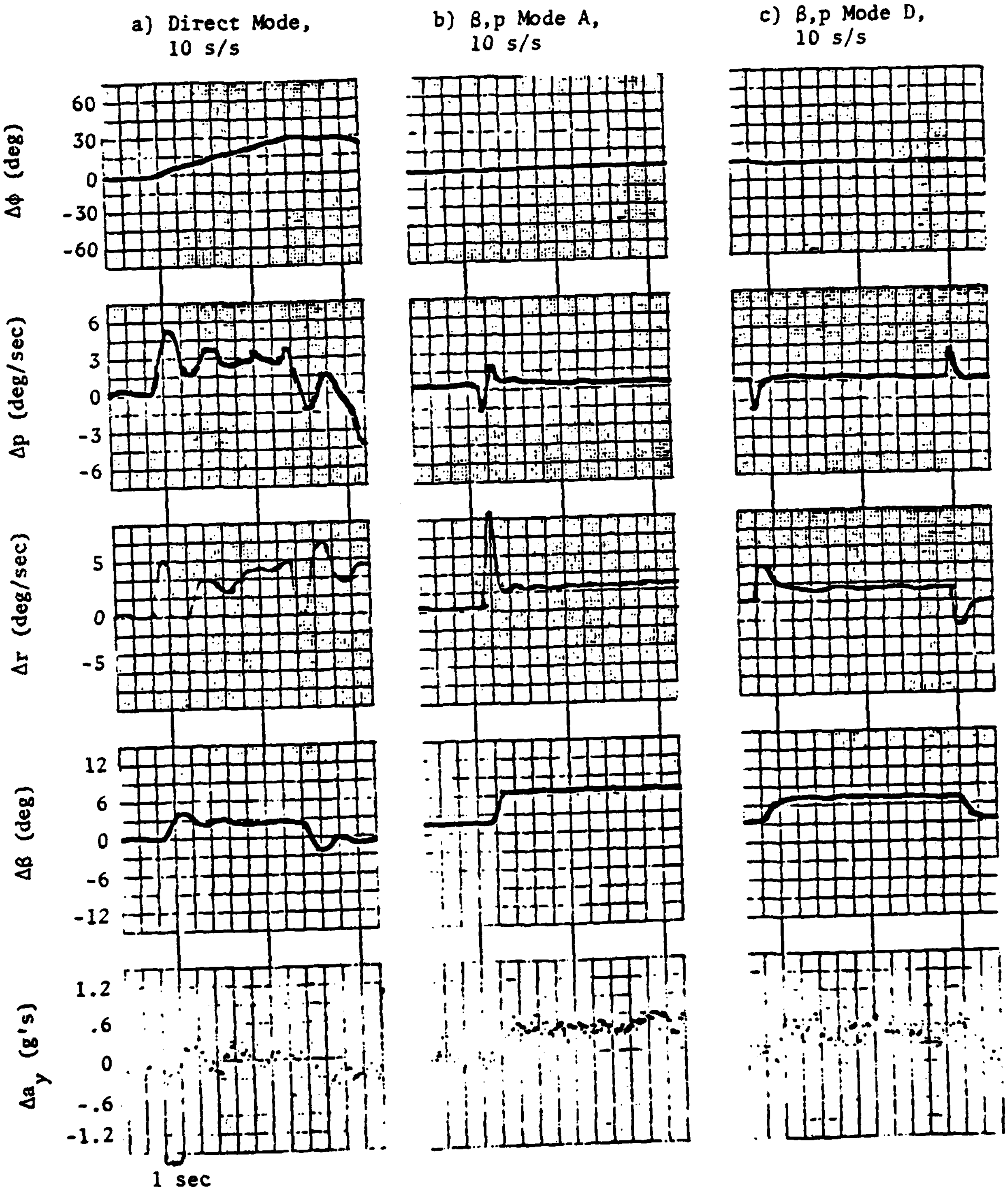

Figure 4-5. VRA Step Responses to Sideslip Angle Commands.

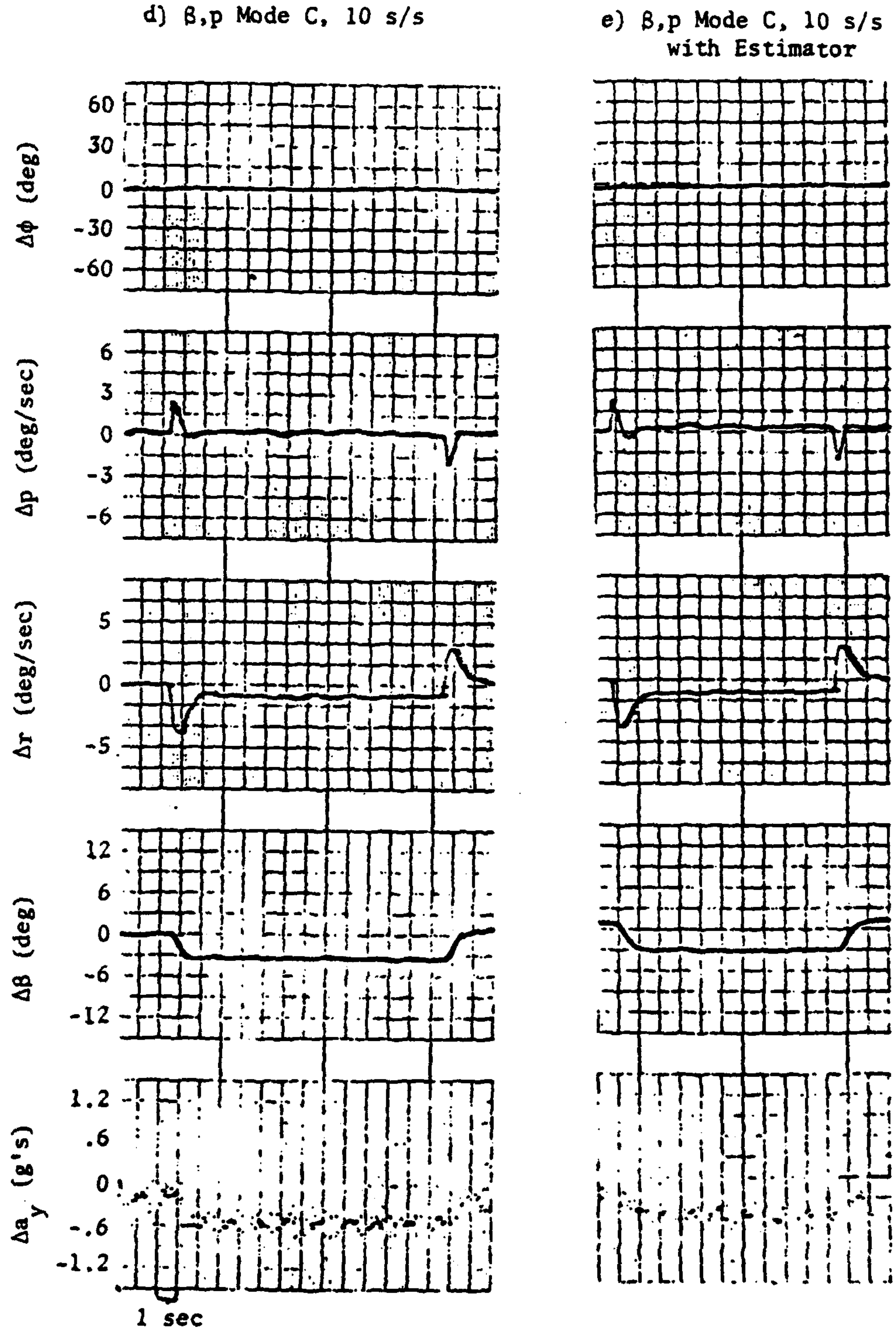

Figure 4-5. VRA Step Responses to Sideslip Angle Commands. (continued)

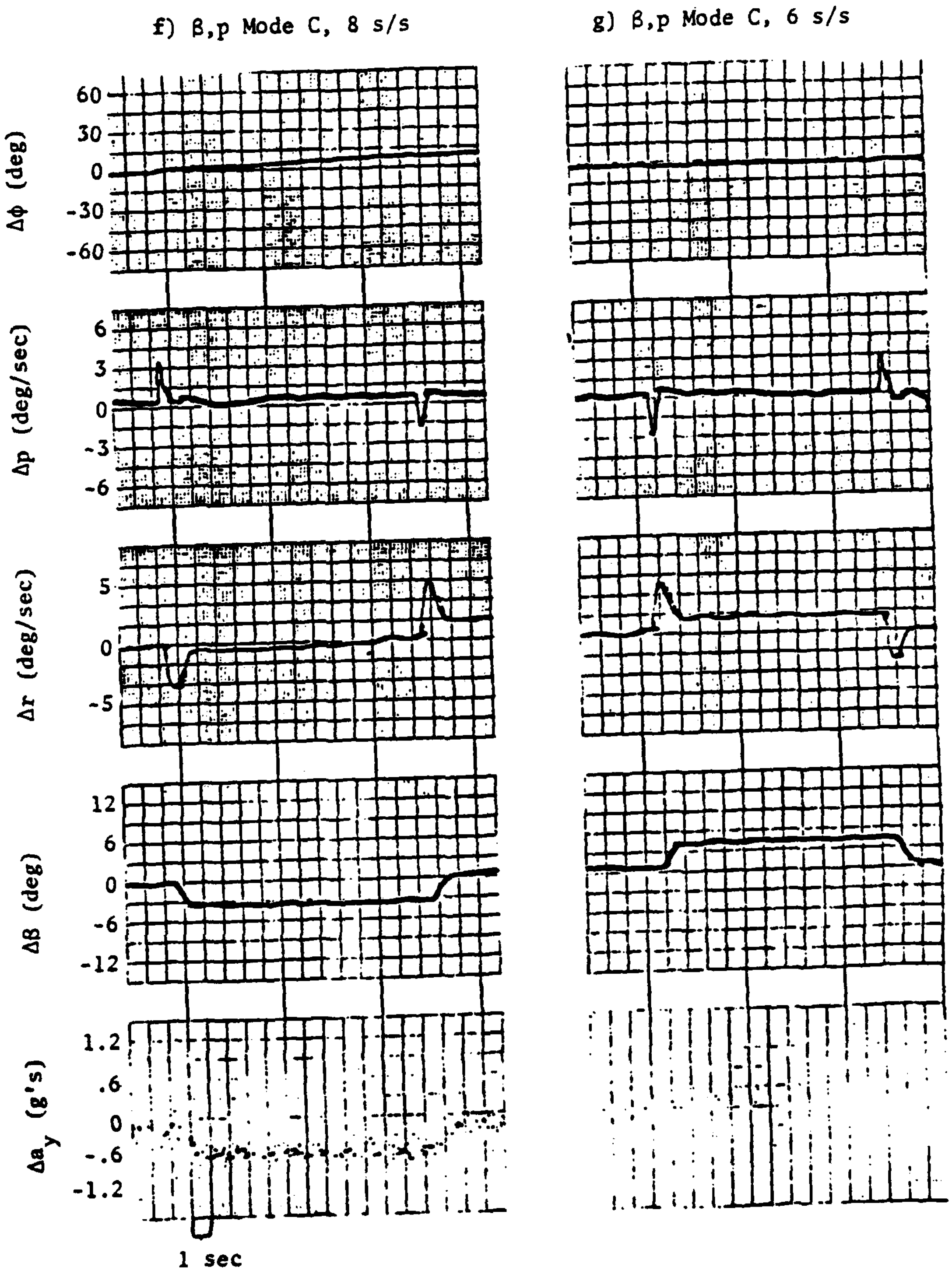

Figure 4-5. VRA Step Responses to Sideslip Angle Commands. (continued)

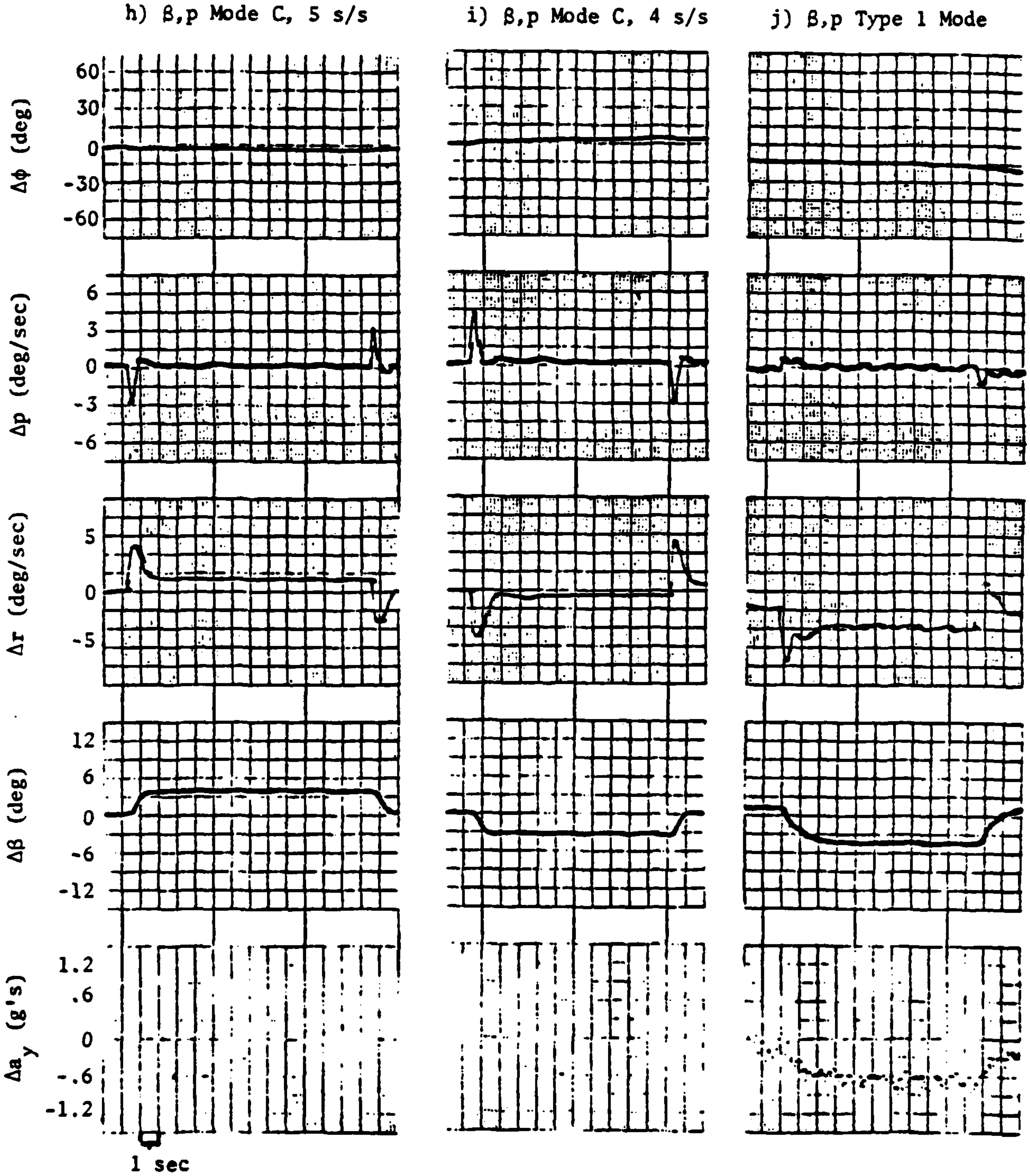

Figure 4-5. VRA Step Responses to Sideslip Angle Commands.

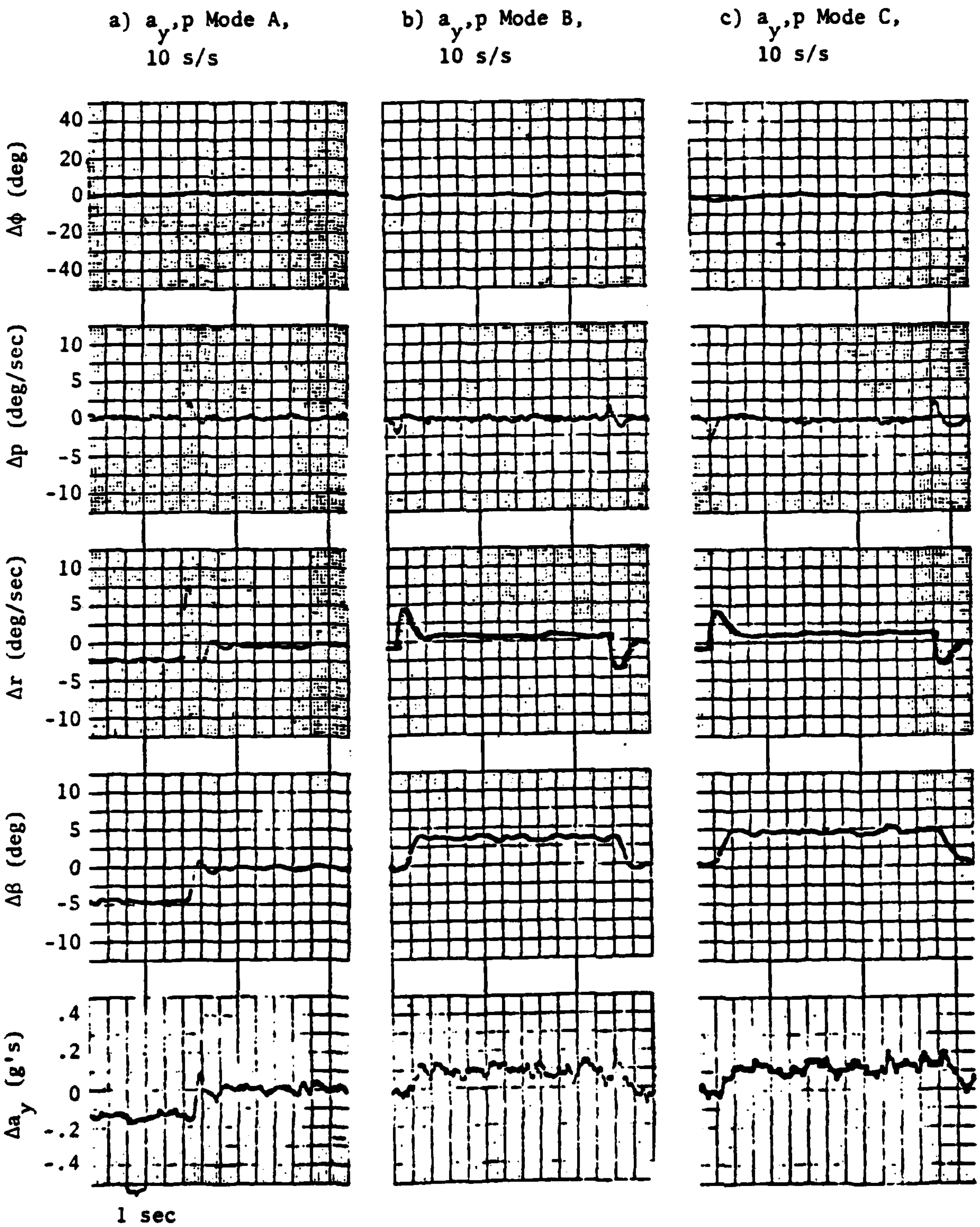

Figure 4-6. VRA Step Responses to Lateral Acceleration Commands.

first-order low-pass filters in series, each with a bandwidth of 1.6 Hz.

The step inputs were commanded using the calibrated step input routine described in Appendix D; command values for roll rate, sideslip angle, and lateral acceleration flight test responses were 5 degrees per second, 5 degrees, and 0.1 g's, respectively. These values are identical to those used in the hybrid simulation tests, except for lateral acceleration commands; hence, only those differences between the corresponding results or important aspects of the flight test results are presented here.

Two minor differences are immediately apparent in the flight test results. One is that the sense of the recorded sideslip angle response trace is opposite to that used in earlier analyses. The second difference is the drop-off that occurs in the roll rate response trace following a roll rate command. This is not a function of the control law itself; it merely reflects the safety pilot returning the VRA to the nominal flight condition.

Other observations of the flight test results are more substantial in nature. Obvious in the traces are the expected improvements of the Micro-DFCS responses over the unaugmented VRA responses. Improvements in roll rate command responses can be seen in the Δr and $\Delta\beta$ traces, where the adverse yaw is eliminated (Δr) and where turn coordination is provided (zero $\Delta\beta$ during a steady turn). More dramatic are the effects of the Micro-DFCS on the sideslip angle command response traces, where great improvements in decoupling and command response are seen in the traces of $\Delta\phi$, Δp, and $\Delta\beta$. Also expected and present in the traces is the sensitivity to disturbances of the Type 1 system.

In addition to producing expected and desired results, the flight test results revealed several unexpected phenomena. First was the

large overshoot of the Type 1 response in roll to roll rate command. This characteristic bears out the pilot comment that this configuration had a "faster than desired" roll response that did not occur with the hybrid simulation test response. Again, this could be due to the fact that the controller is very sensitive to disturbances. A second inconsistency in the flight test results is the fact that the roll rate and sideslip angle command responses did not appear to reach their commanded values. This could possibly be due to either the sensitivity or the scaling of the recorder. A closer examination of the responses leads to another explanation, however. In one case the responses reached their commanded values; the Type 1 responses to both roll rate and sideslip angle commands reached the commanded values while the Type 0 command responses did not. This would indicate that a degree of model mismatch existed between the linear model used in the design process and the actual VRA dynamic characteristics (See Section 2.5.6 for further explanation).

This concludes the results of the in-flight testing of the Micro-DFCS. The following chapter summarizes this investigation, and presents conclusions and recommendations for further study in this area.

5. CONCLUSIONS AND RECOMMENDATIONS

The microprocessor-based digital flight control system operating on Princeton University's Variable Response Research Aircraft has demonstrated, in flight, advanced concepts of command and stability augmentation. Using linear-quadratic sampled-data regulator theory, Type 0 regulators with control rate restraint and equivalent Type 1 regulators have been developed for singular command inputs. These allow the precise following of a command (roll rate) whose integral (roll angle) appears in the state vector, and they have been demonstrated successfully in flight. In addition, an alternative method of defining control structures for control rate outputs, one which uses the Tustin transform to characterize the control derivative in the discrete-time domain, has been developed.

5.1 CONCLUSIONS

The specific objectives of this investigation, outlined in Chapter 1, were to develop and present design and analysis methodologies for digital control structures, to demonstrate and compare these control laws in flight, and to determine the effects of design parameters on the resulting control law. These objectives have been achieved; the methodologies employed and the theoretical and actual flight test results and analyses have been presented in the body of this text. A summary of the major conclusions follows:

- The step response traces of the digital model, hybrid simulation, and flight test reveal nearly identical response characteristics at all sampling rates, indicating that the closed-loop characteristics of the controller are unaffected by the sampling rate when sampled-data regulator theory is used. The HQR given by the evaluation pilots indicate that the lower bound on the sampling rate in this study is a function of the task and of pilot preference.

- The Type 1 control law proved superior to the equivalent Type 0 control law in achieving the desired command response when the linear dynamic model used in the design process differed from the actual aircraft dynamic characteristics. Altering the actual aircraft stability derivatives did little to affect the step response characteristics of the Type 1 system, while causing the Type 0 controller to settle at mismatched values of state and control.

- The Type 0 control law proved superior to the Type 1 system in disturbance suppression and response. Hybrid simulation and flight test results show the equivalent Type 1 system to be unduly sensitive to disturbance inputs and measurement noise, indicating the need for state estimation and/or restructuring of the control law. The Type 0 control law provided improved performance over the open-loop system without state estimation.

- Satisfactory levels of closed-loop lateral-directional control can be achieved without an operationally difficult measurement of sideslip angle. Lateral acceleration/roll rate control structures provided nearly identical command response characteristics as sideslip angle/roll rate controllers, while using feedback of lateral acceleration rather than sideslip angle. In addition, the Type 0 control law using a first-order sideslip angle estimator based on a Kalman filter provided identical command response as the Type 0 control law using the actual sideslip angle measurements.

- In the Type 0 regulator with rate restraint, using the Tustin transform to characterize the control derivative in the discrete-time domain proved theoretically advantageous to using a first-difference approximation. Using the first-difference approximation, the initial response of the controller is independent of the parameters used in the design process; it depends only upon the steady-state values of the control. In some instances, this may not be acceptable; an alternate method of defining the initial responses or an

alternate form of the control law may be desired. The Tustin transform approach provides an alternative form; using this approach, the initial command response characteristics are shaped by the choice of weighting factors used in the design process. These results are borne out by computer generated response traces based on the digital model, although this alternate form was not implemented in the Micro-DFCS.

- The equations of modern control theory can be used to define command structures for singular command inputs through simple matrix manipulation. By removing the integral of the command variable from the state vector and treating it as a disturbance, and by moving its dynamics from the system dynamics matrix to the disturbance effects matrix, the system can be treated as non-singular with known disturbances. This manipulation is required in computing steady-state relationships and in defining equivalent Type 1 command structures.

- The equations of modern control theory combined with microcomputer technology provide substantial capacity for conducting advanced research in digital flight control. The microcomputer used in this study has the speed to execute advanced control laws at the sampling rates afforded by modern control theory design concepts. Execution of the Type 0 regulator with control rate restraint using two pilot inputs, two aircraft controls, and four-state feedback utilized a maximum of 37% of the available duty cycle at a sampling rate of 10 sps; this figure could have been reduced had the entire control algorithm been optimized with respect to time. The speed of this computer coupled with its ease of expansion (additional memory, analog channels, or other peripheral devices), make the microcomputer/modern control theory combination an attractive means of future research in the area of digital flight control.

5.2 RECOMMENDATIONS

Based on experiences gained and results gathered from this investigation, recommendations are made for the continuation of research into digital flight control using microprocessor technology. These include the following:

- A Type 0 regulator with control rate restraint designed using the Tustin transform to characterize the control derivative should be coded and implemented in the Micro-DFCS. Preliminary investigation indicates that this form of the control law is advantageous in that the initial response is dependent upon the design parameters. It remains to be seen whether the implementation and the overall closed-loop performance of such a control law prove superior to its alternate form and warrant its inclusion in an operational system.

- Further investigation into the Type 1 regulator is warranted. Initial investigation revealed that the Type 1 system did null steady-state errors, even in the presence of severe model mismatch, although this was severely outweighed by its undesirable characteristics, notably its extreme sensitivity to disturbance and noise and its instability when used with the sideslip angle estimator. Areas of investigation should include possible restructuring of the control law itself, and the use of state estimation. While it was the state estimation which caused the Type 1 system to become unstable, it should be noted that it was a first-order Kalman filter with constant gains, whose use may be unjustified in the case of the Type 1 system. A higher order Kalman filter could improve the situation and should be investigated.

- Consideration should be given to filtering all the signals from the sensors and pilot controls before the A/D conversion to prevent high frequency noise from being folded into the frequencies of interest by the sampling process. If this high frequency content

is large in magnitude relative to the frequencies of interest, the actual sampled data is distorted and the performance of the Micro-DFCS is adversely affected. In an operational system, all inputs would be filtered to guard against noise, and such measures are recommended here, especially for further research into the Type 1 system. Only the a_y signal was filtered in this investigation.

- The flight tests conducted in this investigation were conducted in smooth air. Further tests should be conducted in turbulent air to reevaluate the closed-loop dynamics in the presence of disturbances. Emphasis should be placed on determining the effects of the sampling rate on closed-loop control with disturbances present.

- As the control algorithms become more complex, extreme care should be taken to ensure that all Flight Control Routines are written to conserve time, not memory. The most critical element in the control calculation is the time between input and output; the time between pilot command and controller response must be kept at an absolute minimum. The experimental system should have enough memory so that space conservation is not a consideration. Time should be conserved by minimizing the number of necessary computations, eliminating generalized subroutines from the control program, and by making each Flight Control Routine specific to its task.

APPENDIX A

Derivation of the Linear-Quadratic Regulator with Rate Restraint Using the Tustin Transform

An alternate form of the Type 0 control law with control rate restraint is desired for the reasons presented in Section 2.3-3. Using a first-difference approximation for control rate, the initial control response is independent of the weighting factors used in the design process. By using the Tustin Transform instead of the first-difference approximation, an alternate form of the control law is derived which allows shaping the initial command response with weighting factors. This derivation proceeds as follows.

The following relationships are defined as before:

$$\Delta\underline{\tilde{u}} = \Delta\underline{u} - \Delta\underline{u}^* \tag{A-1}$$

$$\Delta\underline{\tilde{x}} = \Delta\underline{x} - \Delta\underline{x}^* \tag{A-2}$$

$$\Delta\underline{\tilde{v}} = \Delta\underline{\dot{u}} - \Delta\underline{\dot{u}}^* = \Delta\underline{\dot{u}} \tag{A-3}$$

since $\Delta\underline{\dot{u}}^* = 0$. The desired control law is given by

$$\Delta\underline{\tilde{v}}_k = -K_1\,\Delta\underline{\tilde{x}}_k - K_2\,\Delta\underline{\tilde{u}}_k \tag{A-4}$$

or

$$\Delta\underline{\dot{u}}_k = -K_1\,\Delta\underline{\tilde{x}}_k - K_2(\Delta\underline{u}_k - \Delta\underline{u}_k^*) \tag{A-5}$$

Taking the Laplace Transform of this yields

$$(sI + K_2)\,\Delta\underline{u}_k(s) = -K_1\,\Delta\underline{\tilde{x}}_k(s) + K_2\,\Delta\underline{u}_k(s) \tag{A-6}$$

Defining the Tustin Transform as

$$s = \frac{2}{\Delta t}\left(\frac{z-1}{z+1}\right) \quad ; \quad \Delta\underline{u}_k(s) \rightarrow \Delta\underline{u}_k(z) = \Delta\underline{u}_k \tag{A-7}$$

and substituting it into A-5 yields

$$\left[\frac{2}{\Delta t}\left(\frac{z-1}{z+1}\right) + K_2\right]\Delta\underline{u}_k = -K_1\,\Delta\tilde{\underline{x}}_k + K_2\,\Delta\underline{u}^*_k \tag{A-8}$$

Expanding equation A-8 leads to

$$\left[\left(\frac{2}{\Delta t} I + K_2\right)z + \left(K_2 - \frac{2}{\Delta t} I\right)\right]\Delta\underline{u}_k = (z+1)\left[-K_1\Delta\tilde{\underline{x}}_k + K_2\Delta\underline{u}^*_k\right] \tag{A-9}$$

Transforming this back to the discrete domain and shifting the sampling index using

$$z\Delta\underline{u}_k \to \Delta\underline{u}_k \quad ; \quad \Delta\underline{u}_k \to \Delta\underline{u}_{k-1}$$

gives

$$\left(\frac{2}{\Delta t} I + K_2\right)\Delta\underline{u}_k + \left(K_2 - \frac{2}{\Delta t} I\right)\Delta\underline{u}_{k-1} = -K_1\left(\Delta\tilde{\underline{x}}_k + \Delta\tilde{\underline{x}}_{k-1}\right) + K_2\left(\Delta\underline{u}^*_k + \Delta\underline{u}^*_{k-1}\right) \tag{A-10}$$

The final form of the control law is

$$\Delta\underline{u}_k = \left(\frac{2}{\Delta t} I + K_2\right)^{-1}\left[\left(\frac{2}{\Delta t} I - K_2\right)\Delta\underline{u}_{k-1} - K_1\left(\Delta\tilde{\underline{x}}_k + \Delta\tilde{\underline{x}}_{k-1}\right) + K_2\left(\Delta\underline{u}^*_k + \Delta\underline{u}^*_{k-1}\right)\right] \tag{A-11}$$

This form must satisfy two conditions to provide the desired properties: the initial response should depend upon the optimal gains, and the control should reach the desired steady state in the limit. Suppose that the system is at rest with

$$\Delta\underline{y}_{k-1} = \Delta\underline{u}_{k-1} = \Delta\underline{u}^*_{k-1} = \Delta\underline{x}_{k-1} = \Delta\underline{x}^*_{k-1} = \Delta\underline{x}_k = 0$$

Then for some initial commands

$$\Delta\underline{y}_k \neq 0$$

Equation A-11 provides that

$$\Delta\underline{u}_k = \left(\frac{2}{\Delta t} I + K_2\right)^{-1}\left[K_1\,\Delta\underline{x}^*_k + K_2\,\Delta\underline{u}^*_k\right] \tag{A-12}$$

and the first condition is met. Similarly, under steady state conditions,

$$\Delta \underline{x}_{k-1} \rightarrow \Delta \underline{x}_k \rightarrow \Delta \underline{x}_k^* \quad ; \quad \Delta \underline{u}_{k-1} \rightarrow \Delta \underline{u}_k \rightarrow \Delta \underline{u}_k^*$$

and

$$\Delta \tilde{\underline{x}}_k = \Delta \tilde{x}_{k-1} = 0$$

Then Equation A-11 reduces to

$$\Delta \underline{u}_k = \left(\frac{2}{\Delta t} I + K_2\right)^{-1} \left[\left(\frac{2}{\Delta t} I - K_2\right)\Delta u_k^* + 2K_2 \; \Delta \underline{u}_k^*\right]$$

$$= \left(\frac{2}{\Delta t} I + K_2\right)^{-1} \left[\left(\frac{2}{\Delta t} I + K_2\right)\Delta u_k^*\right]$$

$$= \Delta \underline{u}_k^*$$

and the second condition is met. Thus Equation A-11 is the desired form of the Type 0 controller with control rate restraint.

APPENDIX B

Derivation of a Type 1 Control Law for Commands Whose Integral Appears in the State Vector

An equivalent Type 1 controller is derived for a command whose integral appears in the state vector. When this is not the case, a Type 0 control law is transformed into an equivalent Type 1 controller by simple manipulation of the gains according to the relationship presented in Section 2.3.4,

$$[C_1 \quad C_2] = [\Delta t\ K_1 \quad t\Delta K_2] \begin{bmatrix} (\Phi - I) & \Gamma \\ H_x & H_u \end{bmatrix}^{-1} \tag{B-1}$$

When the integral of a command appears in the state vector, however, the compound matrix in Equation B-1 is non-invertible, and a new relationship must be found. The development of the control law for this case is presented.

The state vector is first redefined as in Equation 2.3-26,

$$\Delta \underline{x}'^T = [\Delta r \quad \Delta \beta \quad \Delta p] \tag{B-2}$$

and $\Delta\phi$ is treated as a disturbance. Using this relationship, the Type 0 control law, Equation 2.3-55,

$$\Delta \tilde{\underline{u}}_k = (I - \Delta t K_2)\Delta \tilde{\underline{u}}_{k-1} - \Delta t K_1\ \Delta \tilde{\underline{x}}_{k-1} \tag{B-3}$$

can be rewritten as

$$\Delta \tilde{\underline{u}}_k = (I - \Delta t K_2)\Delta \tilde{\underline{u}}_{k-1} - \Delta t K_1'\ \Delta \tilde{\underline{x}}'_{k-1} - \Delta t K_\phi\ \Delta \tilde{\phi}_{k-1} \tag{B-4}$$

where K_1' represents the first three columns of K_1 and K_ϕ represents the optimal gains for roll angle (i.e., the last column of K_1). Using this reduced-order vector, a relationship similar to Equation B-1 is defined, where the primed terms indicate a reduced-order matrix:

$$[C_1' \quad C_2] \begin{bmatrix} (\Phi - I)' & \Gamma' \\ & \\ H_x' & H_u \end{bmatrix} = [\Delta t K_1' \quad \Delta t K_2] \tag{B-5}$$

Now this matrix is non-singular, and the equivalent Type 1 controller can be defined.

Expanding Equation B-5 gives the desired relationships

$$\Delta t K_1' = C_1'(\Phi - I)' + C_2 H_x' \tag{B-6}$$

$$\Delta t K_2 = C_1' \Gamma' + C_2 H_u \tag{B-7}$$

Substituting these into Equation B-4,

$$\begin{aligned} \Delta\tilde{\underline{u}}_k - \Delta\tilde{\underline{u}}_{k-1} = & -C_1'(\Phi'\Delta\tilde{\underline{x}}_{k-1}' + \Gamma'\Delta\tilde{\underline{u}}_{k-1}) - C_1'\Delta\tilde{\underline{x}}_{k-1} - C_2(H_x'\Delta\underline{x}_{k-1}' + H_u\Delta\tilde{\underline{u}}_{k-1}) \\ & -\Delta t K_\phi \, \Delta\tilde{\phi}_{k-1} \end{aligned} \tag{B-8}$$

Recalling that when ϕ is treated as a disturbance,

$$\Phi'\Delta\underline{x}_{k-1}' + \Gamma'\Delta\underline{u}_{k-1} + \Lambda'\Delta\phi_{k-1} = \Delta\underline{x}_k \tag{B-9}$$

Equation B-8 can be rewritten as

$$\Delta\tilde{\underline{u}}_k - \Delta\tilde{\underline{u}}_{k-1} = -C_1'(\Delta\tilde{x}_k - \Delta\tilde{x}_{k-1}') - C_2(H_x'\Delta\tilde{\underline{x}}_{k-1} + H_u\Delta\tilde{u}_{k-1}) - (C_1\Lambda' - \Delta t K_\phi)\Delta\tilde{\phi}_{k-1} \tag{B-10}$$

Using the assumption that each command can be treated as a step input, that is that $\Delta\underline{y}_d$ remains constant over the interval and the pilot commands state variables directly, and using Equations 2.3-35 through 2.3-38,

$$\Delta\underline{x}_k^* - \Delta\underline{x}_{k-1}^* = S_{11}' \, \Lambda \, (\Delta\phi_k^* - \Delta\phi_{k-1}^*) \tag{B-11}$$

$$\Delta \underline{u}_k^* - \Delta \underline{u}_{k-1}^* = S_{21}' \Lambda \, (\Delta \underline{\phi}_k^* - \Delta \phi_{k-1}^*) \tag{B-12}$$

and

$$\Delta \phi_k^* - \Delta \phi_{k-1}^* \approx \Delta p^* \, \Delta t \tag{B-13}$$

Substituting these into Equation B-10 yields the final form of the equivalent Type 1 controller,

$$\Delta \underline{u}_k = \Delta \underline{u}_{k-1} - S_{11}' \Lambda (\Delta p^* \Delta t) - C_1' [(\Delta \underline{x}_k' - \Delta x_{k-1}') + S_{11}' \Lambda (\Delta \bar{p}^* \Delta t)]$$

$$- C_2 (H_x' \Delta \underline{x}_{k-1}' - \underline{y}_{d_k}) + (C_1' \Lambda - \Delta t K_\phi)(\Delta \phi_k - \Delta \phi_{k-1}^*) \tag{B-14}$$

The final term in Equation B-14 was assumed to be negligible in the body of this work.

APPENDIX C

Description of APL Functions for Generating Optimal Gains and Time Histories

The equations from modern control theory presented in Chapter 2 are coded in APL functions. A description of each of the functions, presented in Table C-1, is given below:

AUG - Builds a discrete control effects matrix for the augmented system given by Equations 2.3-45 and 2.3-46. Γ' is returned in variable GAMPR.

AUGPHI - Builds a state transition matrix for the augmented system given matrices Φ and Γ. Φ' is returned in variable STMPR.

DCOV - Calculates discrete-time covariance matrix for Kalman filter gain calculations. Uses simple Euler integration in 100 steps. Uses Equation 2.4-15.

FCLOOP - Calculates the closed-loop F matrix for the augmented system given Φ', Γ', and the optimal gains. F_{CL} is returned in variable FCL. Uses Equation 2.3-17.

GAIN - Calculates optimal gains according to Equation 2.5-51. Gains are returned in variables K1 and K2.

GAIN 1 - Calculates Type 1 optimal gains using Equation 2.3-68. Gains returned in variables C_1 and C_2.

GAMMA - Calculates the discrete control effects matrix, Γ, using Equation 2.3-6. Given the state transition matrix, Φ, it returns Γ in variable GAM.

GENSTM - Generates 100 Φ matrices using time intervals of 1 percent increments of the sampling interval. These matrices are for

use in the generation of the discrete weighting matrices.

IDENT - Builds an identity matrix of dimension specified as the argument. Matrix is returned in variable I.

KALG - Calculates the steady-state discrete time state covariance, Φ, and Kalman filter gains, K, using Equation 2.4-35 and 2.4-36.

LAMBDA - Calculates the disturbance effects matrix, Λ, given the matrix Φ, using Equation 2.3-39. Result returned in variable LAM.

OLMOD - Calculates time histories for the open-loop response and Kalman filter response. Uses Equations 2.3-4 and 2.4-7. Aircraft response is stored in matrix Δx while estimator histories are stored in matrix XET. These matrices are used in the 10 LINPLOT routines to plot the time histories.

QMR - Calculates discrete weighting matrices $\hat{Q}$, $\hat{N}$, and $\hat{R}$ from continuous Q' and R'. Uses simple Euler integration in 100 steps according to Equations 2.3-47 through 2.3-49.

RICCATI - Solves Riccati equation (Equation 2.3-52). Result returned in variable P.

QPRIME - Calculates the continuous matrix Q' based on state, state rate, and control weightings. Uses Equation 2.3-76. Result returned in variable Q'.

SMATRIX - Computes the steady-state relationships S_{11}, S_{12}, S_{21}, and S_{22} using Equation 2.3-34.

STATECOV - Propagates the state covariance matrix P and stores the results for plotting. Uses simple Euler integration and Equation 2.3-14. Results stored in matrix PT for plotting using the 10 LINPLOT routines.

STMDYN - Calculates the state transition matrix, Φ, given the time interval and matrix F. Uses Equation 2.3-5. Result returned in variable PHI.

SYSMODEL - Generates a time history for the closed-loop system. The function will ask if a printed table is desired (answer yes or no). The time history will run for 5 seconds unless 'BREAK' is depressed. The histories are stored in matrices DELX and DELV. DELX contains the histories of Δr, $\Delta\beta$, Δp, and $\Delta\phi$. DELV contains the histories of $\Delta\delta R$ and $\Delta\delta A$. The histories are plotted using the 10 LINPLOT functions. Uses Equations 2.3-4 and 2.3-56.

SYSMODEL 1 - Generates time histories for the type 1 system. Results are stored in matrices DELX and DELU, as in SYSMODEL. Uses Equations 2.3-4 and 2.3-75.

TABLE C-1. Listing of APL Functions

```
      ∇AUG[⎕]∇
      ∇ AUG TI
[1]   ⍝CALCULATES GAMMA PRIME FOR AUGMENTED STATE VECTOR
[2]    GAMPR← 6 2 ⍴0
[3]    GAMPR[5;1]←TI
[4]    GAMPR[6;2]←TI
      ∇

      ∇AUGPHI[⎕]∇
      ∇ AUGPHI FI
[1]   ⍝CALULATES PHI PRIME FOR AUGMENTED STATE VECTOR
[2]    STMPR←(FI,GAM),[1]((2 4 ⍴0),(2 2 ⍴ 1 0 0 1))
      ∇

      ∇DCOV[⎕]∇
      ∇ DCOV CC
[1]   ⍝FINDS DISCRETE TIME COVARIANCE MATRIX FROM
[2]   ⍝THE CONTINUOUS TIME DISTURBANCE COVARIANCE MATRIX.
[3]   ⍝LINE 10 MUST BE ALTERED DEPENDING ON THE ORDER OF THE SYSTEM.
[4]    DCO←STM-STM
[5]    T←STEP←DT÷100
[6]    C←1
[7]   LOOP:C←C+CC
[8]    D←C+1
[9]    DD←D+1
[10]   STATETM←⍉STATETM← 2 2 ⍴GSTM[;C],GSTM[;D]
[11]   ID←STEP×(STATETM+.×L+.×CCOV)+.×(⍉L)+.×(⍉STATETM)
[12]   DCO←DCO+ID
[13]   →(T=DT)/0
[14]   T←T+STEP
[15]   →LOOP
      ∇

      ∇FCLOOP[⎕]∇
      ∇ FCLOOP;SM;R;FACTOR;INDEX;I;IFCL
[1]   ⍝CALCULATES C.L. F MATRIX FOR THE AUGMENTED SYSTEM
[2]    RR←(⍴,STMPR)*0.5
[3]    I←(⍳RR)∘.=⍳RR
[4]    N←0
[5]    FCL←I-I
[6]    STMCL←STMPR-GAMPR+.×K
[7]    STMI←I
[8]   LO:N←N+1
[9]    STMI←(STMCL-I)+.×STMI
[10]   FACTOR←((¯1)*N+1)×STMI
[11]   IFCL←FCL+FACTOR÷N
[12]   INDEX←(+/|,FCL-IFCL)÷RR*2
[13]   FCL←IFCL
[14]   →(N=100)/STP
[15]   →(INDEX>0.00001)/LO
[16]   →CONT
[17]  STP:'DID NOT CONVERGE ON C.L.F  MATRIX IN 100 ITERATIONS.'
[18]  CONT:FCL←FCL÷DT
      ∇
```

Table C-1 Continued

```
      ∇GAIN[⎕]∇
      ∇ GAIN
[1]   ⍝CALCULATES OPTIMAL GAINS
[2]   K←(⌹RH+(⍉GAMPR)+.×P+.×GAMPR)+.×((⍉GAMPR)+.×P+.×STMPR)+⍉NH
[3]   K1←⍉K1← 4 2 ⍴K[;1],K[;2],K[;3],K[;4]
[4]   K2←⍉K2← 2 2 ⍴K[;5],K[;6]
      ∇

      ∇GAIN1[⎕]∇
      ∇ GAIN1
[1]   ⍝CALCULATES TYPE 1 GAINS FROM TYPE 0 GAINS
[2]   PHIR← 3 3 ↑(STM-IDENT 4)
[3]   GAMR← 3 2 ↑GAM
[4]   TFM←(PHIR,GAMR),[1]((2 3 ↑HX),HU)
[5]   KR←DT×((2 3 ↑K1),K2)
[6]   CC←KR+.×(⌹TFM)
[7]   C13← 2 3 ↑CC
[8]   C2← 2 ¯2 ↑CC
[9]   C1←C13, 2 1 ⍴0
[10]  C←C1,C2
      ∇

      ∇GAMMA[⎕]∇
      ∇ GAMMA STM
[1]   ⍝  CALCULATES GAMMA MATRIX
[2]   GAM←STM+.×(⌹F)+.×(I-(⌹STM))+.×G
      ∇

      ∇GENSTM[⎕]∇
      ∇ GENSTM;STEP
[1]   ⍝ GENERATES 100 TRANSITION MATRICES FOR QMR
[2]   T←STEP←DT÷100
[3]   GSTM←I
[4]  AGAIN:STMI←T STMDYN F
[5]   GSTM←GSTM,STMI
[6]   →(T=DT)/0
[7]   T←T+STEP
[8]   →AGAIN
      ∇

      ∇IDENT[⎕]∇
      ∇ I←IDENT N
[1]   ⍝  MAKES IDENTITY MATRIX OF SIZE N
[2]   I←⍳N
[3]   I←I∘.=I
      ∇
```

Table C-1 continued

```
      ∇KALG[⎕]∇
      ∇ KALG
[1]   ⍝COMPUTES STEADY STATE DISCRETE TIME STATE COVARIANCE
[2]   ⍝MATRIX AND KALMAN ESTIMATOR GAINS
[3]    P←DCO
[4]    COUNT←0
[5]    ERROR←1E¯12
[6]   LOOP:GPS←STM+.×P+.×⍉HX
[7]    NP←(STM+.×P+.×⍉STM)−(GPS+.×(⌹(HX+.×P+.×⍉HX)+MCOV)+.×⍉GPS)−DCO
[8]    COUNT←COUNT+1
[9]    DIFF←NP−P
[10]   P←(NP+⍉NP)÷2
[11]   A←(|DIFF)>ERROR
[12]   B←+/A
[13]   C←+/B
[14]   →(COUNT=100)/STOPS
[15]   →(C≥1)/LOOP
[16]   K←(P+.×⍉HX)+.×(⌹(HX+.×P+.×⍉HX)+MCOV)
[17]   →0
[18]  STOPS:'DID NOT CONVERGE IN 100 ITERATIONS.'
[19]   →0
      ∇
      ◆

      ∇LAMBDA[⎕]∇
      ∇ LAMBDA STM
[1]   ⍝CALCULATES LAMBDA MATRIX
[2]    LAM←STM+.×(⌹F)+.×(I−(⌹STM))+.×L
      ∇
      ◆

      ∇OLMOD[⎕]∇
      ∇ OLMOD
[1]   ⍝CALCULATES OPEN LOOP RESPONSE AND ESTIMATOR RESPONSE
[2]   ⍝AND STORES RESULTS FOR GRAPHING.  LINE 11
[3]   ⍝MUST BE CHANGED ACCORDING TO THE MEASUREMENT VECTOR
[4]    DELX←DELXY←∆X← 4 1 ⍴0
[5]    XE←XET←L−L
[6]    TIME←T←BA←0
[7]   GO:T←T+DT
[8]    DELX←(STM+.×DELX)+(GAM+.×YD)
[9]    DELXY←(STMY+.×DELXY)+(GAMY+.×YD)
[10]   NY←DELXY[2;]
[11]   ∆Z← 2 1 ⍴DELX[1;],NY
[12]   XEM←(STME+.×XE)+(GAME+.×YD)
[13]   XE←XEM+K+.×(∆Z−((HX+.×XEM)+(HU+.×YD)))
[14]   TIME←TIME,T
[15]   XET←XET,XE
[16]   ∆X←∆X,DELX
[17]   →(T=15)/0
[18]   →GO
      ∇
```

Table C-1 continued

```
      ∇QMR[⎕]∇
      ∇ QMR;STEP
[1]   ⍝  CALCULATES Q HAT, N HAT , R HAT
[2]    NH← 6 2 ⍴0
[3]    QH← 6 6 ⍴0
[4]    RH← 2 2 ⍴0
[5]    T←STEP←DT÷100
[6]    C←1
[7]   LOOP:C←C+4
[8]    D←C+1
[9]    CC←D+1
[10]   DD←CC+1
[11]   STATETM←⍉STATETM← 4 4 ⍴GSTM[;C],GSTM[;D],GSTM[;CC],GSTM[;DD]
[12]   GAMMA STATETM
[13]   AUGPHI STATETM
[14]   AUG T
[15]   IQ←STEP×(⍉STMPR)+.×QPR+.×STMPR
[16]   QH←QH+IQ
[17]   IN←STEP×(⍉STMPR)+.×QPR+.×GAMPR
[18]   NH←NH+IN
[19]   IR←STEP×R+(⍉GAMPR)+.×QPR+.×GAMPR
[20]   RH←RH+IR
[21]   →(T=DT)/0
[22]   T←T+STEP
[23]   →LOOP
      ∇

      ∇RICCATI[⎕]∇
      ∇ RICCATI
[1]   ⍝ CALCULATES SS P FROM RICCATI EQUATION
[2]    P←QH
[3]    COUNT←0
[4]    ERROR←0.001
[5]    GAMMA STM
[6]    AUGPHI STM
[7]    AUG DT
[8]    GAMPRT←⍉GAMPR
[9]    NT←⍉NH
[10]  LOOP:GPS←NT+GAMPRT+.×P+.×STMPR
[11]   NP←QH+((⍉STMPR)+.×P+.×STMPR)-(⍉GPS)+.×(⌹RH+GAMPRT+.×P+.×
                                                    GAMPR)+.×GPS
[12]   COUNT←COUNT+1
[13]   DIFF←NP-P
[14]   P←NP
[15]   P←(P+⍉P)÷2
[16]   A←(|DIFF)>ERROR
[17]   B←+/A
[18]   C←+/B
[19]   →(COUNT=100)/STOPS
[20]   →(C≥1)/LOOP
[21]   →0
[22]  STOPS:'DID NOT CONVERGE ON RICCATI SOLUTION IN 100 ITERATIONS.'
[23]   →0
      ∇
```

Table C-1 continued

```
       ∇QPRIME[⎕]∇
       ∇ QPRIME
[1]   ⍝CALCULATES Q PRIME FOR THE AUGMENTED CONTINUOUS
[2]   ⍝TIME COST FUNCTIONAL
[3]    QPR←SCW+((⍉F,G)+.×SRW+.×(F,G))
       ∇
       ⋄
       ∇SMATRIX[⎕]∇
       ∇ SMATRIX
[1]   ⍝CALCULATES FEED FORWARD GAINS S11,S12,S21,S22
[2]    S←⌹((STM-I),GAM),[1](HX,HU)
[3]    S11← 3 3 ↑S
[4]    S21← ¯2 3 ↑S
[5]    S12← 3 ¯2 ↑S
[6]    S22← ¯2 ¯2 ↑S
       ∇
       ⋄
       ∇STATECOV[⎕]∇
       ∇ STATECOV
[1]   ⍝PROPOGATES THE STATE COVARIANCE MATRIX AND STORES
[2]   ⍝RESULTS FOR GRAPHING
[3]    COUNT←DT←TIME←0
[4]    P←P-P
[5]    PT← 4 1 ⍴0
[6]    STEP←0.005
[7]   GO1:COUNT←1
[8]   GO:PDOT←(P+.×P)+(P+.×⍉P)+((L×Q)+.×⍉L)
[9]    P←P+PDOT×STEP
[10]   P←(P+⍉P)÷2
[11]   DT←DT+STEP
[12]   →(DT>0.5)/0
[13]   →(COUNT=10)/GO2
[14]   COUNT←COUNT+1
[15]   →GO
[16]  GO2:TIME←TIME,DT
[17]   PT←PT, 4 1 ⍴P[1;1],P[2;2],P[3;3],P[4;4]
[18]   →GO1
       ∇
       ⋄
       ∇STMDTN[⎕]∇
       ∇ PHI←DT STMDTN A;R;N;FACTOR;INDEX
[1]   ⍝ CALCULATES TRANSITION MATRIX
[2]    R←(⍴,A)*0.5
[3]    I←(⍳R)∘.=⍳R
[4]    N←0
[5]    PHI←I
[6]    FACTOR←I
[7]   L0:N←N+1
[8]    FACTOR←FACTOR+.×A×DT÷N
[9]    PHI←PHI+FACTOR
[10]   INDEX←(+/|,FACTOR)÷R*2
[11]   →(INDEX>EPS)/L0
       ∇
```

Table C-1 continued

```
      ∇STSMODEL[⎕]∇
      ∇ STSMODEL TD
[1]   ⍝GIVES RESPONSE OF 4TH ORDER SYSTEM TO INPUTS TD
[2]   ⍝AND STORES TIME HISTORY FOR GRAPHING
[3]   ⍝NOTE; ANSWER WITH 'NO' IF TABLE NOT DESIRED.
[4]    T←TIME←ΔR←ΔBETA←ΔP←ΔPHI←0
[5]    DELU←DELTD← 2 1 ⍴0
[6]    ΔPHIST←0
[7]    DELX←ΔX← 4 1 ⍴0
[8]    A←B←1
[9]    I←IDENT 2
[10]   TD1←TD
[11]   'IS A PRINTED TABLE DESIRED'
[12]   →('N'=1↑ANS←⍞)/LOOP
[13]   'TIME            ΔBETA                    ΔUR
[14]  LOOP:YKM1← 2 1 ⍴DELTD[;A]        ΔUA                      ΔP'
[15]   XKM1← 4 1 ⍴DELX[;B]
[16]   UKM1← 2 1 ⍴DELU[;A]
[17]   ΔUSKM1←(-S21+.×LAM×ΔPHIST)+S22+.×YKM1
[18]   ΔXSKM1←((-S11+.×LAM×ΔPHIST)+S12+.×YKM1),[1] ΔPHIST
[19]   ΔPHIST←ΔPHIST+ΔXSKM1[3;]×DT
[20]   ΔXSK←((-S11+.×LAM×ΔPHIST)+S12+.×TD),[1] ΔPHIST
[21]   ΔUSK←(-S21+.×LAM×ΔPHIST)+S22+.×TD
[22]   ΔU←ΔUSK+((I-DT×K2)+.×(UKM1-ΔUSKM1))-DT×K1+.×(XKM1-ΔXSKM1)
[23]   →('N'=1↑ANS)/SKIP
[24]   1 5 ⍴T,ΔX[2;],ΔU[1;],ΔU[2;],ΔX[3;]
[25]  SKIP:ΔX←(STM+.×ΔX)+GAM+.×ΔU
[26]   →(T=5)/STOP
[27]   T←T+DT
[28]   DELX←DELX,ΔX
[29]   DELU←DELU,ΔU
[30]   DELTD←DELTD,TD
[31]   TIME←TIME,T
[32]   A←A+1
[33]   B←A-1
[34]   →LOOP
[35]  STOP:DELU← 0 1 ↓DELU
      ∇
```

Table C-1 continued.

```
      ∇SYSMODEL1[⎕]∇
      ∇ SYSMODEL1 YD
[1]   ⍝GIVES RESPONSE FOR TYPE 1 SYSTEM TO INPUTS YD
[2]   ⍝AND STORES RESULTS FOR GRAPHING
[3]    T←TIME←ΔR←ΔBETA←ΔP←ΔPHI←⍳0
[4]    DELU←DELYD← 2 1 ⍴0
[5]    ΔPHIST←⍳0
[6]    DELX←ΔX← 4 1 ⍴0
[7]    A←B←1
[8]    I←IDENT 2
[9]    'TIME                BETA                ΔUR                ΔUA
[10]  LOOP:YKM1← 2 1 ⍴DELYD[;A]                                      ΔP'
[11]   XKM1← 4 1 ⍴DELX[;B]
[12]   UKM1← 2 1 ⍴DELU[;A]                                   XYD[2;]))
[13]   PHIFACT←-((S21+.×LAM×DT×YD[2;])+((2 3 ↑C1)+.×S11+.×LAM×DT
[14]   ΔU←UKM1+(C2+.×(YD-HX+.×XKM1))+PHIFACT-(C1+.×(ΔX-XKM1))
[15]   1 5 ⍴T,ΔX[2;],ΔU[1;],ΔU[2;],ΔX[3;]
[16]   ΔX←(STM+.×ΔX)+GAM+.×ΔU
[17]   →(T=5)/STOP
[18]   T←T+DT
[19]   DELX←DELX,ΔX
[20]   DELU←DELU,ΔU
[21]   DELYD←DELYD,YD
[22]   TIME←TIME,T
[23]   A←A+1
[24]   B←A-1
[25]   →LOOP
[26]  STOP:DELU← 0 1 ↓DELU
      ∇
```

Using these programs, and following the algorithm outlined in Figure 3, the following sequence outlines the steps used in finding the optimal gains. The public workspace 3 EIGENVAL is used in calculating eigenvalues.

```
apl


      V S   A P L

CLEAR WS
      )LOAD OPTIMAL
SAVED 13:14:15 08/23/79
      •

      FF
  ¯0.75    5.9    ¯0.26    0
  ¯1      ¯0.4     0       0.181
   1.16  ¯11.5    ¯6.5     0
   0       0       1       0
      •

      GG
  ¯6.1    ¯0.252
  ¯0.07    0
   0.58   21
   0       0
      •
      F←3 3↑FF
      •
      G←3 2↑GG
      •
      L←3 ¯1↑FF
      •
      F
  ¯0.75    5.9    ¯0.26
  ¯1      ¯0.4     0
   1.16  ¯11.5    ¯6.5
      •
      G
  ¯6.1    ¯0.252
  ¯0.07    0
   0.58   21
      •
      L
 0
 0.181
 0
      •
      I←IDENT 3
      •
      HX←2 3⍴ 0 1 0 0 0 1
      •
      HX
 0 1 0
 0 0 1
      •
```

```
      STM←DT STMDYN F
      ⋄
      GAMMA STM
      ⋄
      LAMBDA STM
      ⋄
      SMATRIX
      ⋄
      S11
¯3.943587974E¯1   ¯1.027233010E1     1.408734036E¯3
 4.504074140E¯16  ¯7.194324853E¯16   1.111907579E¯17
¯2.601035115E¯17   3.988253843E¯17  ¯6.843380963E¯19
      ⋄
      S22
 1.002469182    ¯0.05594623759
 0.5459032558    0.3108526659
      ⋄
      S12
¯4.701728428E¯1    3.916236631E¯3
 1.000000000E0     1.209553011E¯17
 1.587715185E¯17   1.000000000E0
      ⋄
      S21
¯1.646309097     1.717631875    ¯0.05084765749
 0.04084629988   0.8277927557    0.6488070443
      ⋄
      F←FF
      ⋄
      G←GG
      ⋄
      HX←2 4⍴0 1 0 0 0 0 1 0
      ⋄
      HX
0 1 0 0
0 0 1 0
      ⋄
      I←IDENT 4
      ⋄
      STM←DT STMDYN F
      ⋄
      GAMMA STM
      ⋄
      GENSTM
      ⋄
      SCW←6 6⍴25 0 0 0 0 0 0 30 0 0 0 0 0 0 10 0 0 0 0 0 0 .5
      ⋄
      R←IDENT 2                   0 0 0 0 0 0 15 0 0 0 0 0 0 15
      ⋄
      SRW←4 4⍴0
      ⋄
      QPRIME
```

```
      QFR
 25     0     0     0     0     0
  0    30     0     0     0     0
  0     0    10     0     0     0
  0     0     0   0.5     0     0
  0     0     0     0    15     0
  0     0     0     0     0    15
      ∘
      QMR
      ∘
      RICCATI
      ∘
      GAIN
      ∘
      K1
 ¯2.226868062  ¯3.482421716   0.1035423573  0.1503060991
  0.4338562581 ¯2.209187887   0.4328194312  0.6572397435
      ∘
      K2
  7.072997099     0.3615541911
 ¯0.04492466455   6.677442616
      ∘
      FCLOOP
      ∘
      .001 EIGVAL FCL
 ¯7.028011028   4.597493194
 ¯7.028011028  ¯4.597493194
 ¯3.870323863   3.745582285
 ¯3.870323863  ¯3.745582285
 ¯1.539527882   0
 ¯0.3334287854  0
      ∘
      YD←2 1⍴0 .1
      ∘
      SYSMODEL YD
IS A PRINTED TABLE DESIRED
YES
```

TIME	ΔBETA	ΔUR	ΔUA	ΔR
0	0	¯0.005594623759	0.03108526659	0
0.1	¯0.00004796264297	¯0.004866934581	0.03333570878	0.0478728
0.2	¯0.0001094206221	¯0.005362393304	0.03508818581	0.07959763158
0.3	¯0.00002476572102	¯0.006323464553	0.03385357105	0.0957416
0.4	0.0002236635395	¯0.007271768894	0.03285612011	0.1020802312
0.5	0.0005870820528	¯0.007986143892	0.03230885035	0.1035968902
0.6	0.001001963709	¯0.008420355734	0.03209420904	0.1032367116
0.7	0.001415919755	¯0.00862039657	0.03205350769	0.102571874
0.8	0.001795670398	¯0.00866437852	0.03207513358	0.1019678947
0.9	0.002125545013	¯0.008627697824	0.03210055823	0.1015743573
1	0.002402455124	¯0.008567784929	0.032107[illegible]	0.1013471427

```
GAIN1

C1
¯1.075109895    3.532031744   ¯0.0139897566   0
 0.01756114422  0.09936841709  0.4335301848   0
C2
 0.4852426399 ¯0.0218050371
 0.1187026755  0.2513070724

GAIN1

C1
¯1.075109895    3.532031744   ¯0.0139897566   0
 0.01756114422  0.09936841709  0.4335301848   0

C2
 0.4852426399 ¯0.0218050371
 0.1187026755  0.2513070724

SYSMODEL1 TD
```

TIME	BETA	ΔUR	ΔUA	ΔF
0	0	¯0.004363573794	0.02506802103	0
0.1	¯0.00003535517831	¯0.006547137916	0.03337741166	0.0386072234
0.2	¯0.0001237182436	¯0.007705845193	0.03439211572	0.07168072985
0.3	¯0.0002087363458	¯0.008451491439	0.03321927425	0.09065698196
0.4	¯0.0002545464886	¯0.009022408929	0.03194236439	0.09888717442
0.5	¯0.0002566288334	¯0.009485466994	0.03110729575	0.1013245337
0.6	¯0.0002279476746	¯0.009856816781	0.03067503517	0.1014066478
0.7	¯0.0001851808205	¯0.01015009785	0.03047871984	0.1008802454
0.8	¯0.0001413430182	¯0.01038566023	0.0303845648	0.1004078801
0.9	¯0.0001038140288	¯0.01058613673	0.03031867401	0.1001320127
1	¯0.00007522442871	¯0.01077091227	0.03025069176	0.1000124243

APPENDIX D

The Micro-DFCS Control Program

D-1 DESCRIPTION OF CAS-4 ROUTINES

The routines of CAS-4 are divided into three categories: Executive, Utility, and Control Routines. Each of these is documented in the source listing with line comments and a header for each subroutine. In addition, a description of the major elements of CAS-4 is presented here.

Executive Routines

The executive program provides for CPU initialization, CDU interface and command recognition, and a memory check error detection routine. INITIALIZATION routines set the hardware timer, the mathematics board, I/O ports (parallel and serial), and the analog board; it also initializes flags, registers, and RAM storage space to be used in other routines. CDU INTERFACE checks for inputs from the CDU and allows the user to set the desired parameters for CAS-4 operation. MEMORY CHECK is one of the error detection routines employed in CAS-4. Every 50 samples it adds the entire contents of CAS-4 in an 8-bit register and, ignoring the overflow, compares the result with a known sum. If the two differ, a message is displayed on the CDU indicating that some part of the memory has been altered.

Utility Routines

The routines CLEARLINE, CONSOLE OUTPUT, NUMERIC INPUT, ENTRY ERROR, SERIAL OUTPUT, HEX INPUT, and CONSOLE IN are used to display and enter data on the CDU. BLINK is a second error detection method that flashes a light on the instrument panel to indicate that the operational CAS-4 program is running properly. It is called once in every flight control interrupt service routine. ANALOG TO DIGITAL CONVERSION selects the proper analog input channel, initiates the conversion, and stores

the results. COUNT UP DISPLAY generates an increasing sequence of numbers 1-9 on the bottom line of the CDU. This indicates the hardware interrupt is working, the time interval between interrupts, the program has been initialized, and that the D/A converters are operating properly. INTERRUPT COUNT increments a timer each time an interrupt service routine is executed. This is used in conjunction with the error detection routines to determine the exact location of the error. LIMIT ANALOG OUTPUT prevents the analog output channels from switching instantly from +10 volts to -10 volts, or vice versa. This condition occurs when the control law calculates a control position corresponding to a voltage magnitude greater than 10 volts because of the method used for converting floating point numbers to fixed point format. MODE CHANGE allows the user to select 1 of 20 possible flight control configurations. In CAS-4, only 13 of these modes were used: one direct mode, three lateral acceleration-roll rate controllers with different gains, four sideslip angle-roll rate modes with different gains, four sideslip angle-roll rate controllers with identical weightings at different sampling rates, and one Type 1 sideslip angle-roll rate control mode. MATH UNIT DRIVER loads the high speed mathematics unit with the two arguments to be operated on, initiates the operation, and stores the result in RAM. This routine is relatively slow (230 msec) and very general in nature; it should not be used in the flight control algorithms where time is a critical factor. MATH ERROR PROCESSOR is the third error detection routine in CAS-4. It checks for errors in the mathematics unit (such as divide by zero). It displays the type of error that has occurred and the number of times the math unit has been used in the current control law execution cycle on the CDU. This allows the user to locate the exact location of the error in the control program. CALIBRATED STEP INPUT allows the pilot to command a step input in any of the analog channel inputs. Once the value of the step is entered, the command is initiated by depressing the CDU's "carriage return" key. The command is halted by depressing any CDU key. TIMER allows the user to reset the interrupt timer through the CDU to change the sampling interval. The user enters the four-digit hexidecimal number corresponding to the desired sampling interval. Two other routines that were not used in this investigation

are available in CAS-4. SET DELAY and DELAY allow the user to insert pure time delays between command input and command response. By entering the delay, either by specifying a number of samples to be delayed or a delay time in milliseconds, the user can evaluate the effects of time delays on control performance factors. Similarly, RESOLUTION allows the user to mask bits from the Micro-DFCS outputs. This allows the user to experiment with an eight-bit controller, for example, to determine the effects of a lower bit resolution on control effectiveness.

Flight Control Routines

The flight control routines are of two types: the flight control mode set-up routine, and the flight control mode interrupt service routine. The flight control mode set-up routines are called using the MODE CHANGE routine. Once the desired mode is entered through the CDU, the control program branches to that mode's set-up routines. These routines are responsible for several key elements in the flight control calculations. First, these routines load the starting address of the desired mode's interrupt service routine (control law execution program) at the interrupt branch point. This allows the desired control program to be executed on each timed interrupt. Second, the set-up routine samples and stores values for all aircraft states and command inputs. These values will be used in the control law to calculate perturbation values. Finally, these routines set the optimal gains which correspond to the selected mode of operation and at a voltage level on the analog status channel to identify the mode of operation. These routines follow the flow chart depicted in Figure D-1.

The flight control interrupt service routines are executed on every timed interrupt according to the flow chart depicted in Figure D-2. Once the starting address for these routines has been set at the interrupt branch point by the set-up routine, these routines are given the highest priority over all other routines. The service routines contain the logic that calculates the desired control perturbation, $\Delta \underline{u}$, based on perturbations in state or command.

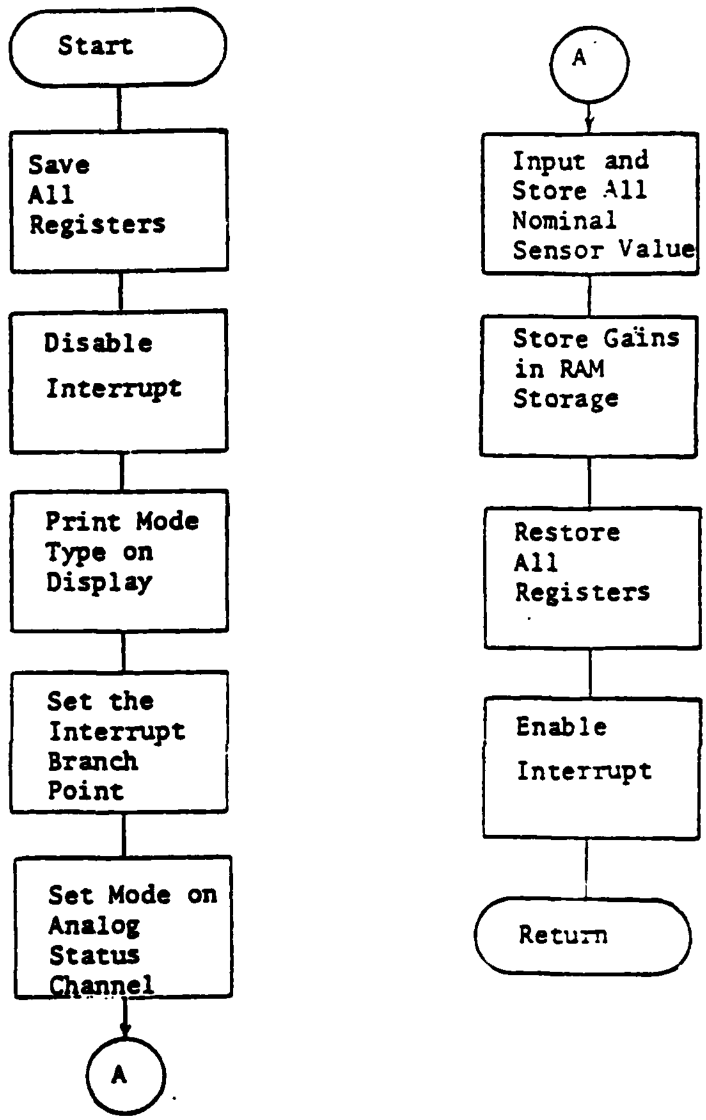

Figure D-1. Flowchart for Typical Mode Set-Up Routine.

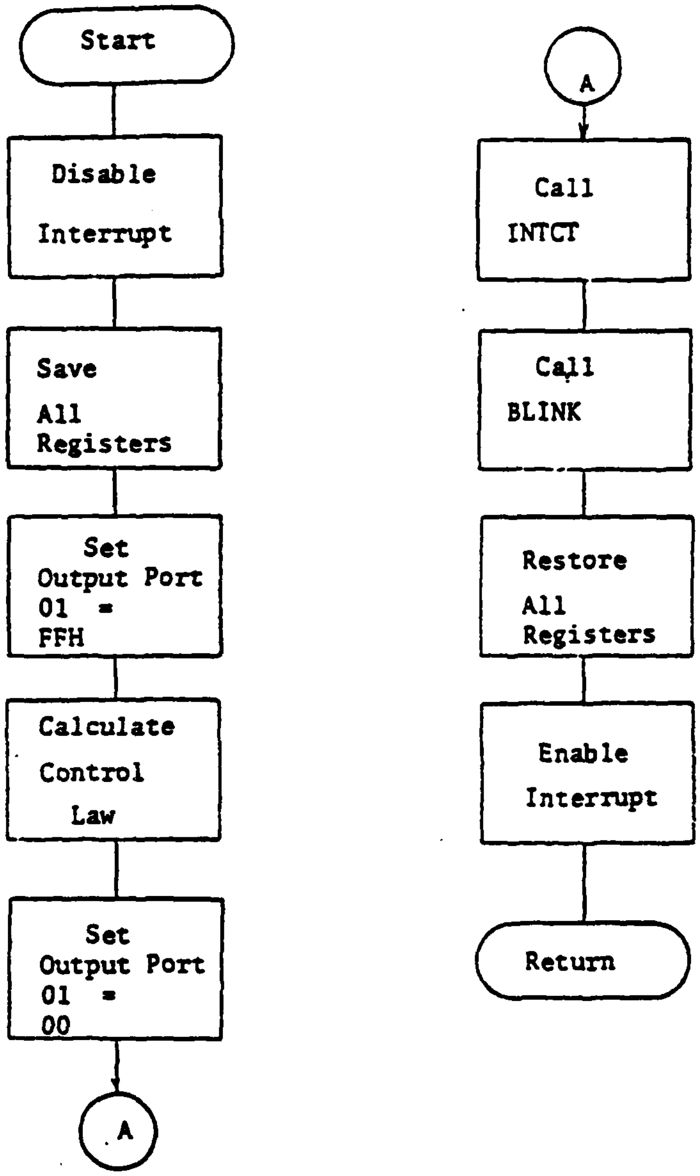

Figure D-2. Flowchart for Typical Flight Control Interrupt Service Routine.

The DIRECT MODE INTERRUPT SERVICE ROUTINE takes in commands from lateral stick and foot pedals, calculates the perturbation in each, adds any step bias, multiplies this by a gearing factor, and sends the values to the ailerons and rudders, respectively.

The LATERAL ACCELERATION-ROLL RATE COMMAND SERVICE ROUTINES calculate aileron and rudder commands, δA and δR, based on measured values of δS, δP, r, a_y, p, and ϕ. The measured inputs first must be formatted and scaled before the control calculations can begin. The analog signals are converted to 12-bit fixed point binary numbers, then to a 32-bit floating point format for use in the mathematics unit. Next, the nominal value for each, stored by the set-up routine, is subtracted from the measured value to calculate the perturbations in each. At this point, if a step bias has been added to any channel using the CALIBRATED STEP INPUT routine, that value is added to the perturbation value. These values must then be scaled to the appropriate units of motion prior to the control law computation. These scaling factors are stored in RAM. Following the control law calculations, the computed values of δA and δR, must first be converted from radians to volts. Finally, they are converted back to 12-bit fixed-point format, converted to analog voltages. and sent to δA and δR. In a similar manner, SIDESLIP ANGLE-ROLL RATE COMMAND INTERRUPT SERVICE ROUTINE and TYPE 1 CONTROL INTERRUPT SERVICE ROUTINE calculate values of δA and δR based on measured values of δS, δP, r, β, p, and ϕ, according to Equations 2.3-56 and 2.3-75.

APPENDIX E

Research Systems

E.1 VARIABLE-RESPONSE RESEARCH AIRCRAFT (VRA)

The VRA is a highly-modified Navion equipped with inertial, air data, and navigation sensors, as well as six independent force and moment controls. The VRA, shown in Figure E-1, has been used to conduct a broad range of experiments in aircraft flying qualities, human factors, and control in the past. The aircraft has played a major role in establishing current military and civil flying qualities criteria, and with the addition of the Micro-DFCS, the VRA is equipped to expand this type of research, as well as to investigate advanced digital control concepts [29].

Independent control of three forces and three moments is provided by commands to the elevator, ailerons, rudder, throttle, direct-lift flaps, and side-force panels (Figure E-2). The control surfaces are driven by hydraulic servos originally fitted to the B-58 aircraft. The modified VRA units incorporate solenoid-actuated valves with force-override features for quick disengagement. Characteristics of the control effectors are summarized in Table E-1. Surface rate limits are seen to range from 60 to 110 deg/sec. Bandwidths are given for flat response and 6 db attenuation (in parenthesis), except that thrust bandwidth is specified by the frequency for 3 db attenuation. The aircraft's normal operating speed range is 65 to 120 KIAS; maximum specific forces and moments ("control power") are given for 70 KIAS. At 105 KIAS, maximum direct lift and side-force accelerations are 1 g and 0.5 g, respectively. The sensors used for most flight testing include angular rate gyros and linear accelerometers for all three axes, vertical and heading gyros, dual angle-of-attack and sideslip-angle vanes, radar altimeter, indicated airspeed, control surface positions, and cockpit control positions. Several other signals (e.g., air temperature, barometric altimeter, altitude rate, and TALAR microwave landing system signals) are available for system feedback or telemetry recording. The

Figure E-1. Variable-Response Research Aircraft.

Figure E-1. Variable-Response Research Aircraft.

AD-A110 274 PRINCETON UNIV NJ DEPT OF MECHANICAL AND AEROSPACE --ETC F/6 1/2
DIGITAL COMMAND AUGMENTATION FOR LATERAL-DIRECTIONAL AIRCRAFT D--ETC(U)
MAY 81 D ATZHORN N00014-78-C-0257
UNCLASSIFIED MAE-1511 ONR-CR-300-003-2 NL

3 of 3

END
DATE
FILMED
2-82
DTIC

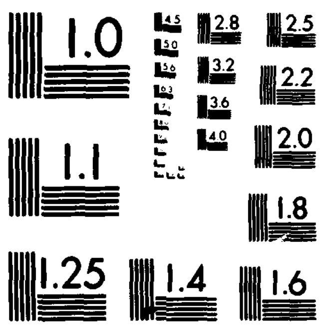

MICROCOPY RESOLUTION TEST CHART

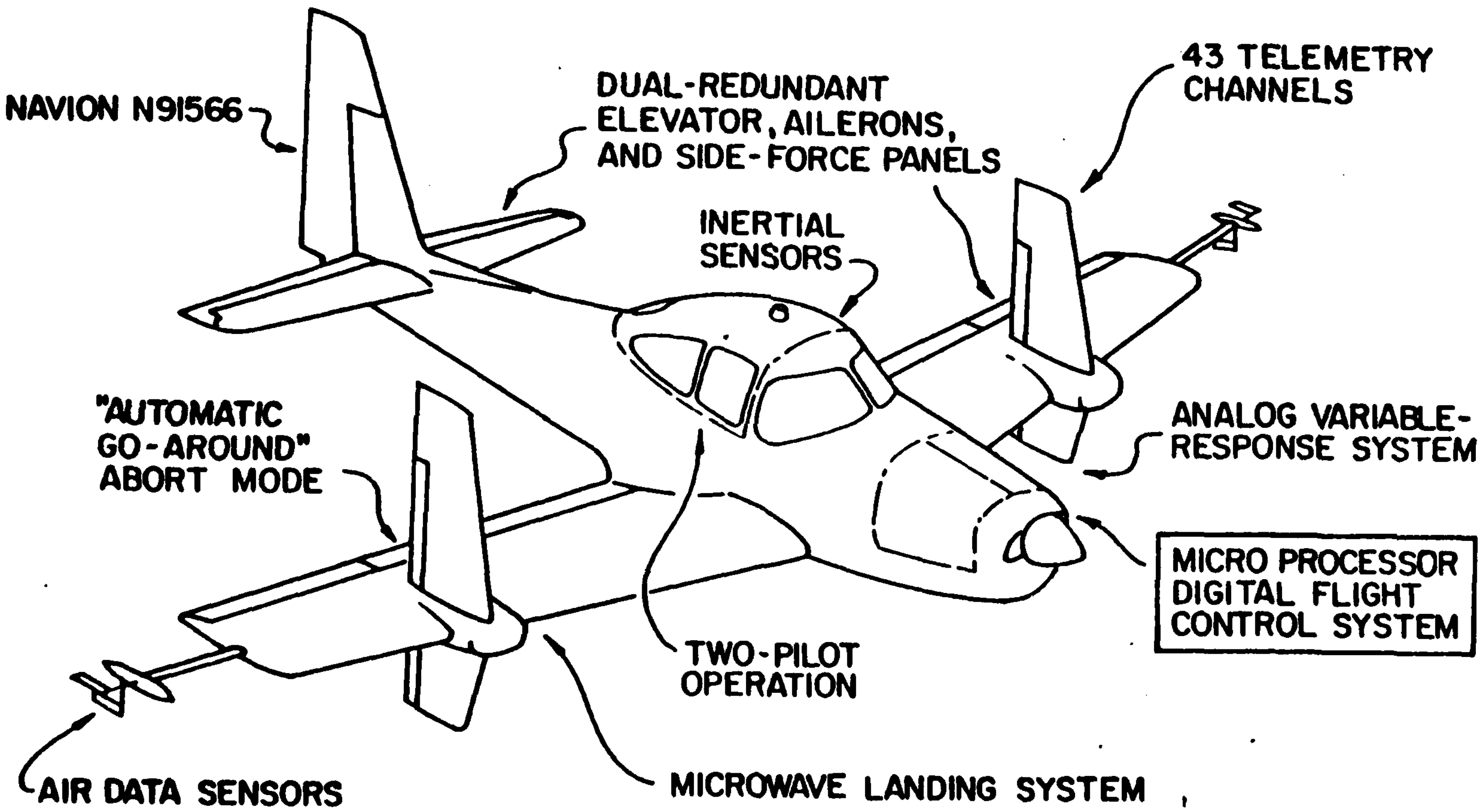

Figure E-2. Variable-Response Research Aircraft (VRA)

Table E-1 VRA Control Characteristics

Control	Displacement Limit, deg	Rate Limit, deg/sec	Bandwidth, Hz	Maximum Specific Force or Moment (IAS = 70kt)
Roll	30.	70.	5 (10)	4.1 rad/sec^2
Pitch	-30. +15.	70.	5 (10)	4.4 rad/sec^2
Yaw	15.	70.	5 (10)	1.9 rad/sec^2
Thrust	--	--	0.6	0.1 g
Side Force	35.	60.	2 (3)	0.25 g
Normal Force	30.	110.	2 (3)	0.5 g

present telemetry system allows 42 data channels to be multiplexed and transmitted to the FRL ground station described below.

The VRA is operated by a two-man crew during all research. In addition to the evaluation and safety pilot mentioned earlier, the safety pilot has at his control an "automatic go-around" abort mode which makes safe experimentation through touchdown possible. This abort mode commands a 20 deg flap setting and climb power when activated; at 70 KIAS on a 6-deg glideslope, and up-flap "hardover" failure can be corrected and climbout can be initiated with a maximum altitude loss of 10 feet.

E.2 EXPERIMENTAL FACILITIES

The VRA is operated from the flight test facility at Princeton University's James Forrestal Campus. The facility includes the FRL hangar, laboratories, and shops, plus a 3000 ft Basic Utility II runway. TALAR 3 and 4 fixed-beam microwave landing systems (MLS) furnish precision approach-path guidance.

The ground station at the FRL is used to receive, record, and analyze the telemetered data from the VRA. It includes a Honeywell seven-channel tape recorder, an FM or AM receiver presently operating at 1458 MHz in the FM mode, a telemetry demultiplexer with five translators, an EAI TR-48 analog computer, a radio telephone, and a six-channel paper strip chart recorder. The PDM telemetry system provides 42 data channels, each sampled at a rate of 20 sps. The telemetry data from the receiver can be recorded on tape and demultiplexed five channels at a time for plotting on the strip chart recorder. The analog computer scales and buffers all input channels from the translators to the strip chart recorder, in addition to providing ground-based simulations for the VRA and other dynamic systems [18].

REFERENCES

1. Brogan, W.L., Modern Control Theory, Quantum Publishers, Inc. New York, 1974.

2. Yopp, N.B. and McDonnell, J.D., "Digital Flight Control Systems--Considerations in Implementation and Acceptance", AIAA Paper No. 75-577, April, 1975.

3. McRuer, D., "New Trends and Problems Areas in Automatic Flight Control", Israel Journal of Technology, Vol. 15, 1977, pp. 1-10.

4. Arnold, J.I., "Future Trends in Highly Reliable Systems", in "Integrity in Electronic Flight Control Systems", AGARD ograph #224, April 1977.

5. Boone, J.H. and Flynn, G.R., "Digital Flight Control is the Answer--What is the Question?", IEEE Transactions on Aerospace and Electronic Systems, Vol. AES-15, No. 5, September 1975, pp. 862-882.

6. Osder, S.S., "Architecture Considerations for Digital Flight Control Systems", IEEE Transactions on Aerospace and Electronic Systems, Vol. AES-11, No. 5, September 1975, pp. 829-840.

7. Osder, S.S., Mossman, D.C. and Devlin, B.T., "Flight Test of a Digital Guidance and Control System in a DC-10 Aircraft", AIAA Paper No. 75-567, April 1975.

8. Mathews, Jr., M.A., "SAAB Digital Flight Control", AIAA Paper No. 74-26, 1974.

9. Yechout, T.R. and Oelschlaeger, D.R., "Digitac Multimode Flight Control System", AIAA Paper No. 75-1085, August 1975.

10. Damman, L., Kennington, R., Kirsten, P., Grabe, R. and Long, P., "Flight Test Development and Evaluation of a Multimode Digital Flight Control System Implemented in an A-7D", Vol. I, AFFTC-TR-76-15, June 1976.

11. Lipari, L.J., "Digitac II Phase I, Yaw Control Laws and Analytical Redundancy Evaluation", AFFTC-TR-79-5, May 1979.

12. Elliot, J.R., "NASA's Advanced Control Law Program for the F-8 Digital Fly-by-Wire Aircraft", IEEE Transactions on Automatic Control, Vol. AC-22, No. 5, October 1977, pp. 753-757.

13. Hartmann, G.L., Hange, J.A. and Hendrick, R.C., "F-8C Digital CCV Flight Control Laws", NASA CR-2629, February 1976.

14. Athans, M., et al, "Investigation of the Multiple Model Adaptive Control (MMAC) Method for Flight Control Systems", NASA CR-3089, May 1979.

15. Stengel, R.F., Broussard, J.R. and Berry, P.W., "Digital Controllers for VTOL Aircraft", IEEE Transactions on Aerospace and Electronic Systems, Vol. AES-14, No. 1, January 1978, pp. 54-63.

16. Kubbat, W.J., "A Multifunctional Guidance and Control System", NAECON '77 Record, Dayton, May 1977.

17. Beh, H., Korte, U. and Löbert, G., "Stability and Control Aspects of the CCV-F104 G", Presented at the AGARD Flight Mechanics Panel Meeting on Stability and Control, Ottawa, September 1978.

18. Anon., "Military Specification, Flying Qualities of Piloted Airplanes", MIL-F-8785B (ASG), August 1969.

19. Seat, J.C., "A Flight Investigation of Digital Control Using Microprocessor Technology", MSE Thesis, MAE Report 1411-T, Princeton University, April 1979.

20. Stengel, R.F., Broussard, J.R. and Berry, P.W. "The Design of Digital Adaptive Controllers for VTOL Aircraft", NASA CR-144912, 12 March 1976.

21. Dorato, P., and Levis, A. H., "Optimal Linear Regulators: The Discrete-Time Case", IEEE Transactions on Automatic Control, Vol. AC-16, No. 6, December 1971, pp. 613-620.

22. Broussard, J.R. and Safanov, M., "Design of Generalized Discrete Proportional Integral Controllers by Linear-Optimal Control Theory", TASC TIM-804-1, October 1976.

23. Berman, H. and Gran, R., "An Organized Approach to the Digital Autopilot Design Problem", AIAA Paper No. 73-848, August 1973.

24. Broussard, J.R., Berry, P.W. and Gully, S.W., "Synthesis of Digital Controllers for a Fighter Aircraft Using Continuous-Time Specifications", Proceedings of the Flight Control Systems Criteria Symposium, Naval Postgraduate School, Monterey, July 1978, pp. 91-111.

25. Sandell, N., Jr. and Athans, M., "On Type-L Multivariable Linear Systems", Automatica, Vol. 9, No. 1, January 1973, pp. 131-136.

26. Stengel, R.F., "Proposal to Continue Digital Flight Control Research Using Microprocessor Technology", Princeton FRL TP-101-2, December 14, 1978.

27. Stengel, R.F., Broussard, J.R. and Berry, P.W., "Command Augmentation Control Laws for Maneuvering Aircraft", AIAA Paper No. 77-1044, August 1977.

28. Gelb, A., Applied Optimal Estimation, M.I.T. Press, Cambridge, 1974.

29. Stengel, R.F., "Some Effects of Parameter Variations on the Lateral-Directional Stability of Aircraft", AIAA Journal of Guidance and Control", Vol. 3, No. 2, Mar-Apr 1980, pp. 124-131.

30. Stengel, R.F., "Digital Flight Control Using Microprocessor Technology", IEEE Transactions on Aerospace and Electronic Systems, Vol. AES-15, No. 3, May 1979, pp. 397-404.

31. Holley, W.E. and Bryson, A.E., Jr., "Multi-Input, Multi-Output Regulator Design for Constant Disturbances and Non-Zero Set Points with Application to Automatic Landing in a Crosswind", SUDAAR NO. 465, August 1973.

Suggested Distribution List

	No. of copies
Office of Naval Research 800 N. Quincy St. Arlington, VA 22217	
Code 260	1
Code 432	2
Commander, Naval Air Development Center Warminster, PA 18974	
Code 6072 (Piranian)	1
Code 6053 (Clark, J.W.)	1
Commander, Naval Air Systems Command Washington, D.C. 20360	
Code AIR 340D	1
Code AIR 53011B	1
Defense Documentation Center Cameron Station Alexandria, VA	12
Commander, David Taylor Naval Ship R & D Center Bethesda, MD 20084	
Code 166 (Nichols)	1